9412071

I

RAPPORT

Jürgen König

Fire Resistance of Timber Joists and Load Bearing Wall Frames

Trätek

INSTITUTET FÖR TRÄTEKNISK FORSKNING

Jürgen König

FIRE RESISTANCE OF TIMBER JOISTS AND LOAD BEARING WALL FRAMES

Trätek, Rapport I 9412071

ISSN 1102 – 1071
ISRN TRÄTEK – R – – 94/071 – – SE

Nyckelord

beams
charring
fire resistance
joists
load bearing capacity
model
tests
timber frame
walls

Stockholm november 1995

Rapporter från Trätek — Institutet för träteknisk forskning — är kompletta sammanställningar av forskningsresultat eller översikter, utvecklingar och studier. Publicerade rapporter betecknas med I eller P och numreras tillsammans med alla utgåvor från Trätek i löpande följd.

Trätek — Institutet för träteknisk forskning — betjänar de fem industrigrenarna sågverk, trämanufaktur (snickeri-, trähus-, möbel- och övrig träförädlande industri), träfiberskivor, spånskivor och plywood. Ett avtal om forskning och utveckling mellan industrin och Nutek utgör grunden för verksamheten som utförs med egna, samverkande och externa resurser. Trätek har forskningsenheter i Stockholm, Jönköping och Skellefteå.

Reports issued by the Swedish Institute for Wood Technology Research comprise complete accounts for research results, or summaries, surveys and studies. Published reports bear the designation I or P and are numbered in consecutive order together with all the other publications from the Institute.

The Swedish Institute for Wood Technology Research serves the five branches of the industry: sawmills, manufacturing (joinery, wooden houses, furniture and other woodworking plants), fibre board, particle board and plywood. A research and development agreement between the industry and the Swedish National Board for Industrial and Technical Development forms the basis for the Institute's activities. The Institute utilises its own resources as well as those of its collaborators and other outside bodies. Our research units are located in Stockholm, Jönköping and Skellefteå.

CONTENTS

PREFACE

The investigation described in this report has been conducted at Trätek - the Swedish Institute for Wood Technology Research. The comprehensive test programme was conducted by Joakim Norén. In the first phase of testing, before Trätek's present fire laboratory was commissioned, the small-scale furnace was employed at the Royal Institute of Technology, Stockholm, Thanks to the generosity of Prof. Kai Ödeen. The full-scale tests were conducted at and in co-operation with the Fire Technology Laboratory of the Technical Research Centre of Finland (VTT) under the responsibility of Jarmo Majamaa.

SUMMARY

The goal of the investigations described in this report was to develop a simple model which can be used in the structural fire design of typical applications in timber frame housing as wall and floor assemblies. Two types of structures exposed to standard fire exposure on one side were considered: load bearing walls and floors acting as a border of a fire compartment.

The experimental investigations in this research project were divided into two parts. In the first, main part timber members were investigated in pure bending using a small-scale furnace. In the second part some full-scale tests were conducted on axially loaded walls, with the aim of seeing whether the results obtained from small-scale tests could be used to describe the full-scale behaviour of a wall.

In the small-scale tests the specimens consisted of the timber frame member itself and surrounding materials such as rock fibre mineral wool and gypsum plasterboards. The load was applied such that the fire exposed side of the timber member was in compression or tension. The dimensions of the timber members were 45 mm × 95 mm, 45 mm × 145 mm and 45 mm × 195 mm. Most of the fire tests were made with unprotected timber members on the fire-exposed side. The wide sides of the timber members were protected by mineral wool. The load level was in relation to the predicted load bearing capacity at normal temperature. By using different load levels in the range between 10 and about 80 %, relationships were determined between the load ratio and time to failure. The decrease of flexural stiffness and the location of the neutral axis were determined as a function of time. The tests show that there exists an influence of the state of stress on the results.

The residual cross sections of the members were recorded by means of a digitizer and the temperature was measured at several points in the timber member. The charring depth was determined and it is shown that this can be defined by the location of the 300-degree isotherm. It is shown that the charring depth is independent of the state of stress (tension or compression).

Test series with variable loads during the fire tests showed that the influence of loading rate on the failure load is small and could be neglected if this method were to be adopted in a standard for fire testing of load bearing timber constructions.

The contribution to fire resistance by means of gypsum plasterboards was studied by comparing the behaviour of test specimens with and without the fire protective boards. It was found that their fire protective effect was a function of time.

Three full-scale fire tests were conducted on load-bearing walls in order to verify the results obtained from the small-scale tests. It was found that there was a good agreement with respect to charring depth and temperature in the timber members.

An empirical analytical model was developed to describe the mechanical properties of the timber members. This consists partly of notional charring rates in order to define an effective rectangular cross section, partly of expressions for the reduction of strength and stiffness parameters due to the influence of fire. A simple model is given for the calculation of the load bearing capacity of axially loaded wall studs.

SAMMANFATTNING

Syftet med undersökningarna beskrivna i denna rapport var att utveckla en enkel beräkningsmodell som kan tillämpas vid dimensionering av typiska bärande träregelkonstruktioner. Två olika fall med ensidig standardbrandbelastning betraktades: Bärande väggar och bjälklag som bildar omslutningen av en brandcell.

De experimentella undersökningarna i detta forskningsprojekt var uppdelade i två delar. I den första delen som utgör merparten av undersökningarna provades träreglar med en ren böjbelastning i en småskaleugn (modellugn). I undersökningens andra del genomfördes några fullskaleförsök med belastade väggar med syftet att ta reda på om resultaten erhållna vid försöken i liten skala skulle kunna användas till att beskriva väggarnas egenskaper i full skala.

Provkropparna vid småskaleprovningen var sammansatta av träregeln och omgivande material (stenullsisolering och gipsskivor). Den mekaniska belastningen påfördes så att träregelns brandexponerade sida antingen var tryckt eller dragen. Träreglarnas dimensioner var 45 mm × 95 mm, 45 mm × 145 mm respektive 45 mm × 195 mm. Det flesta av brandproven genomfördes med oskyddad kantsida. Flatsidorna skyddades av stenull. Lastnivån av den mekaniska belastningen definierades i förhållande till den skattade bärförmågan vid normal temperatur. Genom att välja lastnivåer mellan 10 och ca 80 % bestämdes samband mellan lastnivå och tid till brott. Reduktionstalet för elasticitetsmoduln och neutrala lagrets läge bestämdes som funktion av tiden. Försöken visar att spänningstillståndet påverkar resultaten.

Formen av träreglarnas resttvärsnitt registrerades med hjälp av en digitaliseringsutrustning. Temperaturen mättes i reglarna i flera punkter. Inbränningsdjupet uppmättes och det visas att det kan beskrivas som läget av 300-gradersisotermen. Försöken visar att inbränningsdjupet inte påverkas av spänningstillståndet med avseende på tryck eller dragning.

Resultaten från provserier med variabel mekanisk belastning visar att belastningshastigheten på brottlasten är liten och att den skulle kunna försummas om detta förfarandesätt inkluderades i en standard för brandprovnings för bärande träkonstruktioner.

Gipsskivornas bidrag till brandmotståndet studerades genom jämförelse av provkroppars egenskaper utan och med brandskyddande beklädnad. Det visas att den brandskyddseffekten är tidsberoende.

Tre fullskaleprov med bärande väggar genomfördes för att verifiera resultaten erhållna vid småskaleprovningen. Resultaten visar att de överensstämmer väl avseende inbränningsdjupet och temperaturen i träreglarna.

En empirisk beräkningsmodell utvecklades som beskriver träreglarnas mekaniska egenskaper. Modellen inkluderar dels en fiktiv inbränningshastighet för bestämning av ett effektivt rektangulärt resttvärsnitt, dels uttryck för beräkning av hållfasthets- och styvhetsreduktionen på grund av brandpåverkan. En enkel model presenteras för beräkningen av bärförmågan av axialkraftbelastade väggreglar.

1 INTRODUCTION

The performance of timber structures exposed to fire is characterized by two phenomena. The first is the charring of wood by which the section of the member is reduced, and the second one is the softening and reduction of strength of the residual cross section of the member. Traditionally most research on the behaviour of timber structures exposed to fire has dealt with large sections of solid timber and glued laminated beams. Since charring is the most apparent phenomenon when wood is exposed to fire, most of the research has been concentrating on charring and how it is influenced by other parameters. Typical results of this kind of research are those by Schaffer (1967), Hadvig (1981), Mikkola (1990) and Hao and White (1992).

Our knowledge of the properties of fire-exposed light timber members as they are used in timber frame structures as wall studs and floor joists is still limited, especially when the members are surrounded by other building materials such as mineral wool and boards and therefore are partially protected against the influence of fire. While in heavy-timber members, in standard fire exposure, only the outer part of the cross section near the char layer is affected by fire, in small members the conditions are more complicated, since a greater part of the residual cross section is affected by elevated temperature and changes of moisture content. For example, very little is known as to what extent strength and stiffness are influenced by transient states of temperature and moisture content in the wood.

For timber members exposed to fire on three or four sides, in Eurocode 5, Part 1-2 (ENV 1995-1-2) charring rates are given, and the reduction of strength and stiffness parameters are approximated. These design data may also be used for light timber frame members. For light timber members which are protected on more than one side, no information is given regarding charring rates and the reduction of strength and stiffness parameters.

Therefore, the main goal of the investigations described in this report was to make it possible to develop a simple model which can be used in the design of typical applications in timber frame housing as walls and floors. Secondly, the results should be used in order to verify more sophisticated analytical models.

Two typical types of structures exposed to fire on one side were considered: Load bearing walls and floors acting as a border of a fire compartment. In load-bearing walls the stud deflects towards the unexposed side of the wall, due to increasing eccentricity of the load. The stud acts as a beam-column with a large bending moment which causes compressive stresses on the fire exposed side of the stud. The structural behaviour of such members has been investigated in a simulated fire situation by removing layers of the stud by planing. See König (1988) or König and Källsner (1988) . The failure load of axially loaded timber members is very sensitive to imperfections which are inevitable due to the inhomogeneity of wood. In tests scatter would therefore normally be large and have an influence on the accuracy of the results.

The investigations in this research project were divided into two parts. In the first main part timber members were investigated in pure bending using a small-scale furnace. In the second part some full-scale tests were conducted on axially loaded walls, with the aim of investigating whether the results obtained from small-scale tests could be used to describe the full-scale behaviour of a wall, e.g. by using the analytical models presented by König (1988) or König and Källsner (1988).

In floors the joists are in bending and, since their lower side is exposed to fire, this side is in tension. The wide sides of the wood members are usually protected by mineral wool and the narrow sides by a lining.

The fire resistance of a load bearing structure is dependent on the magnitude of the load acting upon the structure. One of the goals was therefore to establish relationships between fire resistance and load capacity in fire. Since the buckling failure load of a stud is dependent on the flexural stiffness and the location of the centre of gravity of the residual section, it was also important to determine changes in these parameters during the tests.

In fire tests the applied load is normally held constant until failure. Since the effective cross section is decreasing during the test, strains and stresses increase initially at a very slow and approximately constant rate. In the stage close to failure do these rates accelerate. This can be seen from the relationships between deflection and time. See e.g. figure 2.8b. In design by testing the determination of load capacity for a specific fire resistance could be facilitated by increasing the applied loading during the fire test. Thus, in order to investigate the influence of the loading rate, in two of the test series the load was increased during the last stage before failure.

Some of the test results have been published before termination of the whole test programme, see König and Norén (1991) and König (1991). In the latter different ways of modelling are also discussed. In the view of the new findings made during the progress of the work, some of the conclusions in these papers had to be revised. This was necessary with respect to the influence of density on charring and the effective fire protection which can be obtained by the use of a cladding of gypsum plasterboard. Some of the results have been presented by Östman et al. (1994)

2 FIRE TESTING OF MEMBERS

2.1 MATERIALS

In Swedish timber frame housing load bearing members of solid timber normally have dimensions between 45 mm H 95 mm and 45 mm H 220 mm. Members of three different dimensions were included in this investigation. Their width was 45 mm and their depth 95, 145 and 195 mm respectively. All specimens were of spruce (picea abies).

The timber chosen was fairly free from knots. The reason was that this type of material would give test results with smaller scatter than is normal in tests with timber with large knots, and would allow a better prediction of the load bearing capacity at normal temperature. It has been shown by Norén (1988) that the fire resistance of timber members is fairly independent of the existence of knots, with a slight tendency for timber with knots to exhibit longer failure times. Since this influence is very small experimental investigations can be made using more homogeneous material.

All specimens were conditioned in a controlled climate chamber at 20 °C and 65% RH. The resulting moisture content was about 14%. The range of dry density was between 324 and 509 kg/m^3. The dry density was determined by weighting the members and dividing the weight by their volume. The moisture content was determined from small specimens taken from the same pieces of timber prior to the manufacturing of the test specimens. The material data of each specimen in the fire tests is given Appendix D.

The insulation material used was rock fibre manufactured by Rockwool AB, Sweden, Type 1331-00 with a nominal density of 30 kg/m^3 and a nominal thermal conductivity of 0,040 W/mK. The board material used was gypsum plasterboard of type A according to prEN 520 from AB Gyproc, Sweden, with a thickness of 12,5 mm and a weight of 9 kg/m^2. The boards were attached to the wood member using self-drilling screws with a length of 41 mm and a nominal diameter of 3,9 mm.

2.2 REFERENCE TESTS AT NORMAL TEMPERATURE

Reference tests were made at normal temperature conditions, with the aim that the load bearing capacity of each test specimen of the fire tests should be predicted.

The bending strength was determined in short-term tests according to EN 408. The test specimens with a span of 18 times the depth were symmetrically loaded at two points, the distance of the inner load points was 6 times the depth. The test results are presented as bending strength versus dry density in figure 2.1. A regression analysis was performed where a linear expression with intercept equal to zero was chosen to fit the results. A complete list of the test results is given Appendix A.

2.3 TEST PROGRAMME AND SPECIMENS

The test specimens should represent the thermal conditions of two typical applications - in the first case an insulated exterior timber frame wall exposed to fire on the inner side, and in the second case an insulated timber joist floor exposed to fire on its lower side. The test specimens consisted of the timber member, mineral wool protecting its sides from fire, and attached strips

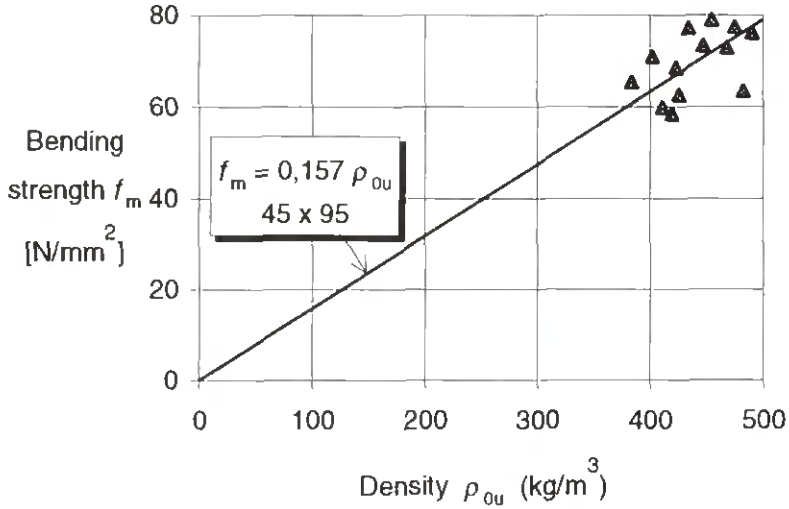

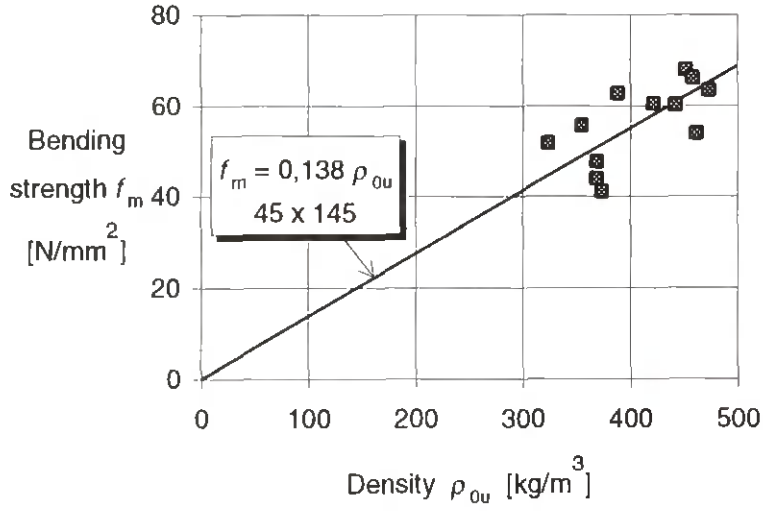

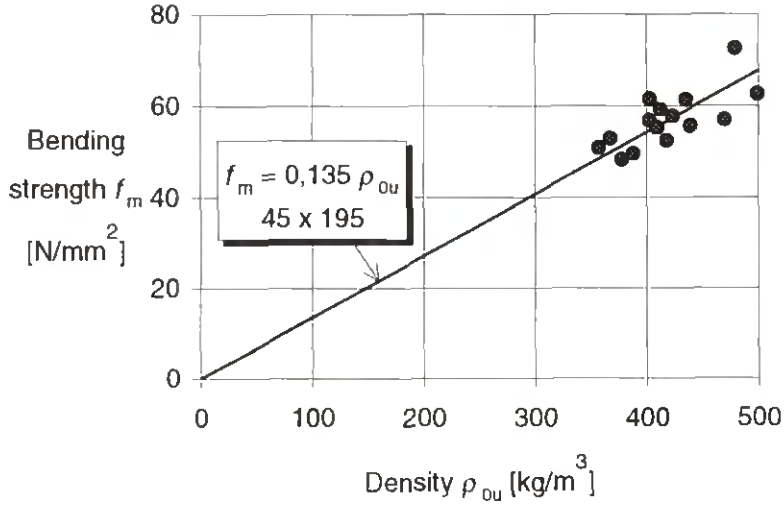

Figure 2.1: Bending strength versus dry density - reference tests series R1 - R3

of gypsum plasterboard on the non fire-exposed side. In series S2, in addition a piece of plasterboard was attached to the fire exposed side of the member. See figure 2.2. The area exposed to fire was 0,6 m H 1,0 m, with the width of 0,6 m representing the distance between the wall studs.

By using strips of board in transversal direction to the span on the unexposed side of the member, composite action was eliminated. In practical applications composite action may

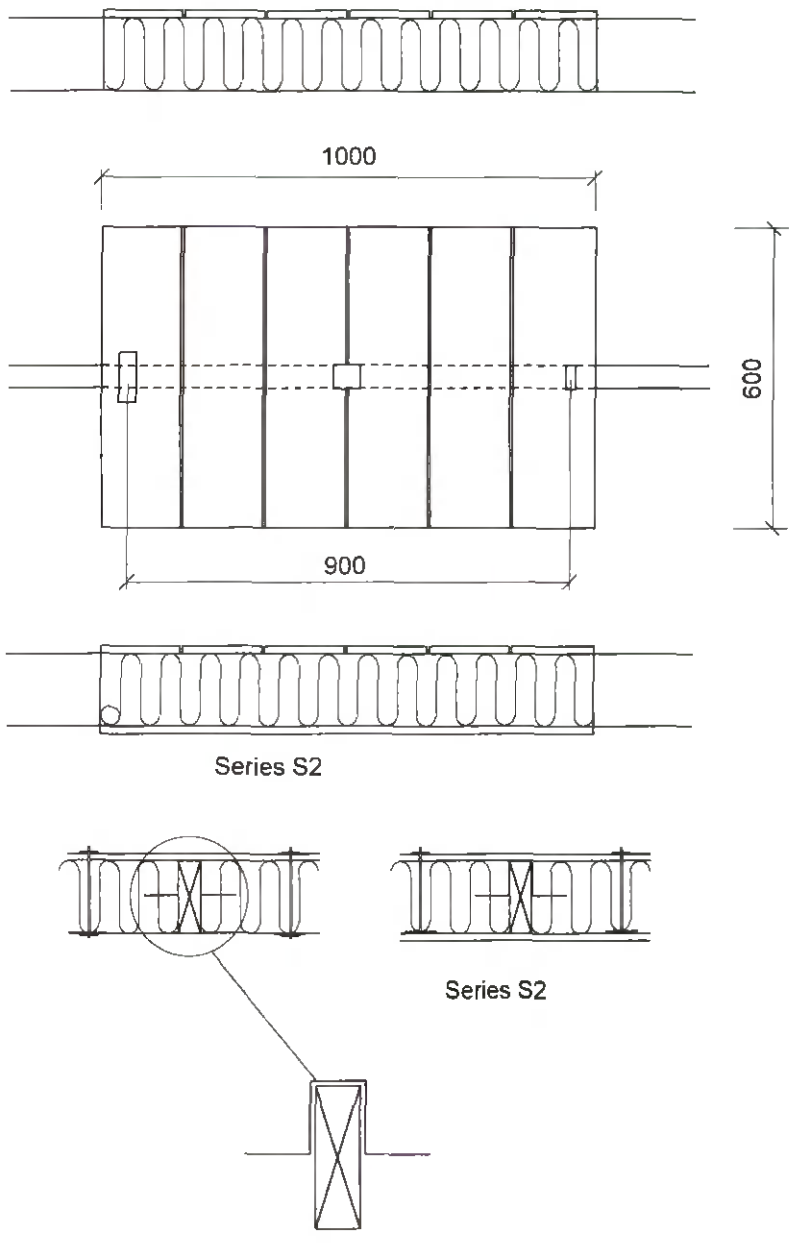

Figure 2.2: Specimen consisting of the member, mineral wool bats and gypsum plasterboard

contribute to a considerable degree to the load bearing capacity of a wall or a floor. This effect can easily be added in the analytical model, allowing for taking into account the beneficial effect of a wide variety of boards and ways of attaching these to the timber member. The mineral wool bats were tied against the member and suspended from the plasterboard strips

attached to the upper side using 4 mm thick steel wires and plates. Furthermore steel sheet clips were used to hold the mineral wool blocks in its position. See figure 2.2.

In table 2.1 an overview of the test programme is given, showing member dimensions, state of stresses on the fire exposed side and further information considering protective cladding and loading procedure. In addition to the tests with external loading two pilot tests (series P) were performed without an exterior static load in order to measure the influence of thermal expansions on the strain and deflection measurements and further tests (series T) in order to make additional temperature measurements.

Table 2.1: Test programme

Test series No.	Dimensions of member $b \times d$ [mm × mm]	Number of tests	State of stress on fire exposed side	Further description
S1	45 × 145	12	Compression	
S1a	45 × 145	13	Compression	Increasing of load [a)]
S2	45 × 145	9	Compression	12,5 mm gypsum plasterboard on fire-exposed side
S3	45 × 145	15	Tension	
S3a	45 × 145	13	Tension	Increasing of load [a)]
S4	45 × 95	12	Compression	
S5	45 × 95	15	Tension	
S6	45 × 195	12	Compression	
S7	45 × 195	12	Tension	
P	45 × 145	2	-	No external load
T	45 × 145	7	-	No external load

a) See 2.7.2.2

2.4 TESTING EQUIPMENT

A small gas-fired furnace with interior cladding of mineral wool was used in the fire tests. Its interior length was 1 m, and its width and depth were 0,6 m. The specimen was placed on two supports outside the furnace, forming a cover to the furnace. See figure 2.3.

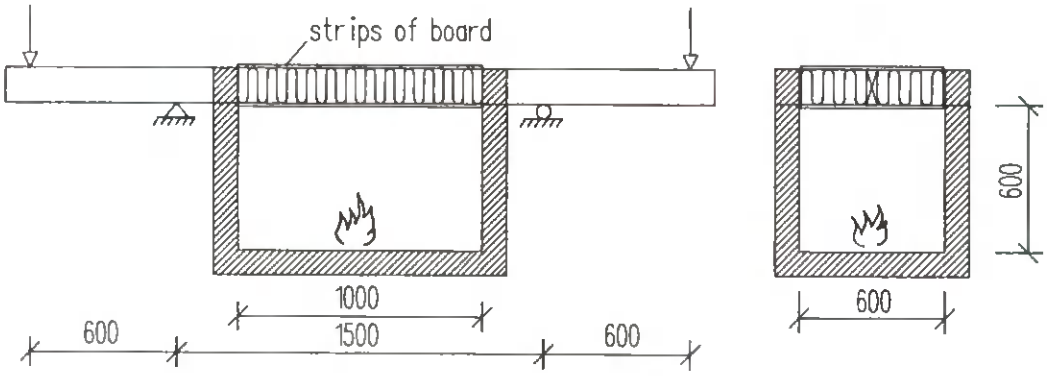

Figure 2.3: Testing equipment: Furnace and principle of loading

The sides of the specimen above the walls of the furnace were protected by insulated frames, which could be removed in order to facilitate the application of the specimen. The load was applied at the ends of the member by means of hydraulic jacks with reversible load directions. A thermocouple for registration of the furnace temperature was located in the middle of the furnace 100 mm below the lower side of the test specimen.

In order to determine the position of the neutral axis of the member during the different stages of the tests, the deflection and strain of the cold side of the member was recorded over the gauge length of 900 mm by means of a device which was attached to the timber member. See figure 2.4.

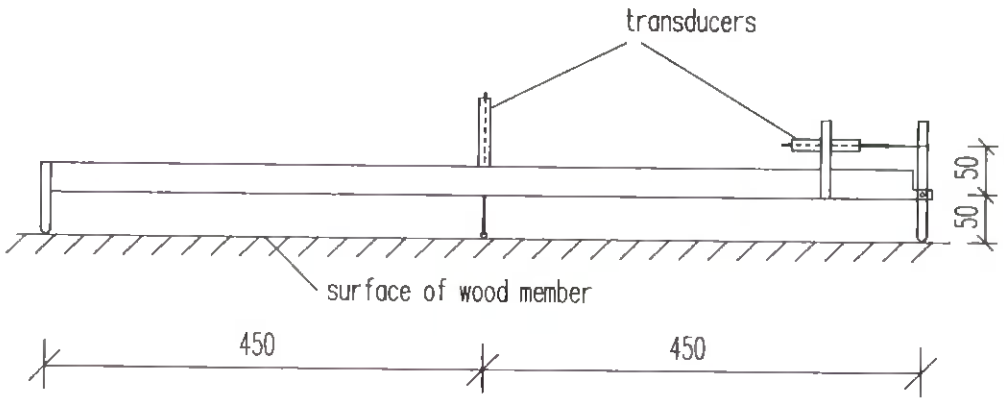

Figure 2.4: Testing equipment: Principle of device for measuring deflection and strain on the upper side of the specimen

2.5 LOCATION OF THERMOCOUPLES

All thermocouples were of chromel-alumel, type K. In series S1 to S6 and T they were attached along the vertical centre line of the cross section at different sections at equal distances of 100 mm in the longitudinal direction of the member. See figure 2.5. The holes for the wire were drilled from and perpendicular to the wide side of the member. In test series S1-S3 two alternative configurations were used. The temperature was recorded in five of the specimens of test series 1 and in all specimens of test series S2 and S3. In test series S4

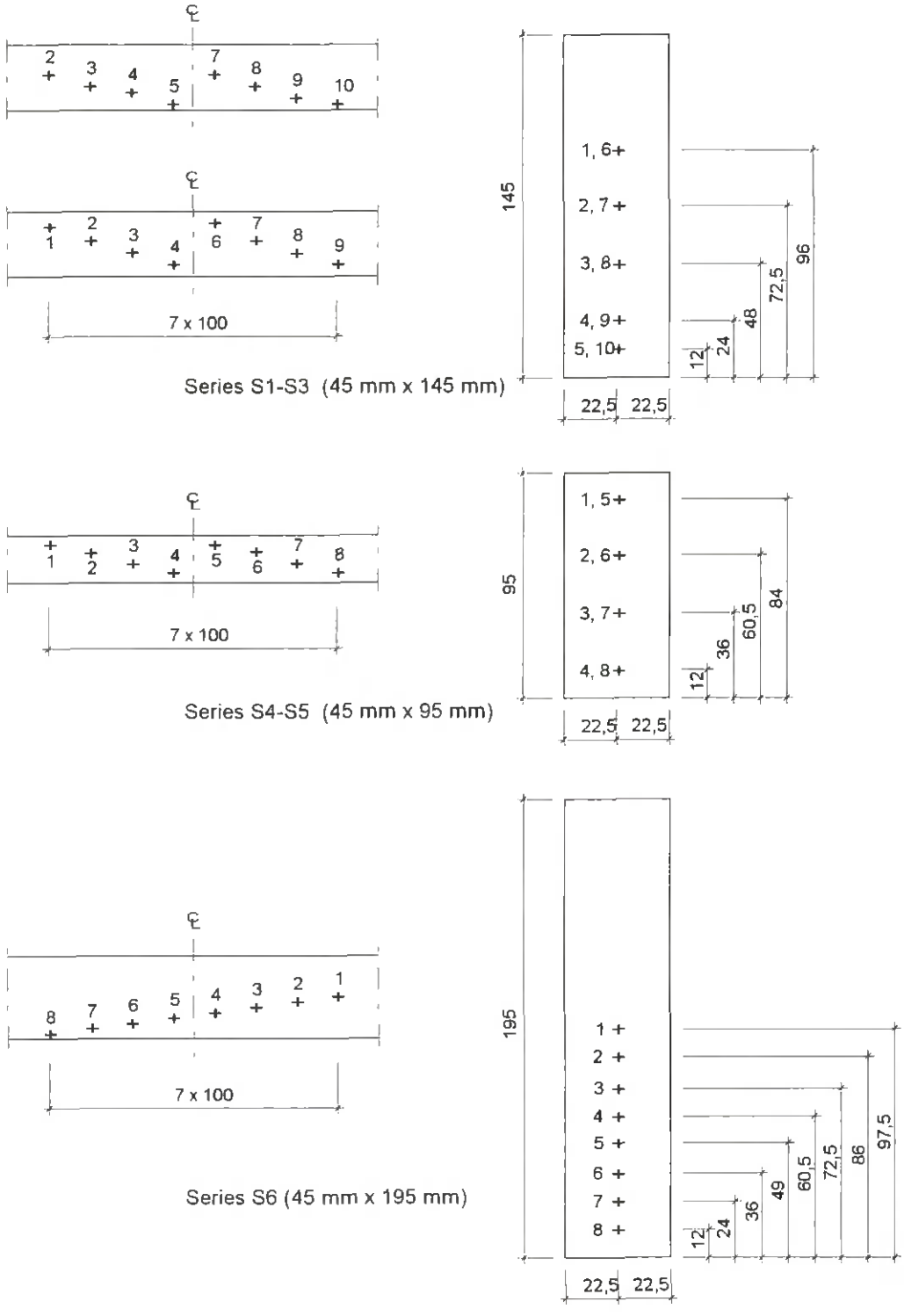

Figure 2.5: Position of thermocouples in series S1-S6

temperature measurements were made in eight of fourteen and in series S5 in all specimens except one where the temperatures could not be recorded due to a defect in the measuring equipment. In series S6 temperature measurements were made in three of eight and in series 7 in none of the specimens.

In specimens 1A, 37A and 37B of test series T the thermocouples were located as shown in figure 2.6. In specimens N1 and F1-F3 the thermocouples were located on the surface of the narrow side and at distances of 12, 24, 36, 48, 60 and 72,5 mm from the edge, similar to series S6.

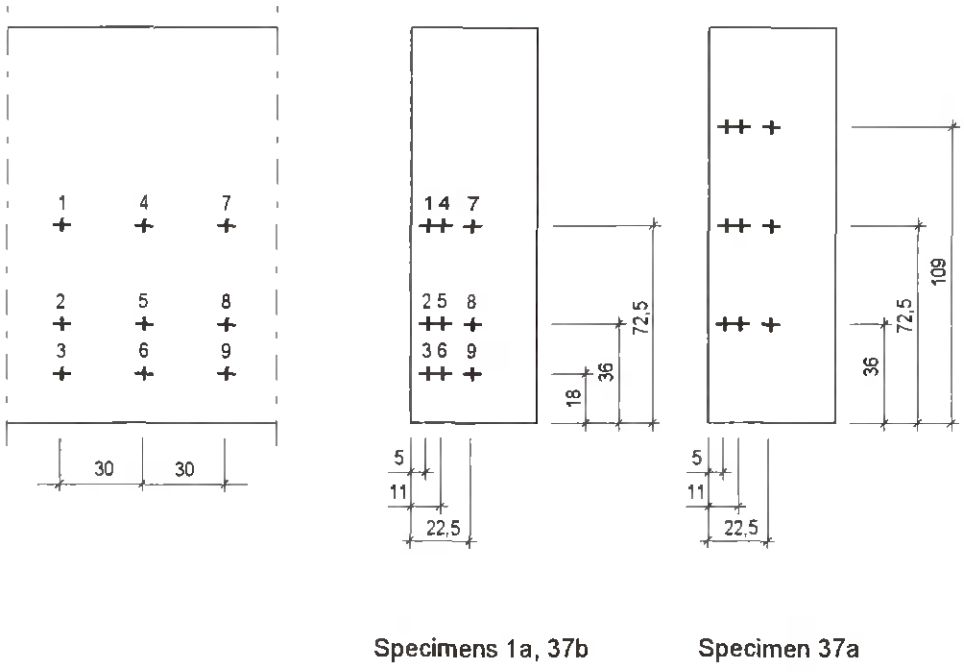

Figure 2.6: Position of thermocouples specimens 1A, 37A and 37B of series T

2.6 TEST PROCEDURE

For each specimen the bending strength was predicted for normal temperature conditions, using the regression lines given in Tables A1 - A3 in Appendix A. For the fire tests a relative load level was chosen in the range between 10 and about 80 percent of the load bearing capacity at normal temperature.

After application of the load, the fire exposure was started and the temperature in the furnace was increased following the standard fire temperature-time curve according to ISO 834. The recorded temperature-time curves during the tests are shown in Appendix B, figures B.1a-i. The load was held constant until failure occurred. The definition of failure was that the load could not be held constant any longer due to collapse or extensive deformations.

In test series 2 the fire-exposed side was protected by a single layer of gypsum plasterboard. In order to determine the flexural stiffness of the members, prior to these fire tests the specimens were loaded without the fire protective board and the deflections and loading were recorded. After unloading the specimen the layer of gypsum plasterboard was attached and the ensuing test procedure was the same as described above.

In test series 1a and 3a the load was constant or zero during the major part of the fire test. In the final stage of the fire test the load was increased until failure at a rate of approximately 25 percent of the load capacity at normal temperature per minute. In these cases the initial constant relative load level was in the range between 0 and 25 percent. The purpose of these tests was to investigate whether the failure load level is influenced by the load rate during the fire test.

After failure the gas burner was immediately turned off, the specimen removed and the fire in the member was extinguished with water. From each specimen five approximately 10 mm thick slices were cut out at approximately equal distances along the charred part of the member. The charcoal was removed and the pieces put back into the climate chamber in order to be re-conditioned. Then the shape of the residual cross section was recorded by means of a digitizer. Some typical residual cross sections are shown in appendix C.

2.7 RESULTS

2.7.1 THERMAL EXPANSIONS

Two tests were performed (series P). The purpose of these tests was to investigate whether the curvature of the members was influenced by the temperature gradient during the fire tests. Such influence could have consequences on the determination of the position of the neutral axis by means of the device shown in figure 2.4. The results are shown in figure 2.7. Specimen P211 was exposed to fire during about 50 minutes. During this time period the maximum deflection v of the member within the gauge length was about 0,5 mm and the maximum thermal expansion u on the cold side of the member was about 0,1 mm. The results of test specimen P243 were of the same order of magnitude. Since these displacements are very small in comparison with the displacements in the tests with static loading, the effect of thermal expansions can be neglected in the evaluation of the tests.

2.7.2 MECHANICAL PROPERTIES

2.7.2.1 Members with unprotected narrow side

Load ratio and time to failure. For each of the test series S1 and S3 to S7 the relationship is determined between time to failure t_u and the load ratio, i.e. the ratio of the ultimate load at failure in the fire test and the predicted load bearing capacity at normal temperature. See figures 2.8a-2.13a where the results are shown together with exponential regression curves determined according to two different assumptions. In the first case a linear regression analysis was performed using the equation

$$\ln \eta = A + Bt_u \quad [\text{min.}] \tag{2.1}$$

Since it is evident that the load ratio is unity for t_u equal to zero, as an alternative a linear regression analysis was performed using the equation

$$\ln \eta = Bt_u \quad [\text{min.}] \tag{2.2}$$

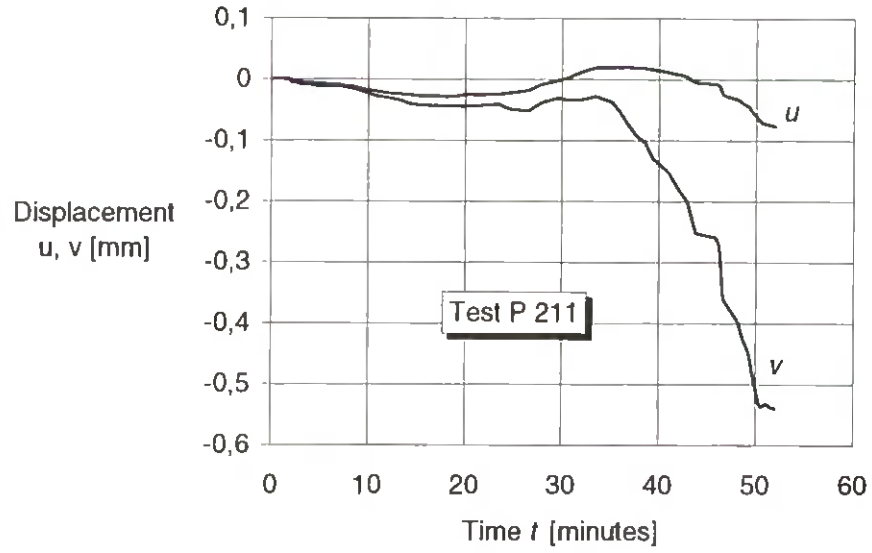

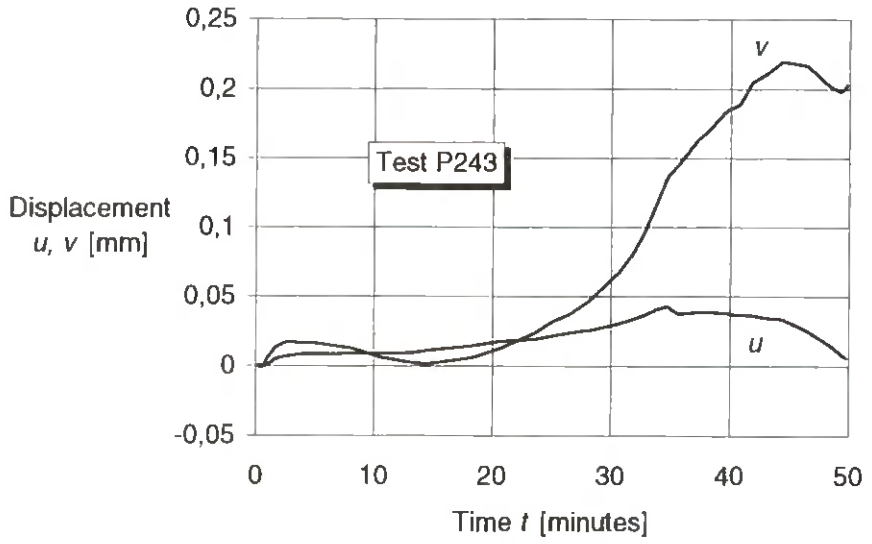

Figure 2.7: Pilot tests: Deflection and displacement on the upper side of the specimen

In these equations

$$\eta = \frac{M_f}{M_0} \tag{2.3}$$

where

M_f Bending moment in fire test
M_0 Predicted bending moment capacity at normal temperature

Complete sets of data of the specimens are given in appendix D, tables D1 to D6, while the parameters of the regression equations are given in table 2.2. To facilitate the values of standard deviation of regression have been included, which are defined by

Table 2.2: Parameters in regression equations (2.1) and (2.2) and standard deviations *s* of regression

Test series No.	Regression equation (2.1)			Regression equation (2.2)	
	A	*B*	*s*	*B*	*s*
S1	0,00285	-0,04904	0,03653	-0,04895	0,03490
S1a	-	-	-	-0,04428	0,06522
S2	0,97702	-0,05545	0,05582	-	-
S3	0,11759	-0,04217	0,09239	-0,03868	0,08763
S3a	-	-	-	-0,03972	0,06318
S4	0,14815	-0,07413	0,05664	-0,06775	0,05115
S5	0,27690	-0,07697	0,07947	-0,06509	0,07731
S6	-0,05522	-0,03230	0,05703	-0,03358	0,05612
S7	0,50479	-0,04610	0,05410	-0,03451	0,05619

$$\hat{\sigma} = \sqrt{\frac{\Sigma(\eta - \hat{\eta})^2}{n - a}} \tag{2.4}$$

where a is the number of parameters in the regression equations (2.1) and (2.2), and η and $\hat{\eta}$ are the test values of load ratios of the individual specimens and the load ratios predicted by the regression equations respectively.

Generally, we can see that time to failure increases when the load ratio is decreasing. Comparing the results of series S1 with those of series S3, we can see that there also exists an influence of the state of stress, i.e. whether the fire-exposed side is in compression or tension. When the fire-exposed side is in compression the slopes of the regression curves are greater than in the case of tension, i.e. the load ratio is reduced more when the fire-exposed side is in compression. In series S4 and S5, as well as in series S6 and S7 the state of stress does not seem to have an influence on the load ratio at failure.

Deflections. The recorded mid-deflections during the fire exposure refer to a gauge length of 900 mm. See figures 2.8b to 2.13b. Generally, we can see that lower load ratios give rise to greater deflections at failure and failure modes with increasing ductility. Moreover, specimens with the fire-exposed side in compression perform failure modes with greater ductility than in the case of tensile stresses on the fire-exposed side.

Flexural stiffness. The variation of the stiffness ratio, during the tests is shown in figures 2.8c to 2.13c where the stiffness ratio is defined as the ratio of the flexural stiffness and its initial value at normal temperature $(EI)_f/(EI)_0$. The flexural stiffnesses $(EI)_f$ and $(EI)_0$ were calculated assuming a constant curvature within the gauge length.

Comparing the diagrams in figures 2.8c and 2.9c we can see that the decrease of the flexural stiffness during the fire tests is dependent on the load ratio and the state of stress on the fire-exposed side. When the fire exposed side is in compression the rate of decrease of stiffness is dependant on the relative load level. For specimens with load ratios below about 0,30 the

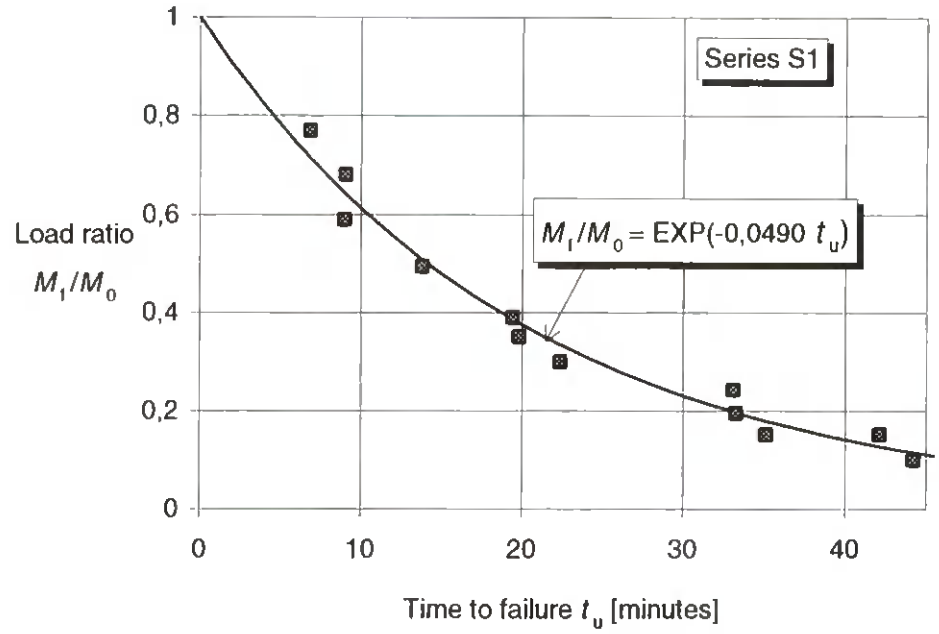

a)

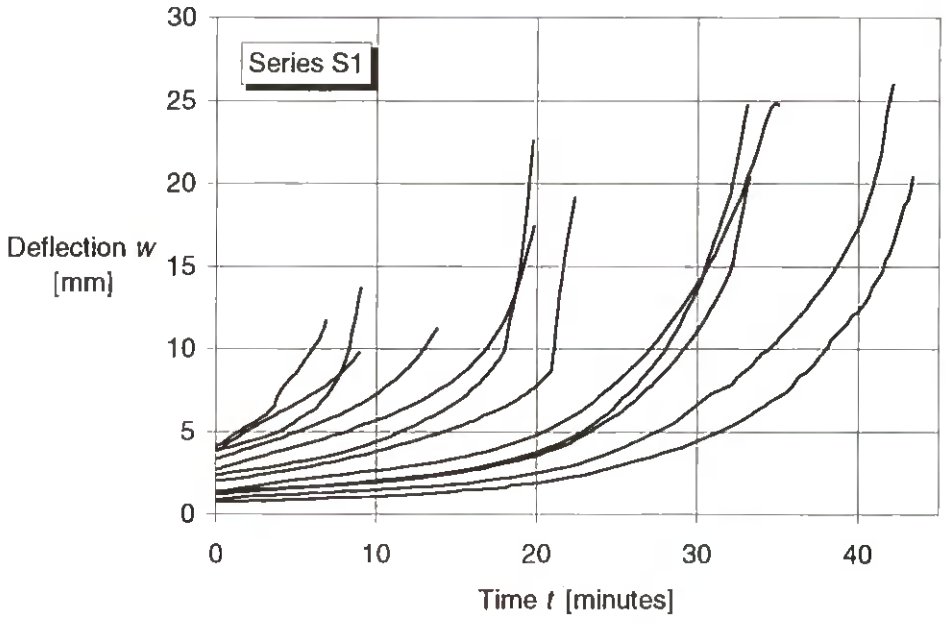

b)

Figure 2.8a-b : Test results of series S1 - Mechanical properties
a) Load ratio versus time of failure
b) Mid-deflection versus time

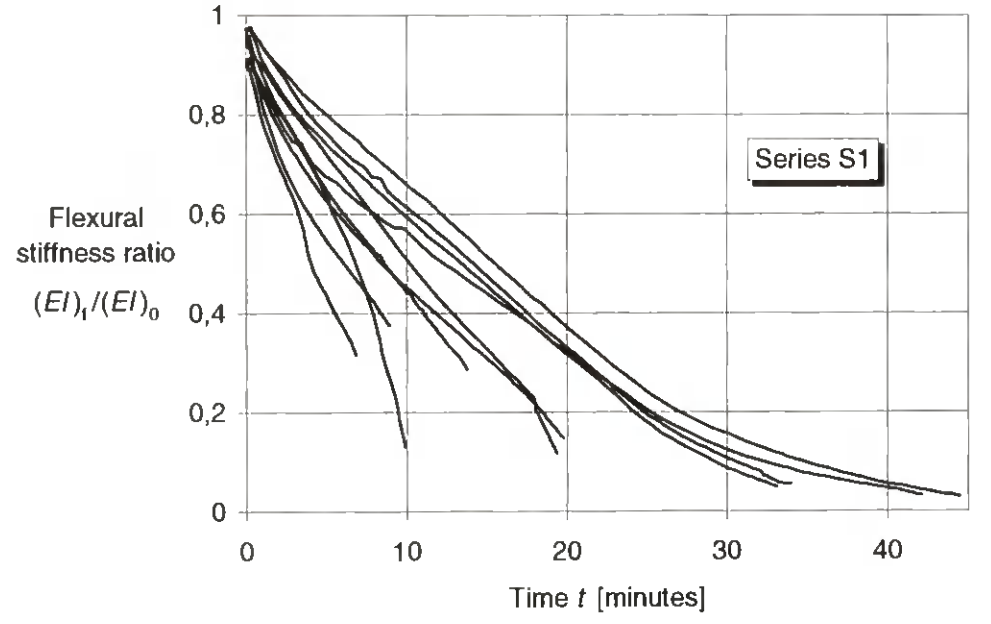

c)

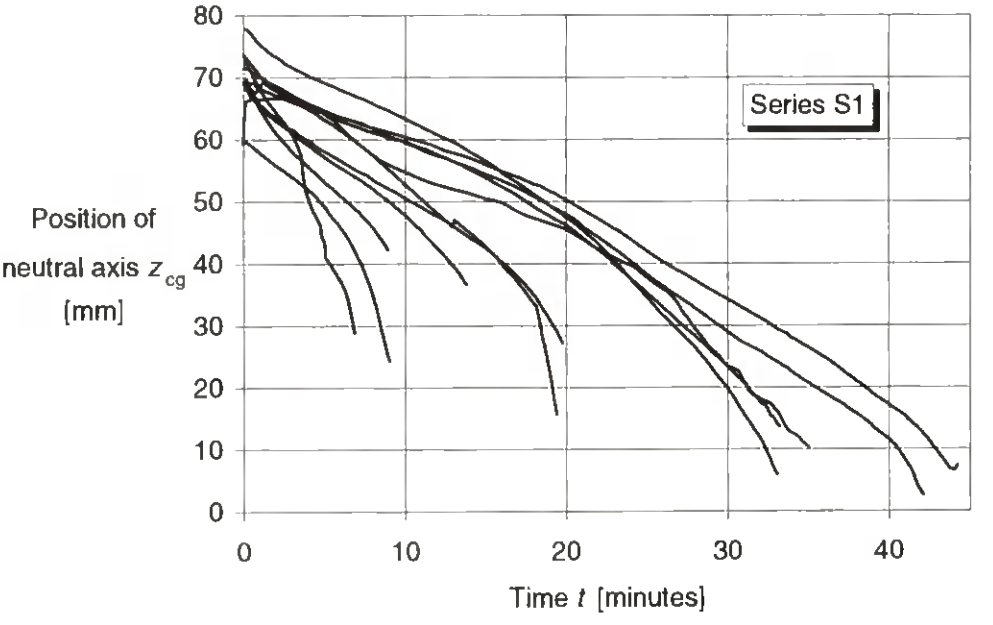

d)

Figure 2.8c-d: Test results of series S1 - Mechanical properties
c) Flexural stiffness ratio versus time
d) Position of neutral axis versus time

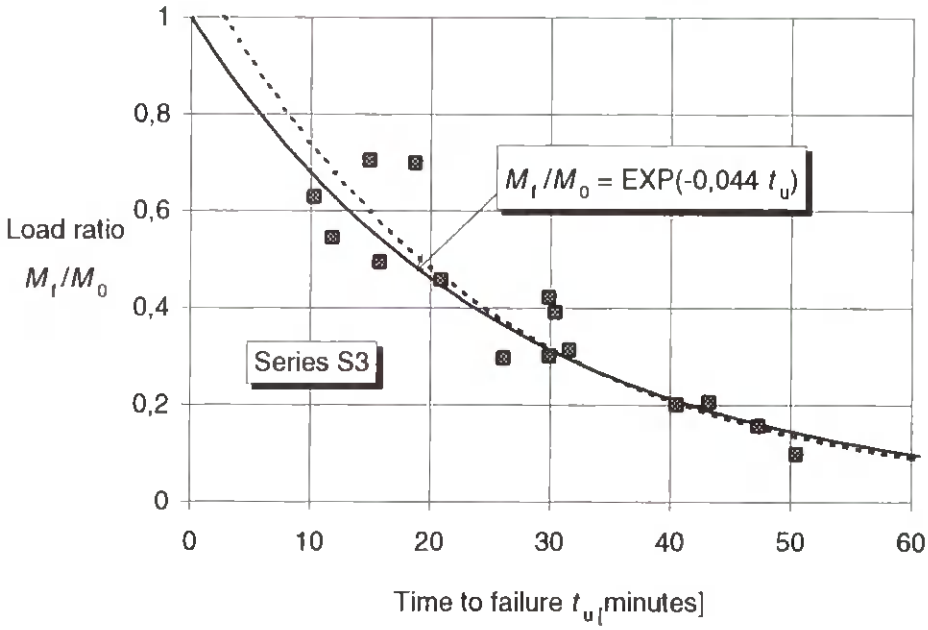

a)

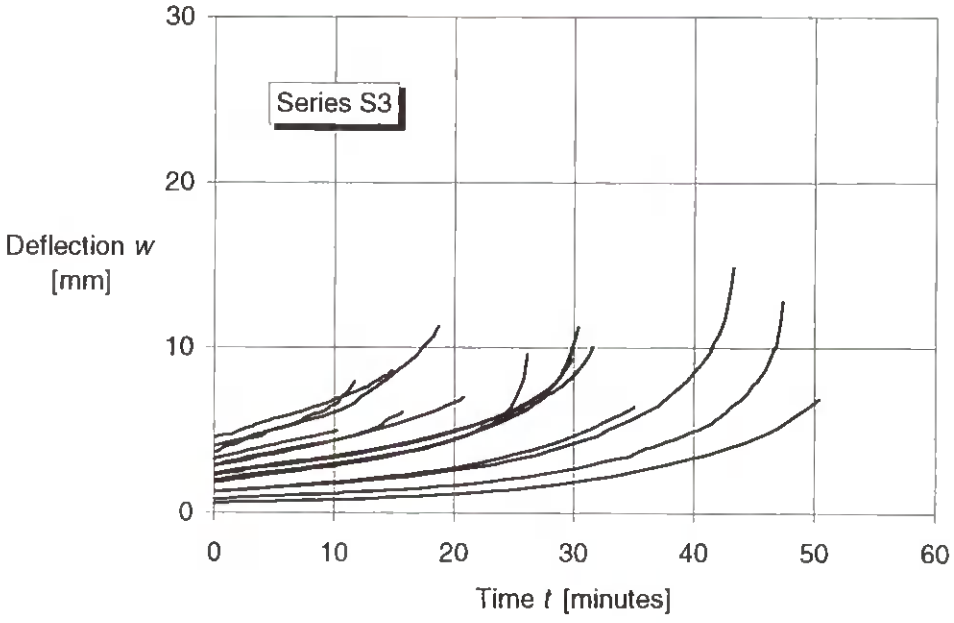

b)

Figure 2.9a-b: Test results of series S3 - Mechanical properties
a) Load ratio versus time of failure
b) Mid-deflection versus time

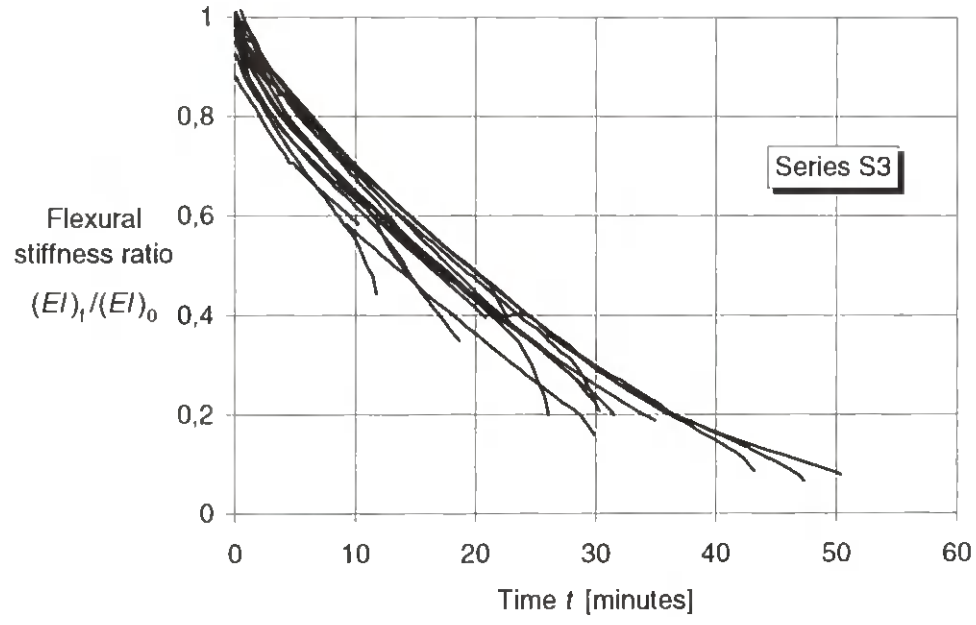

c)

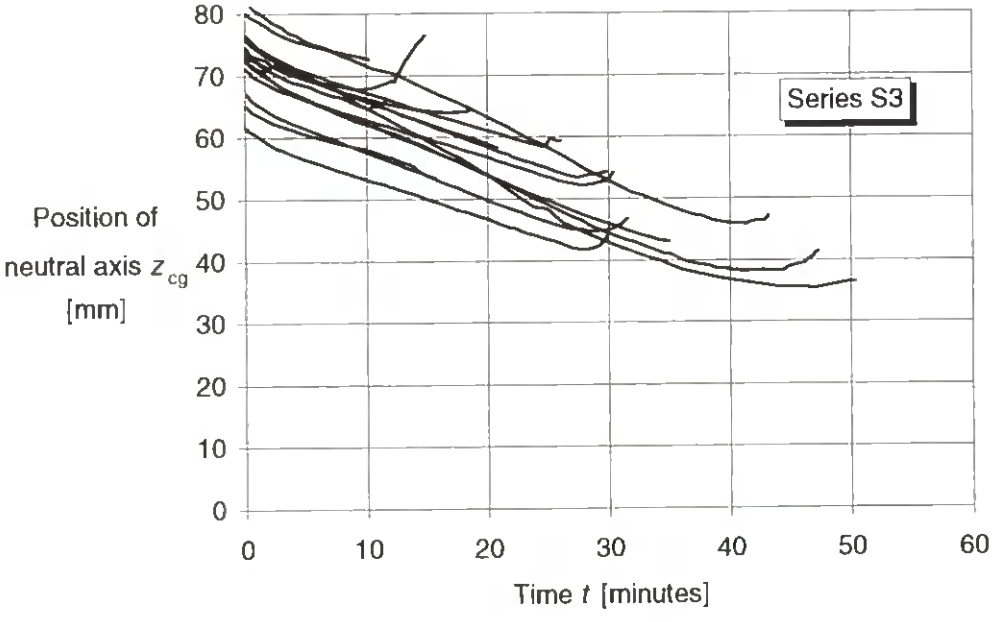

d)

Figure 2.9c-d : Test results of series S3 - Mechanical properties
c) Flexural stiffness ratio versus time
d) Position of neutral axis versus time

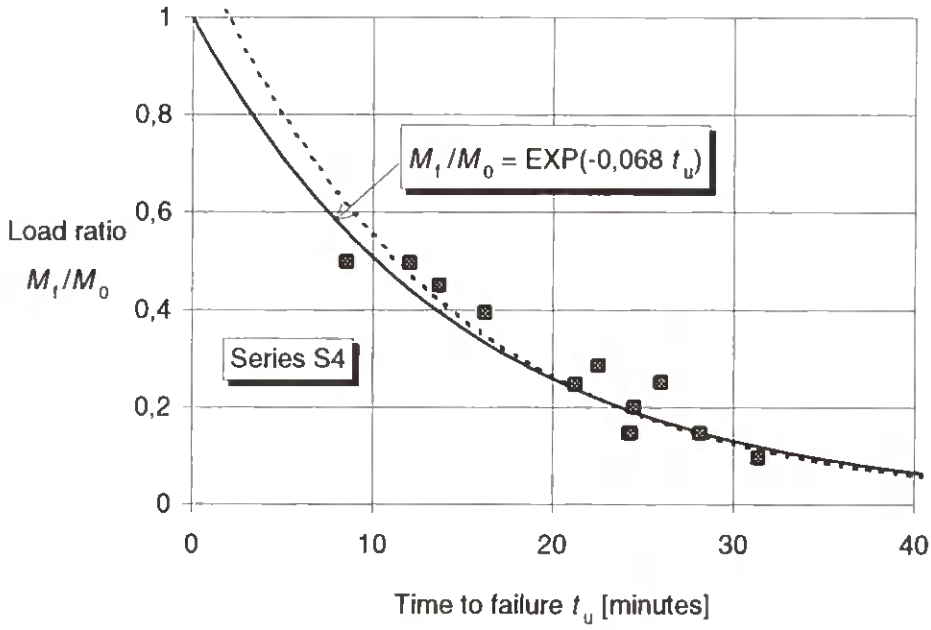

a)

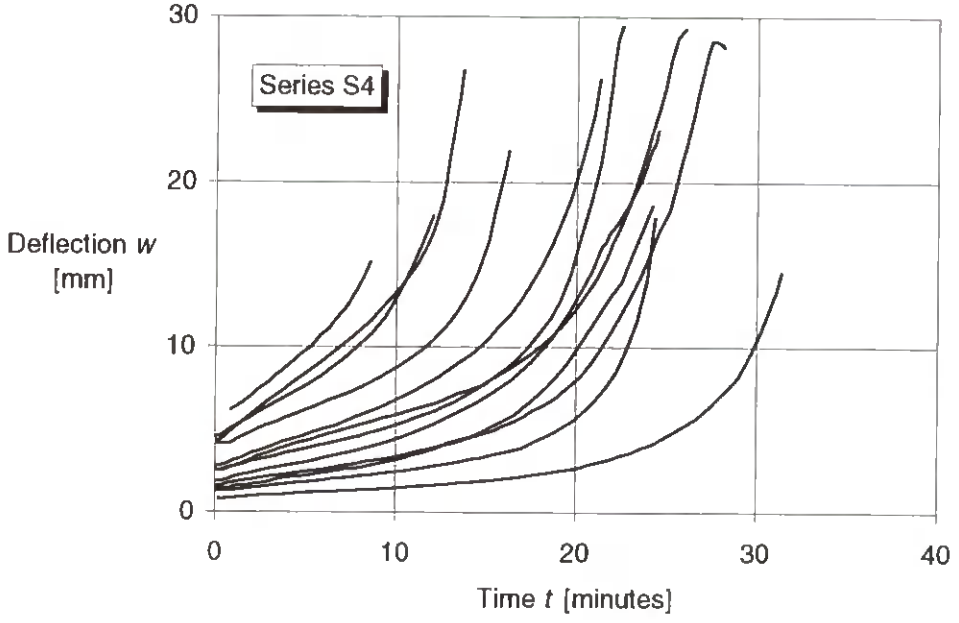

b)

Figure 2.10a-b: Test results of series S4 - Mechanical properties
a) Load ratio versus time of failure
b) Mid-deflection versus time

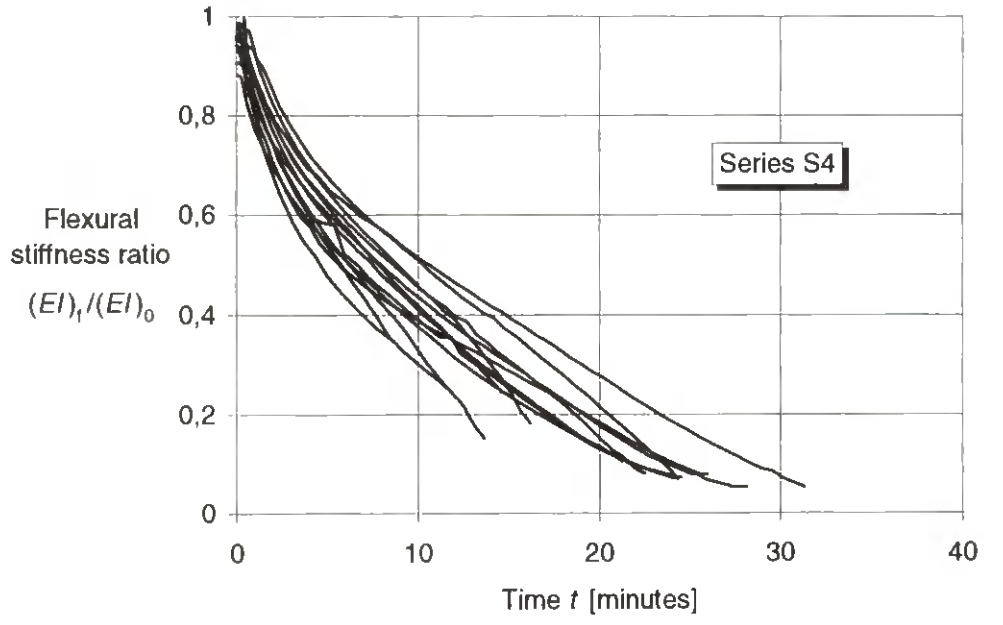

c)

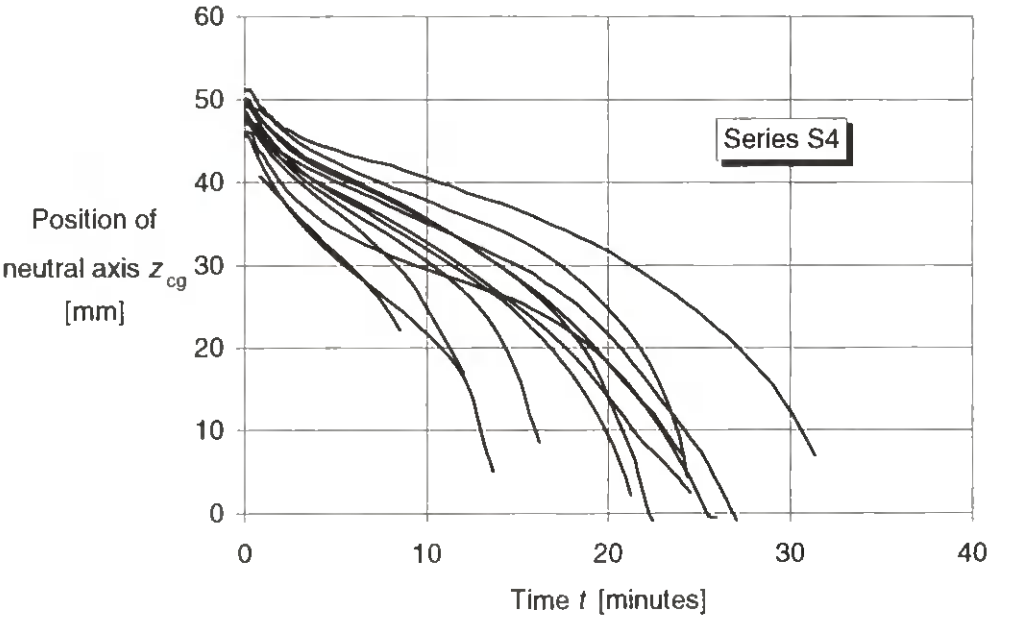

d)

Figure 2.10c-d: Test results of series S4 - Mechanical properties
c) Flexural stiffness ratio versus time
d) Position of neutral axis versus time

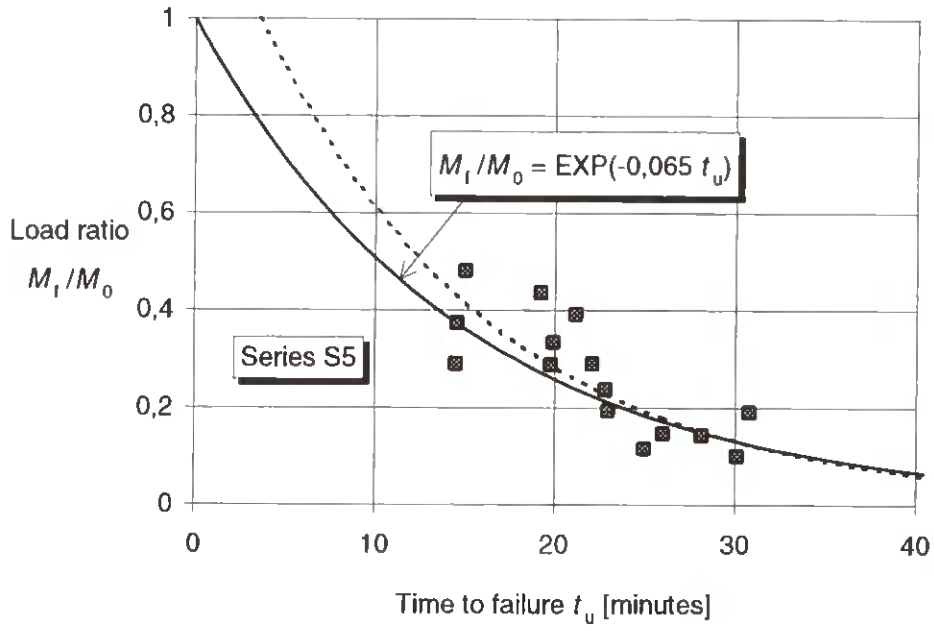

a)

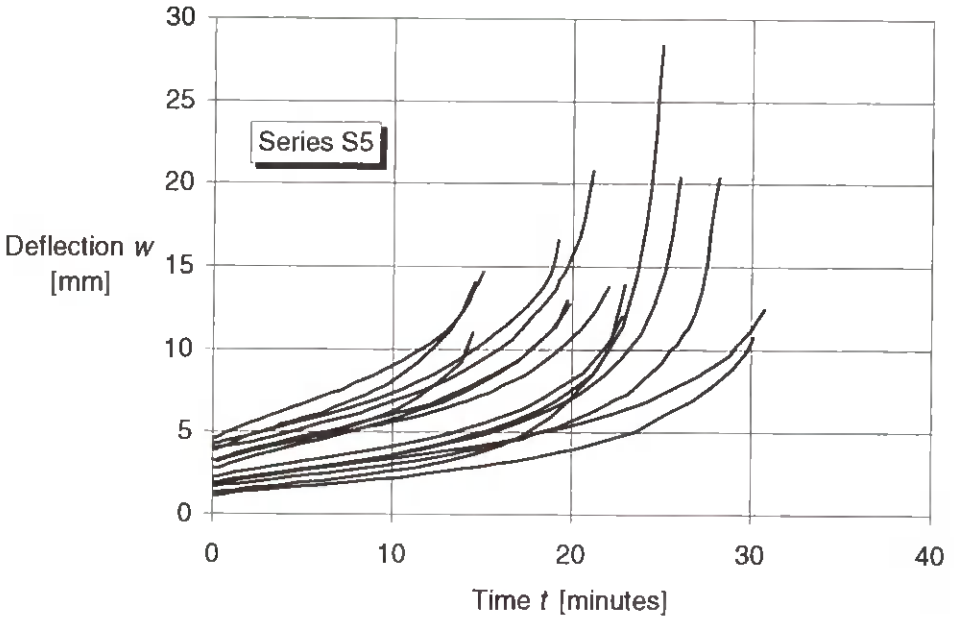

b)

Figure 2.11a-b: Test results of series S5 - Mechanical properties
a) Load ratio versus time of failure
b) Mid-deflection versus time

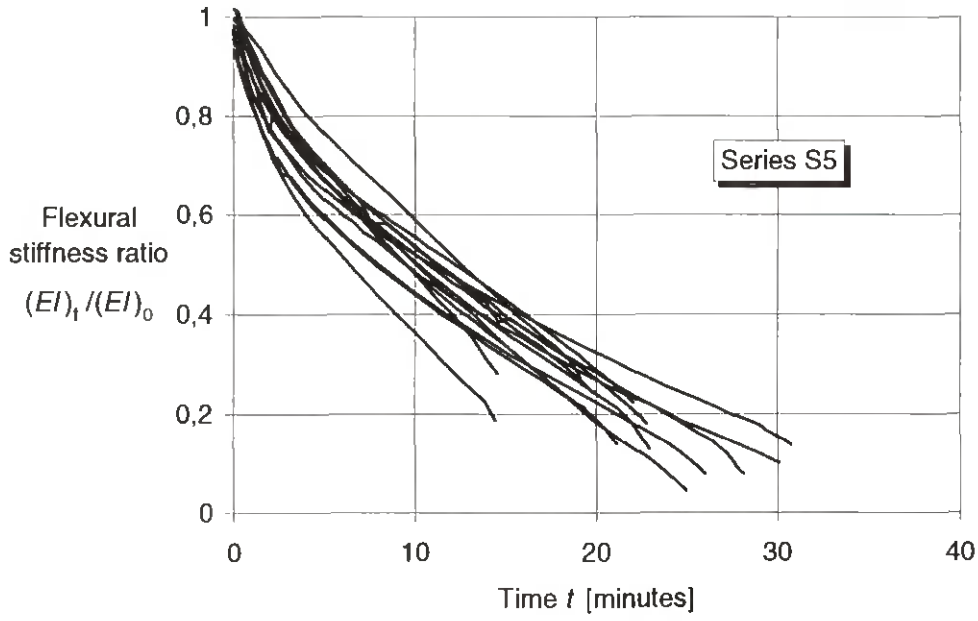

c)

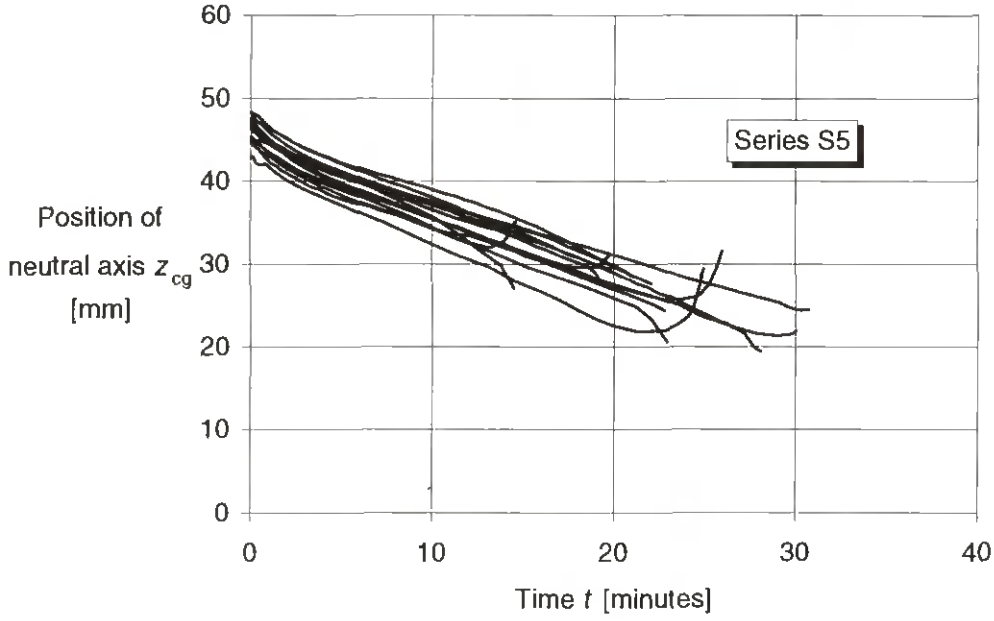

d)

Figure 2.11c-d: Test results of series S5 - Mechanical properties
c) Flexural stiffness ratio versus time
d) Position of neutral axis versus time

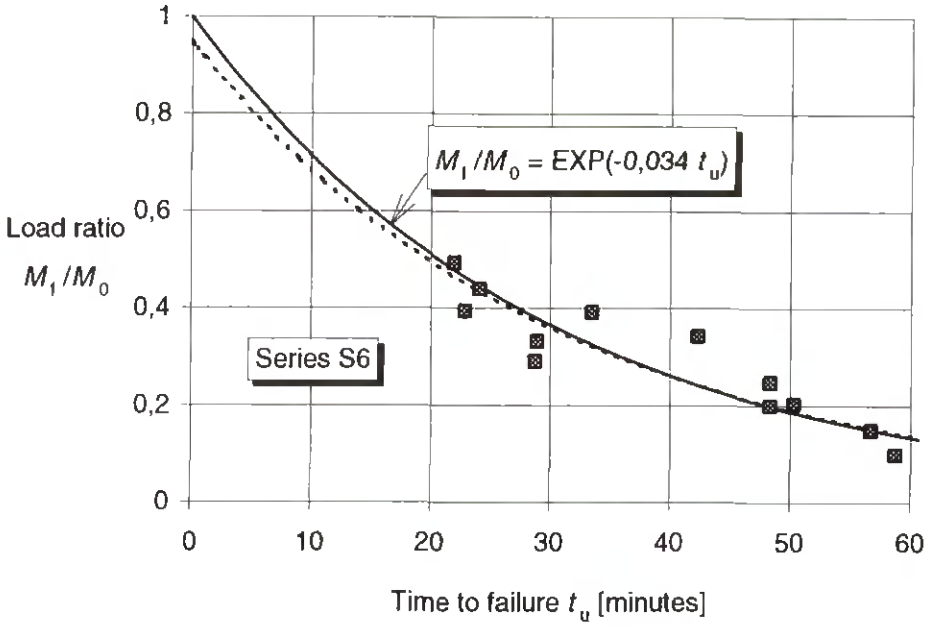

a)

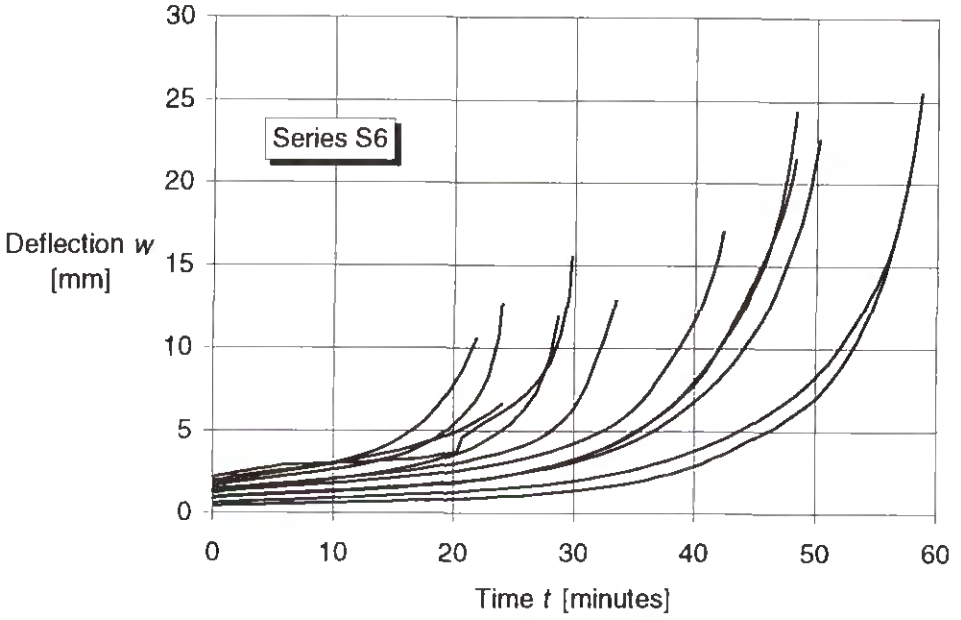

b)

Figure 2.12a-b: Test results of series S6 - Mechanical properties
a) Load ratio versus time of failure
b) Mid-deflection versus time

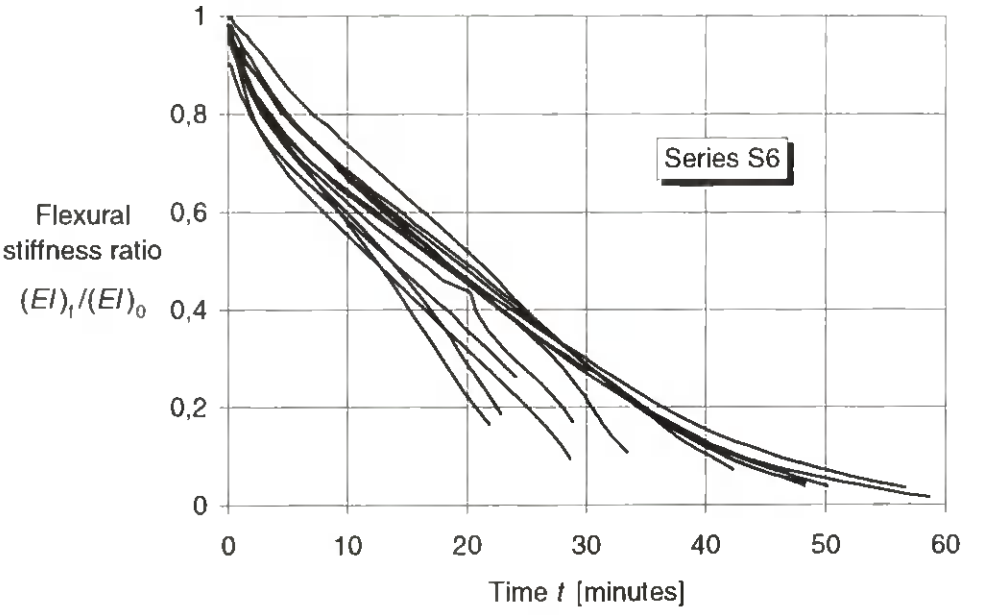

c)

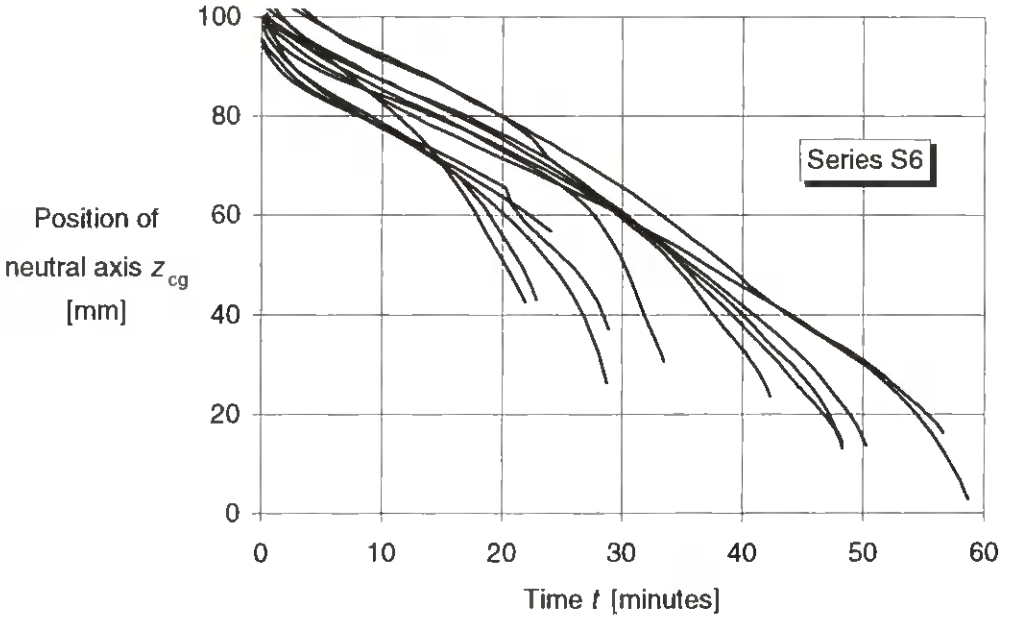

d)

Figure 2.12c-d: Test results of series S6 - Mechanical properties
c) Flexural stiffness ratio versus time
d) Position of neutral axis versus time

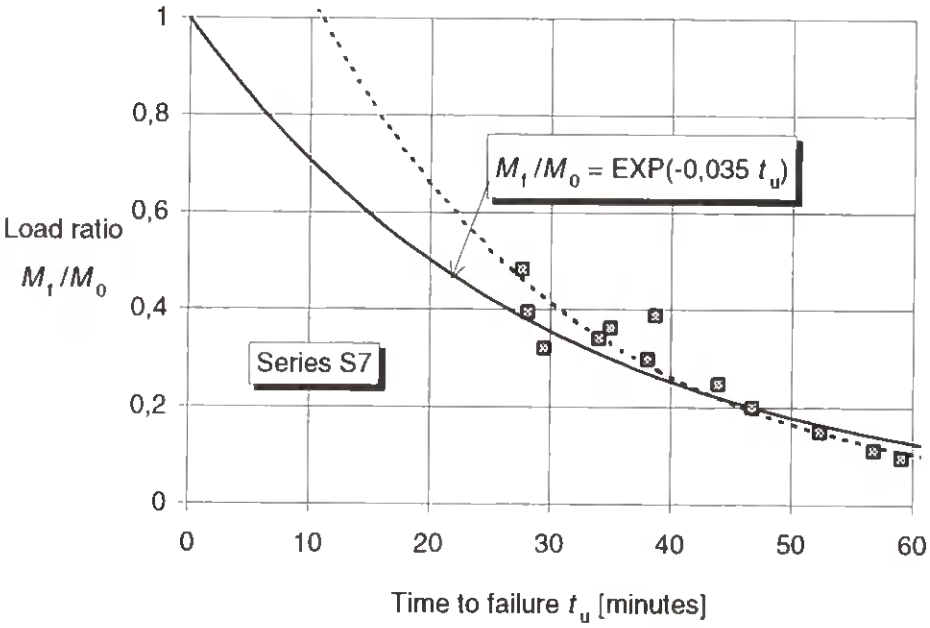

a)

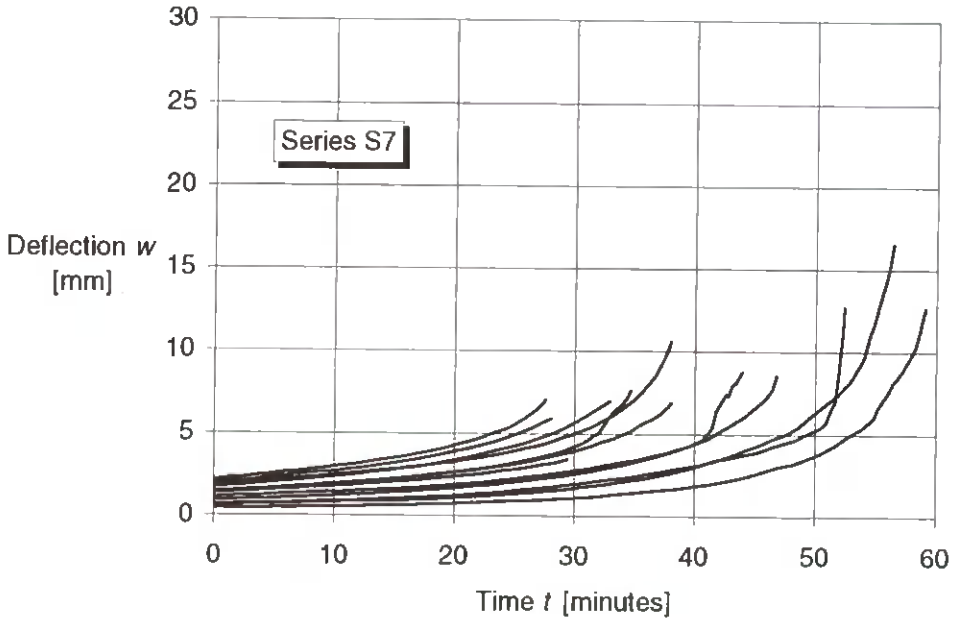

b)

Figure 2.13a-b: Test results of series S7 - Mechanical properties
a) Load ratio versus time of failure
b) Mid-deflection versus time

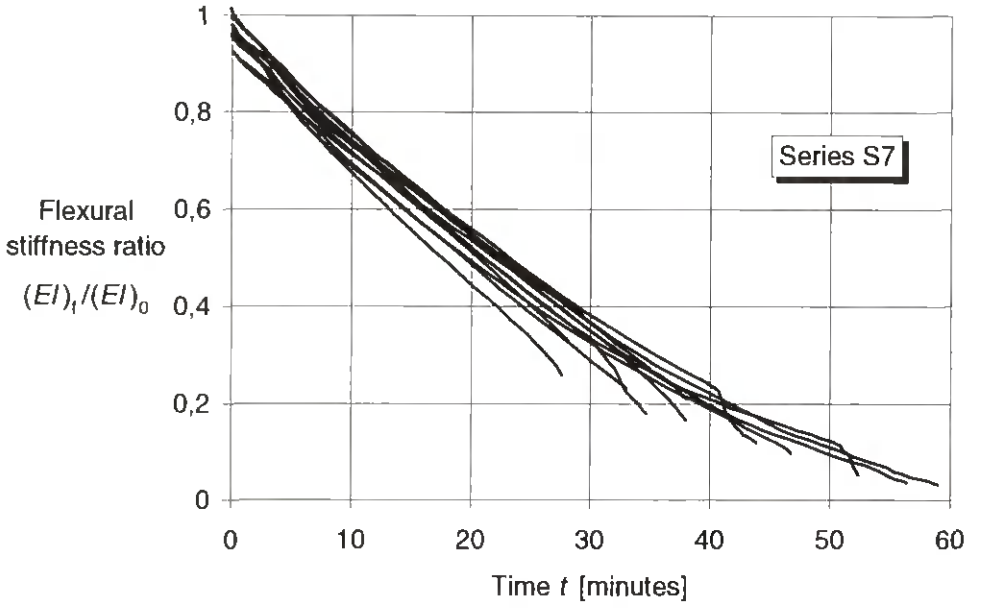

c)

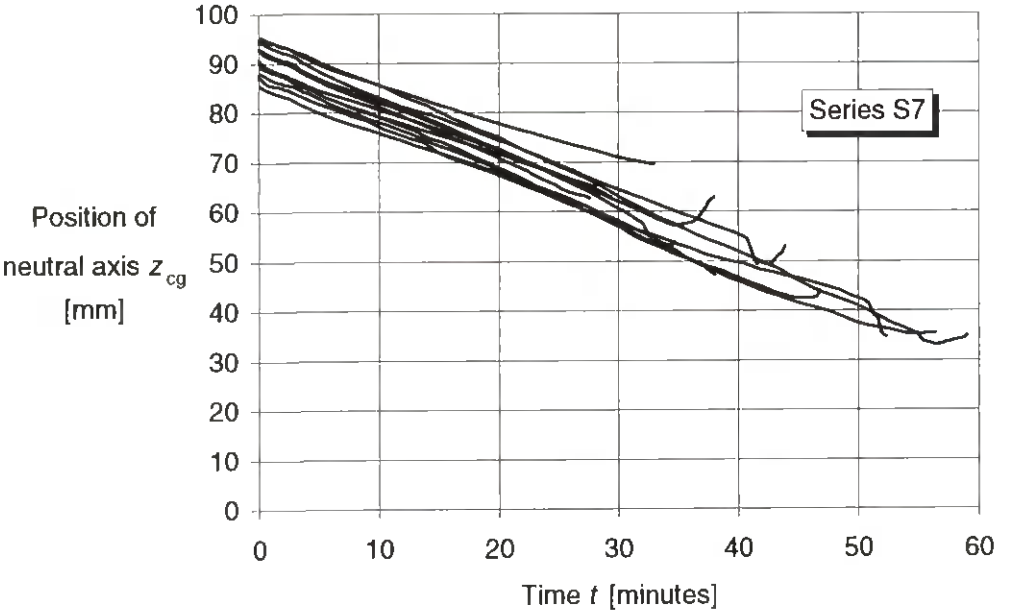

d)

Figure 2.13c-d: Test results of series S7 - Mechanical properties
c) Flexural stiffness ratio versus time
d) Position of neutral axis versus time

rate of stiffness reduction is apparently not influenced by the load ratio. When the fire-exposed side is in tension, firstly there exists no apparent influence of the load ratio, and secondly, the decrease of the stiffness ratio is smaller than in the case of compressive stresses on the fire-exposed side. See figure 2.9c. The same can be seen from figures 2.10c to 2.13c, even though not as clearly since in series S4 to S7 the range of load ratios was not as large.

High loading from the beginning results in large plastic deformations due to buckling failure of the grain of the wood on the compression side of the member. This effect is increased by the elevated temperature.

Position of neutral axis. Plots of the position of the neutral axis given as the distance from the upper unexposed side of the member are presented in figures 2.8d to 2.13d. The values were determined as the mean distance of the neutral axis from the upper unexposed edge of the member within the gauge length L_g. These curves were calculated using the recorded strain values u/L_g and deflections w. Assuming that strain varies linearly across the depth of the section, it can be shown that

$$z_{cg} = -\frac{L_g}{8w}\left[u - L_g + \frac{L_g^2}{4w}\ \arcsin\frac{4w}{L_g}\right] \tag{2.5}$$

The last two terms, which are put in brackets, take into account the shortening of the beam due to deflection.

There is a considerable influence of the state of stresses on the fire-exposed side. In series S1, S4 and S6 with the fire-exposed side in compression the position is also dependent on the load ratio. When the fire-exposed side is in compression, the displacement of the neutral axis is much greater than in beams with this side in tension. In series S1, S4 and S6, due to extensive plastic flow on the fire-exposed compression side, the upward motion of the neutral axis is accelerating near failure. In series S3, S5 and S7 due to plastic flow on the unexposed compression side finally the motion of the neutral axis stops and turns back downwards.

For comparison, in figure 2.14 is shown the displacement of the neutral axis during the stage of load application prior to the fire test for some specimens of series S1 and S3. We can see that the neutral axis is moving towards the edge of the member which is in tension right from the beginning. Since a member is not symmetric about its y-axis due to imperfections as e.g. knots, its neutral axis is normally not located in the middle of the depth of the member, which in these specimens was 72,5 mm from the upper edge.

2.7.2.2 The influence of loading rate - test series S1a and S3a

Load ratio and time to failure. For both series S1a and S3a the relationships between load ratio and time are shown in figures 2.15a and 2.16a, where the values at failure are shown as circles. For complete data see appendix D, tables 7 and 8. Linear regression analyses were performed using the one-parameter equation (2.2), see table 2.2. For comparison, in the figures the results are shown together with the corresponding results of series S1 and S3. We can see that in the case of series S3 and S3a the difference between the two regression curves is very small and statistically not significant. In the case of series S1 and S1a the load bearing capacity is greater when the load is increased prior to failure. By performing a two-sided hypothesis test it was found that the difference of the two regression curves is significant at the level of 5 %. The ratio of the load bearing capacities described by these two curves is

$$\frac{\hat{\eta}_{1a}}{\hat{\eta}_1} = e^{(B_{1a}-B_1)t_u} = 1{,}00468^{t_u} \qquad (2.6)$$

where t_u is in minutes. With t_u = 25 minutes for a load ratio of about 0,3 we get a ratio of 1,12, i.e. by increasing the load during the test the load bearing capacity is overestimated by 12 % when the time to failure is 25 minutes.

Comparing the results of series S1 and S3 with series S1a and S3a we can see that the increase of loading exerts a greater scatter when the fire-exposed side is in compression, c.f. the values of standard variation of regression in table 2.2.

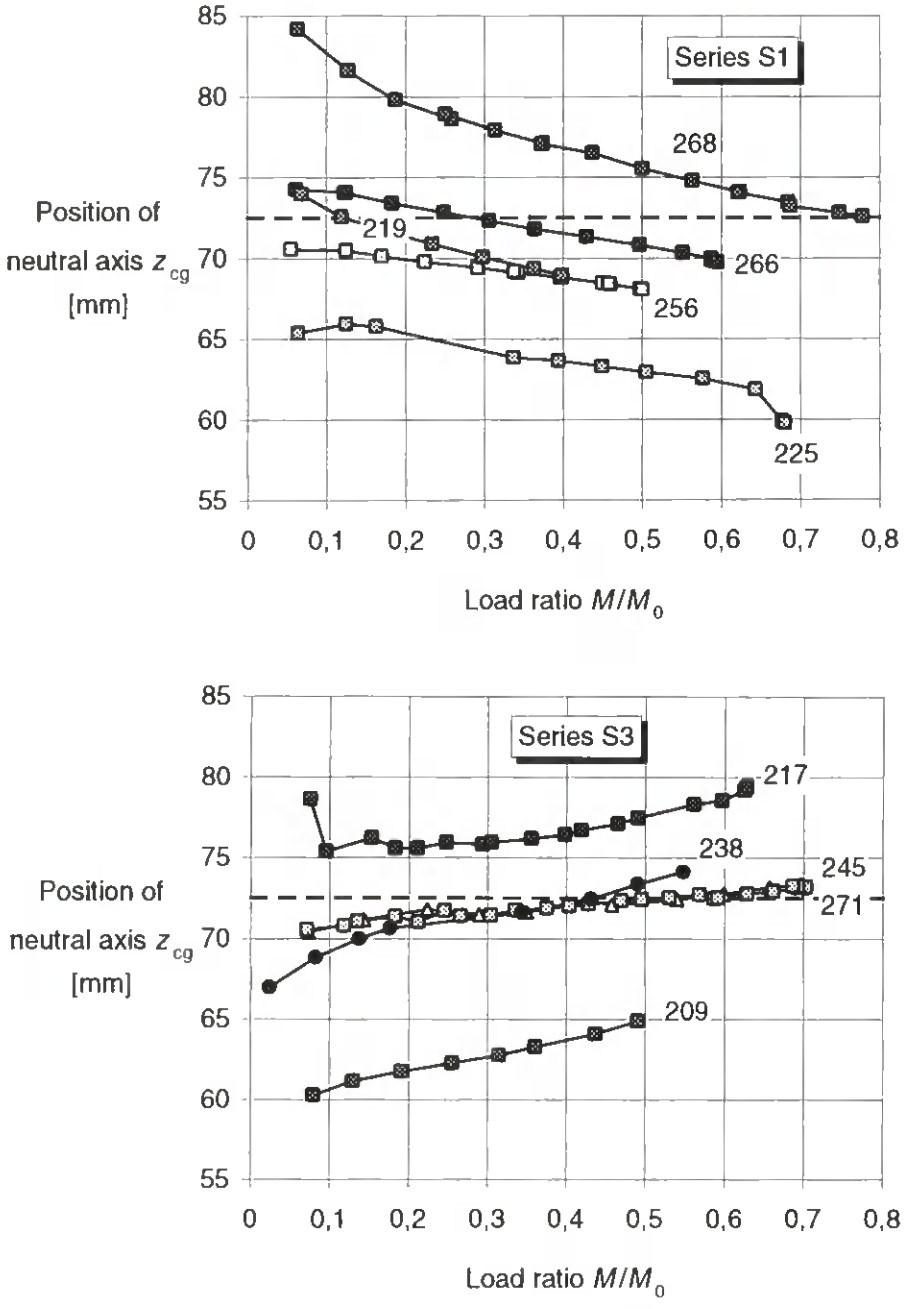

Figure 2.14: Stage of application of load prior to fire test - position of neutral axis versus load ratio for some specimens of series S1 and S3

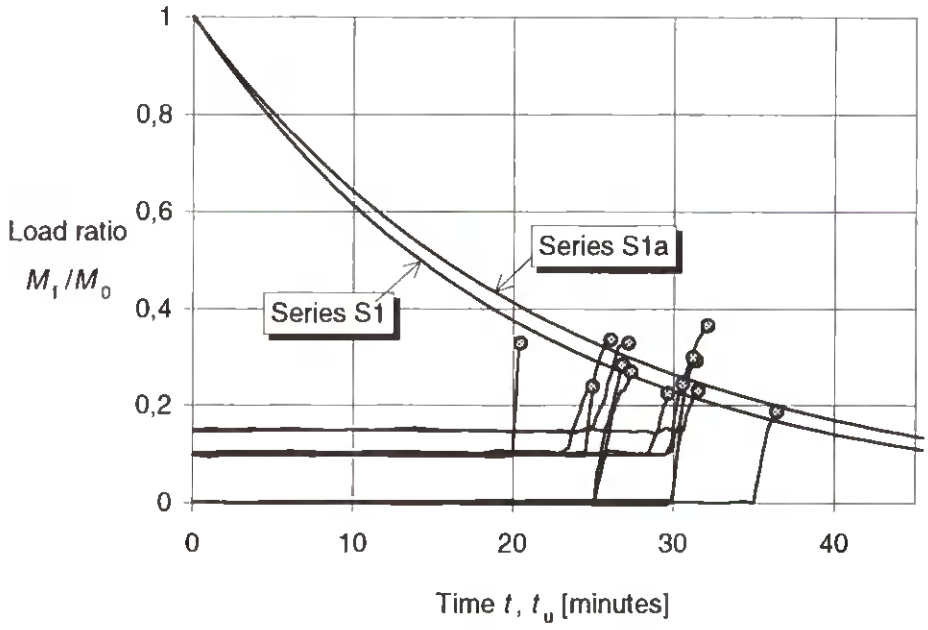

a)

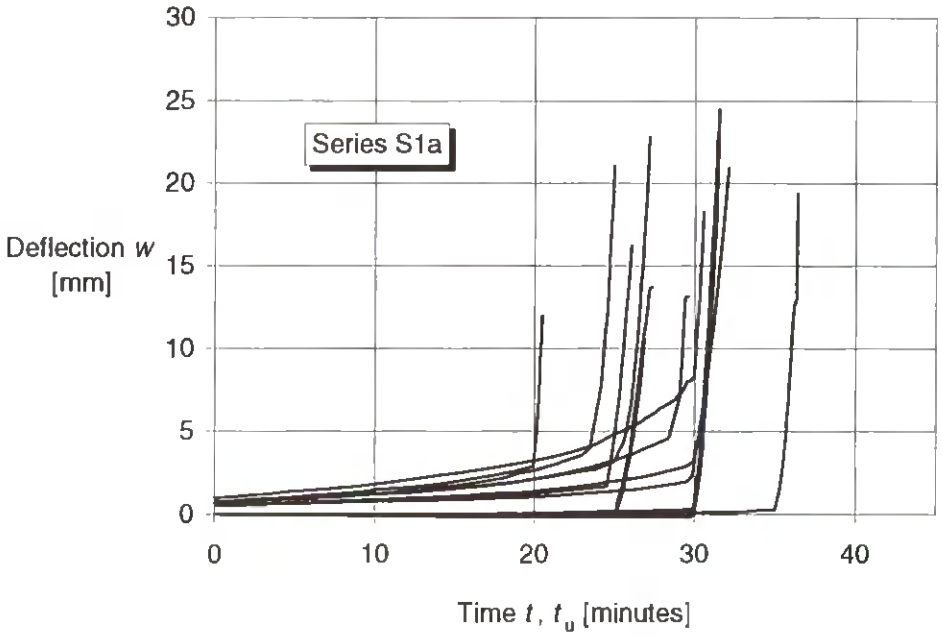

b)

Figure 2.15a-b: Test results of series 1a - Mechanical properties
a) Load ratio versus time of failure in comparison with series S1 (marked by squares)
b) Mid-deflection versus time

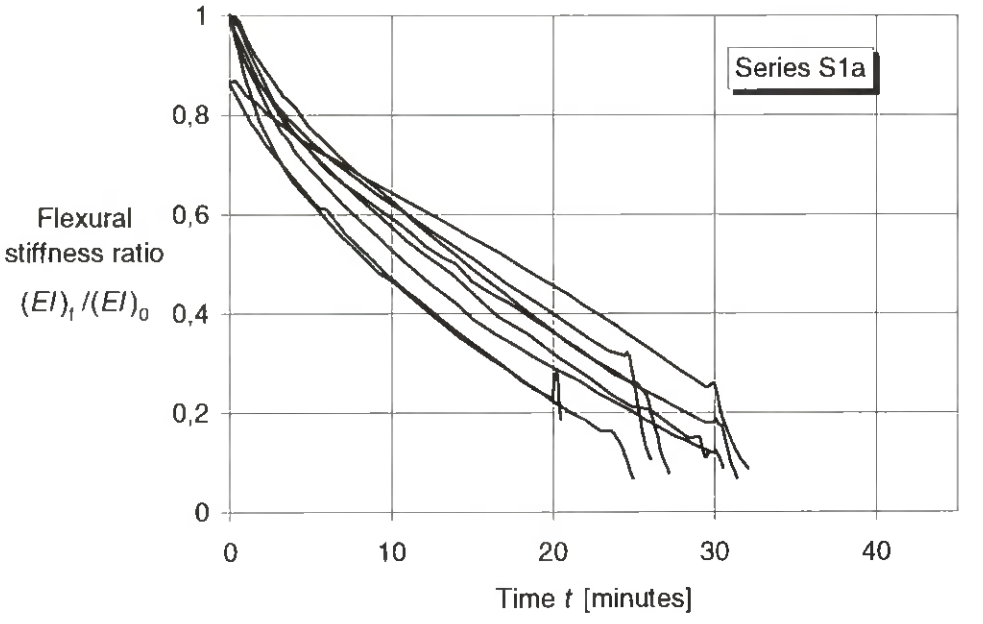

c)

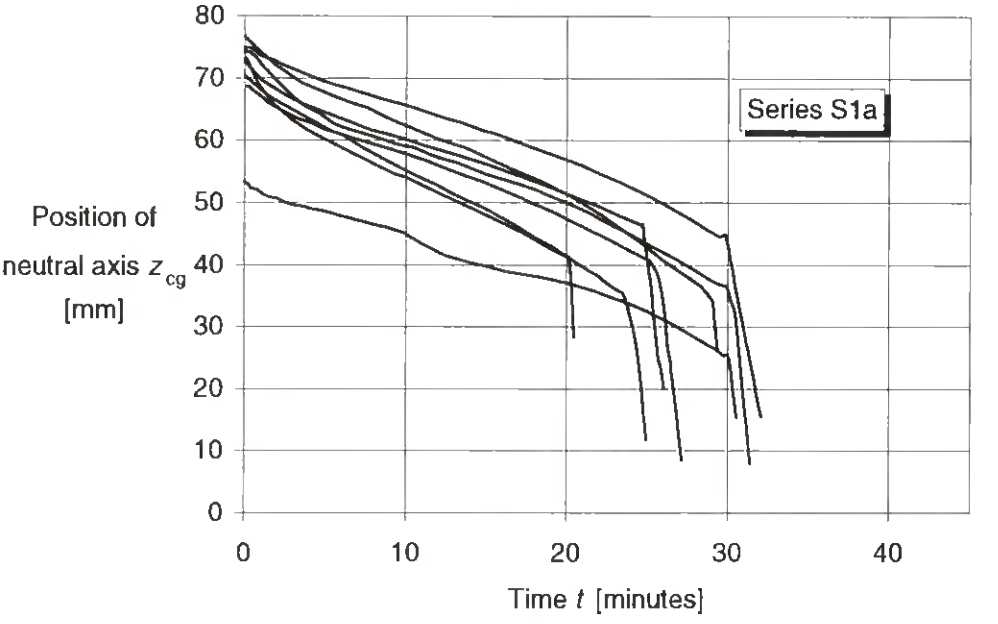

d)

Figure 2.15c-d: Test results of series S1a - Mechanical properties
c) Flexural stiffness ratio versus time
d) Position of neutral axis versus time

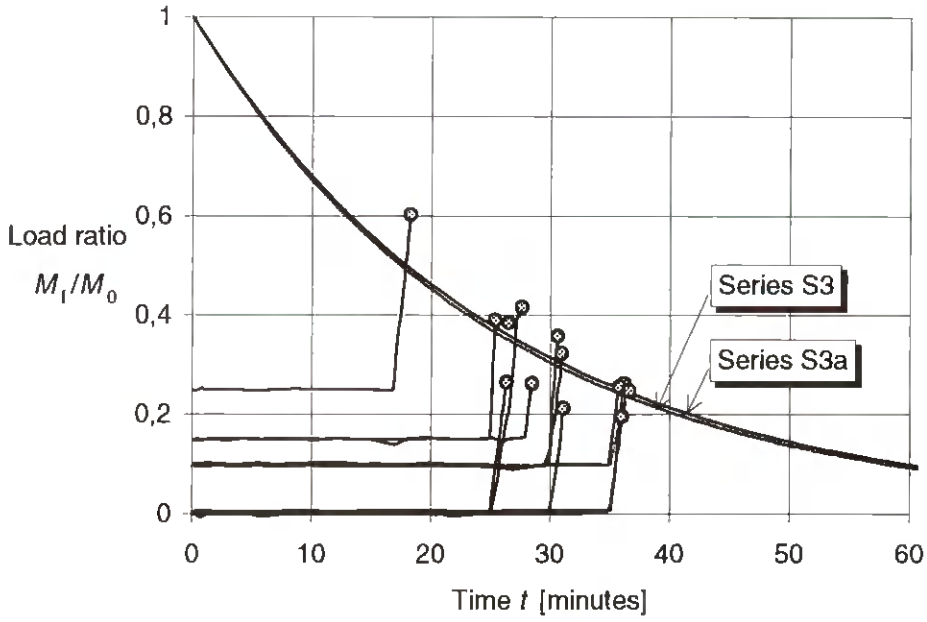

a)

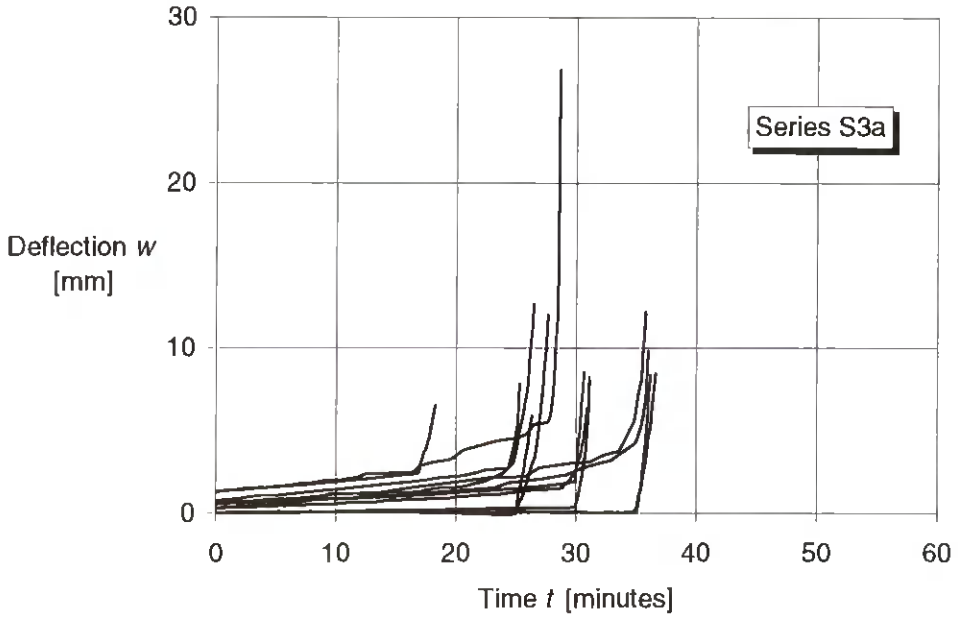

b)

Figure 2.16a-b: Test results of series 3a - Mechanical properties
a) Load ratio versus time of failure in comparison with series S3 (marked by squares)
b) Mid-deflection versus time

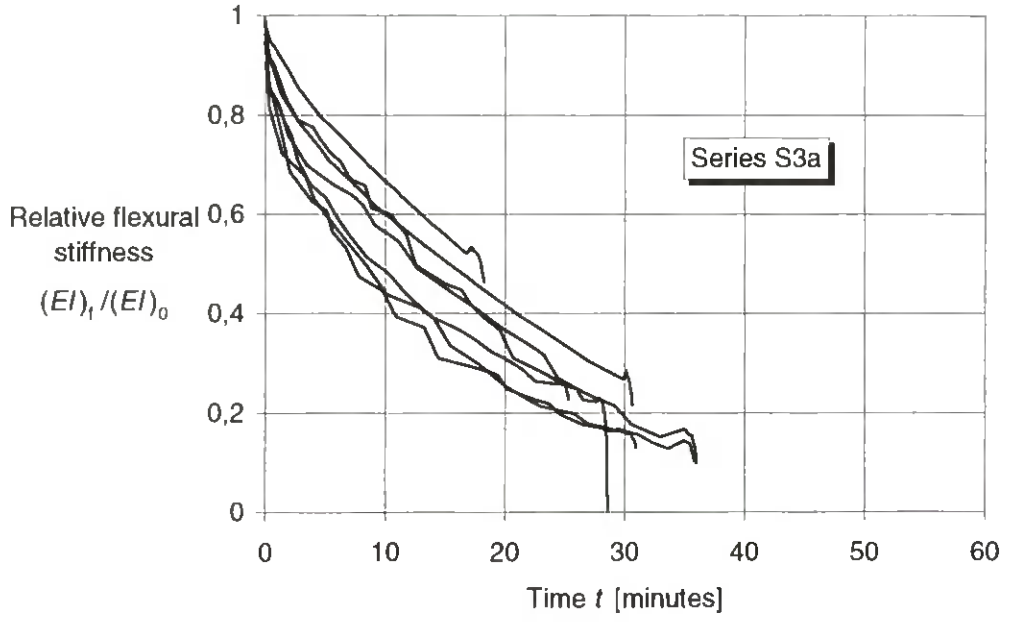

c)

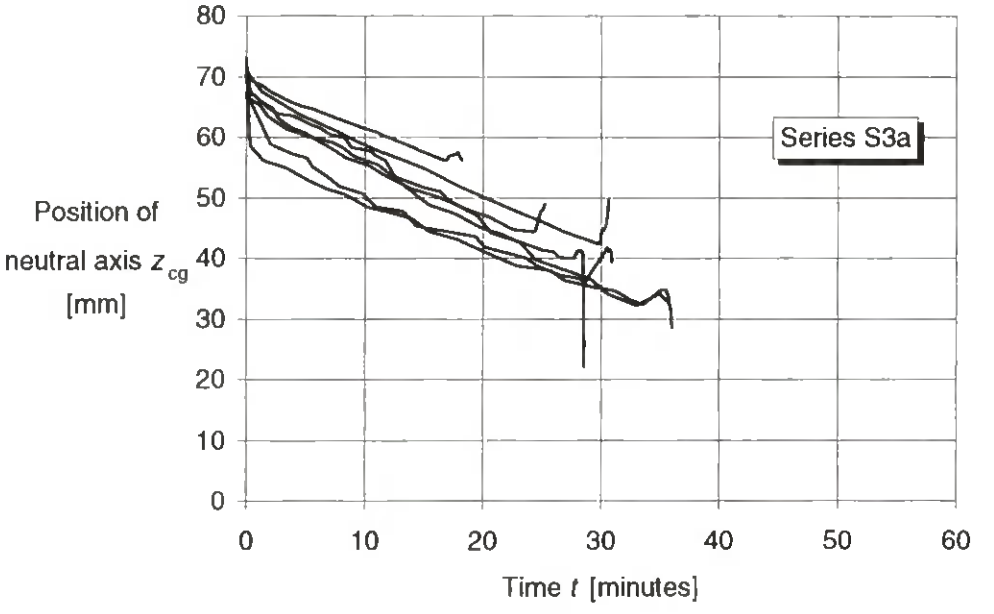

d)

Figure 2.16c-d: Test results of series S3a - Mechanical properties
c) Flexural stiffness ratio versus time
d) Position of neutral axis versus time

Deflections, flexural stiffness and position of neutral axis. Plots of these parameters versus time are shown in figures 2.15b-d and 2.16b-d. Flexural stiffnesses and the position of the neutral axis are not shown for specimens with an initial load ratio equal to zero. The influence of the increase of load can be seen from a sudden change of rate of these parameters.

2.7.2.3 The influence of fire protective gypsum plasterboard - test series S2

In test series S2 the fire-exposed side of the members was protected by a single layer of gypsum plasterboard with a thickness of 12,5 mm in order to determine its contribution to the fire resistance. In all tests this layer of plasterboard was in place during a time period of about 28 minutes. Then it could be heard clearly that the attached gypsum board fell down.

A plot of the results of load ratio versus time to failure is shown in Figure 2.17a. For complete data see appendix D, table D9. The regression curve was determined by linear regression analysis according to Equation (2.1) with parameters A and B according to Table 2.2. For comparison, in the diagram the regression curve according to Equation (2.2) is shown for series S1. The horizontal distance of the two regression curves is the effective failure time of the protective board t_{pr} and defined as

$$t_{pr} = t_{u,2} - t_{u,1} \tag{2.7}$$

where $t_{u,1}$ is the failure time of the unprotected construction and $t_{u,2}$ is the failure time of the protected construction. In other words, the failure time of the protected construction is the sum of the unprotected construction and the failure time of the protective board:

$$t_{u,2} = t_{u,1} + t_{pr} \tag{2.8}$$

Since the two regression curves have different slopes (parameters B, see table 2.2), the failure time of the protective board changes with time. From the two regression equations

$$\ln \hat{\eta}_1 = B_1 \, t_{u,1} \quad [\text{min.}] \tag{2.9}$$

$$\ln \hat{\eta}_2 = A_2 + B_2 t_{u,2} \quad [\text{min.}] \tag{2.10}$$

and with

$$\hat{\eta}_1 = \hat{\eta}_2 = \hat{\eta} \tag{2.11}$$

the difference of time for the same load ratio can be derived as

$$t_{pr} = \frac{\ln \hat{\eta} - A_2}{B_2} - \frac{\ln \hat{\eta}}{B_1} \tag{2.12}$$

where $\hat{\eta}$ is the predicted load ratio by the regression equation and A_2, B_1 and B_2 are the parameters in the regression equations according to Table 2.2. With equation (2.9) we get

$$t_{pr} = \left(\frac{B_1}{B_2} - 1 \right) t_{u,1} - \frac{A_2}{B_2} \tag{2.13}$$

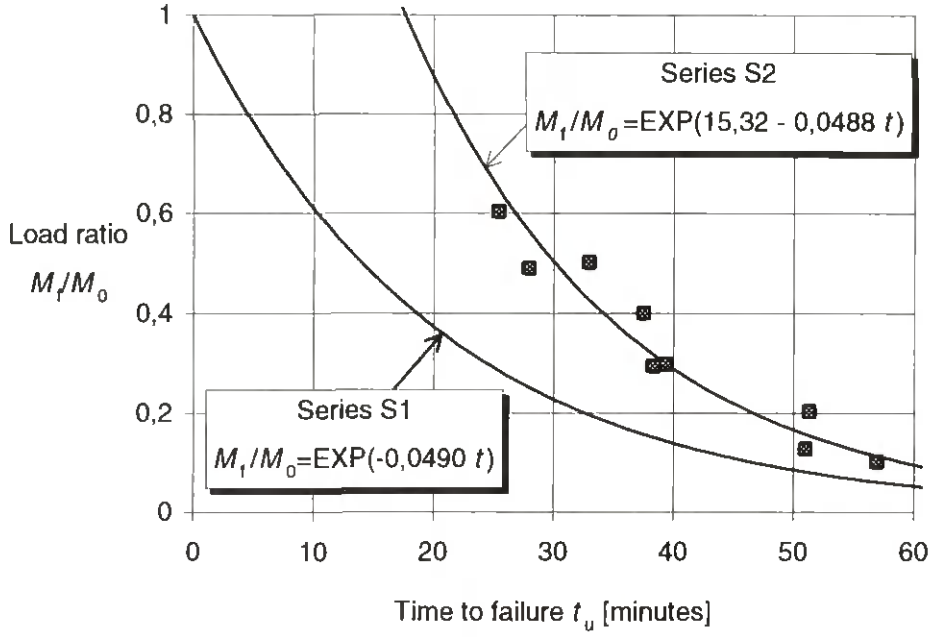

a)

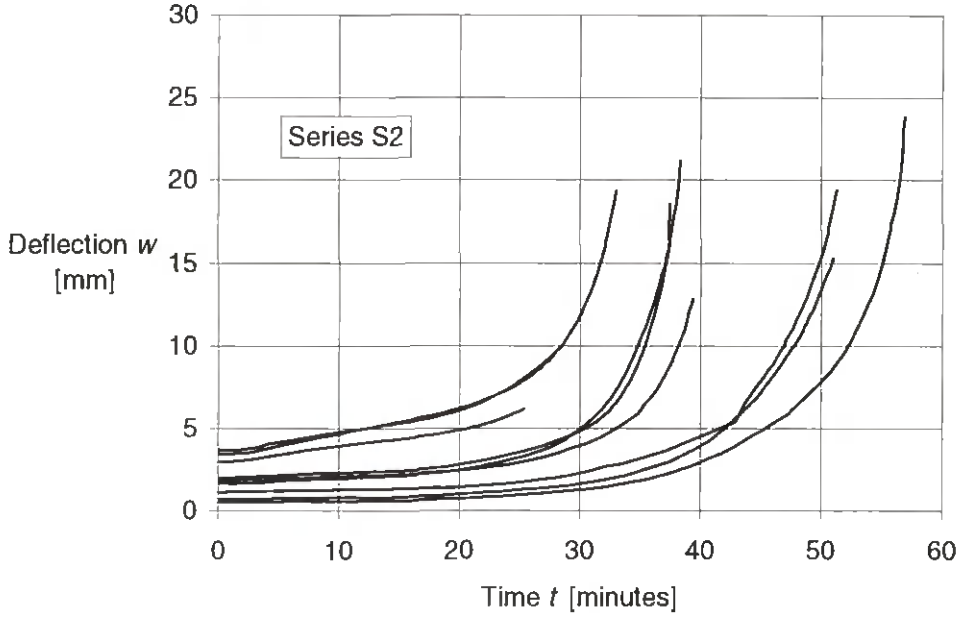

b)

Figure 2.17a-b: Test results of series S2 - Mechanical properties
a) Load ratio versus time of failure
b) Mid-deflection versus time

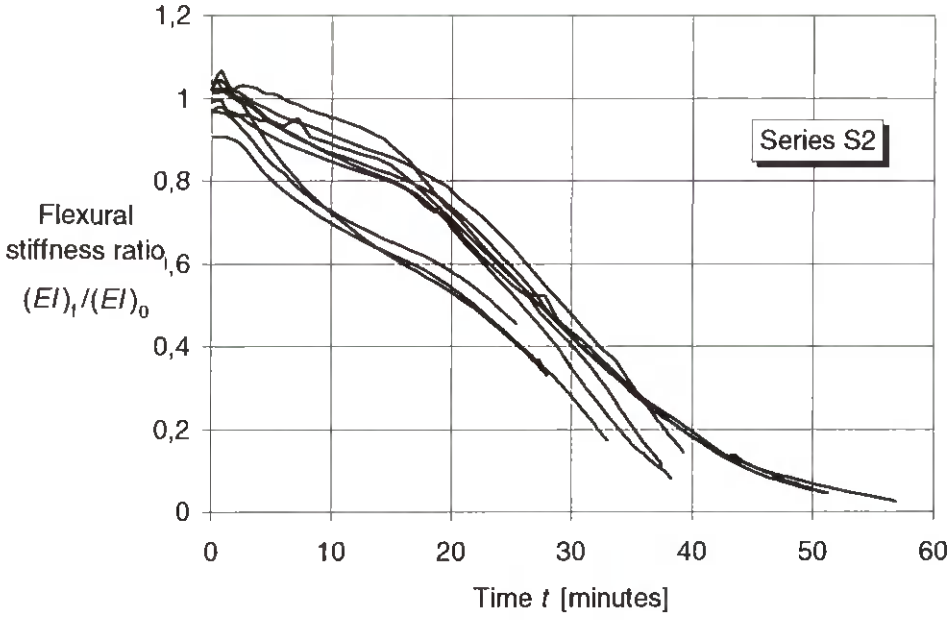

c)

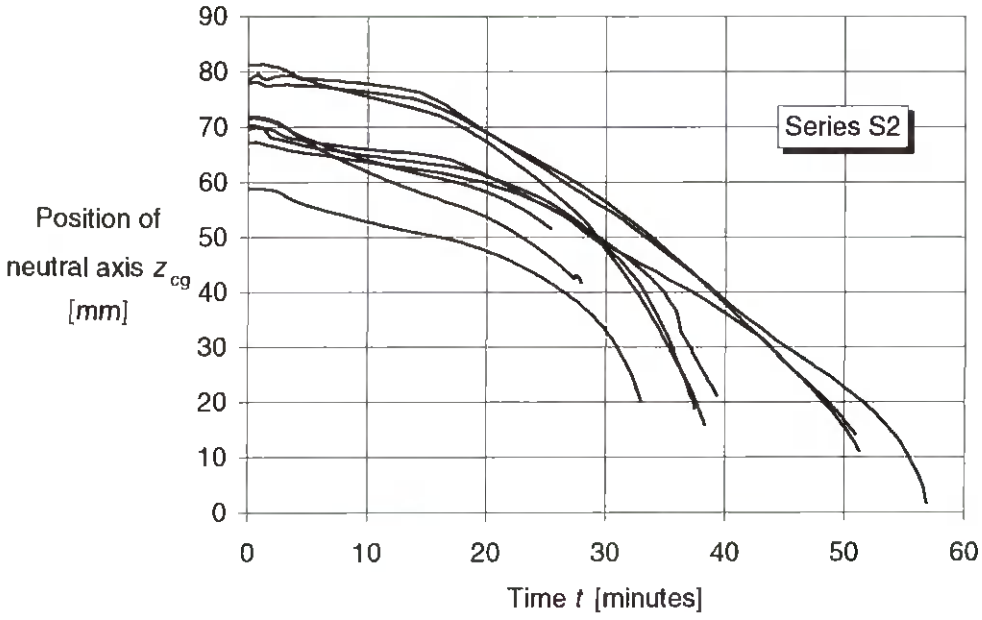

d)

Figure 2.17c-d: Test results of series S2 - Mechanical properties
c) Flexural stiffness ratio versus time
d) Position of neutral axis versus time

A plot of equation (2.7) is shown in figure 2.18. We can see that the protective effect of the gypsum board is dependent on time. The failure time is 17,6 minutes in the beginning while it is only 12,3 minutes when $t_{u,1}$ is 45 minutes. As mentioned above, the gypsum boards were attached to the timber members during approximately 28 minutes.

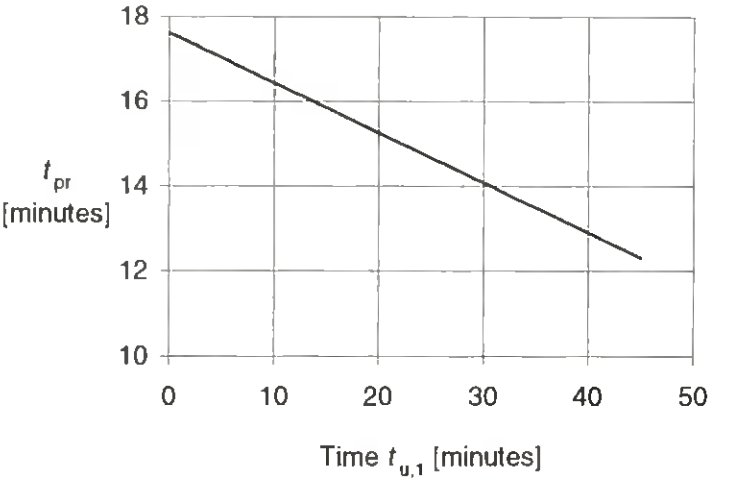

Figure 2.18: The effective failure time of fire-protective plasterboard versus failure time in series S1 - Comparison of test series S2 and S1

Plots of the mid-deflection versus time and the variation of the flexural stiffness ratio during the fire test are shown in figures 2.17a-b. Compared to the results of series S1 the initial flexural stiffness was greater, due to the effect of composite action between the member and the protective board. Consequently, the initial position of the neutral axis is also a little closer to the fire-exposed side, see figure 2.17d.

2.7.3 TEMPERATURE MEASUREMENTS

Series S1 - S7. An example of the relationship between temperature in the member and time during the fire test is shown in figure 2.19. The figures in the diagram refer to the gauge points of thermocouples, see figure 2.5. Temperatures greater than 300 °C are not shown since it is widely accepted that charring occurs at a temperature of about 300 °C. A complete set-up of diagrams is presented in appendix E.

Using these recorded temperatures, temperature profiles along the vertical centre-line of the cross-section were plotted for specific times, see figures 2.20-23.

Series T. Fire tests with specimens 1a, 37a and 37b gave information about temperature profiles in the horizontal direction at some distances from the fire exposed side, see figures 2.24-26.

The fire test N1 was made in order to give information concerning the onset of charring on the surface of the member, since in series S2 the temperature was not recorded on the surface. The results from tests N1 are presented below as the propagation of the 300-degree isotherm, see figure 2.28. Correspondingly four tests F1 to F4 were made in order to give information on the onset of charring on the surface of members protected by a layer of gypsum plasterboard type F as they were used in the wall tests, see section 3.

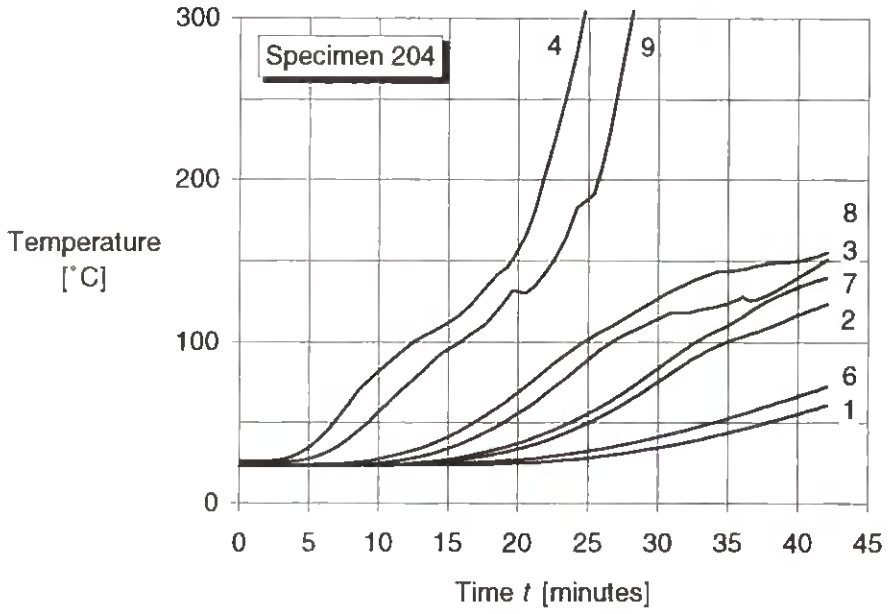

Figure 2.19: Example of the relationship between temperature and time. The numbers refer to gauge points (see figure 2.5)

2.7.4 CHARRING DEPTHS

An example of the residual cross section of a member is shown in figure 2.27. Further examples are shown in appendix C. These were used to determine the average minimum charring depth near the vertical centre-line of the cross-section (see figure 2.28) of each specimen and were plotted versus time, see figures 2.29-31. The results of series with only one size of cross section are shown in one figure. The charring depths of all specimens are also shown in figure 2.32.

The effect of the attached gypsum plasterboard can be seen from Figure 2.29. As before in Figure 2.18, we can see that charring of the protected members in series S2 lags behind charring of the unprotected members in series S1 and S3. The time difference t_{pr} varies with time and is of the same order of magnitude as shown in Figure 2.18.

In addition to the charring depths, curves of the position of the 300-degree isotherm are shown. The plotted values are averaged values of the recorded data, however, in figure 2.29, for series S2, the plotted value for the edge distance of 48 mm is based on only one recorded value. The dotted line representing test N1 (series T) fits better to the recorded values of charring depth (triangles). In series S4 and S5 (see figure 2.30) values exist only for the edge distance of 12 mm, while the curve for series S6 is based on the measurements in only one specimen.

We can see that the state of stress does not influence the charring depth, and that the position of the char-line is fairly well described by the position of the 300-degree isotherm.

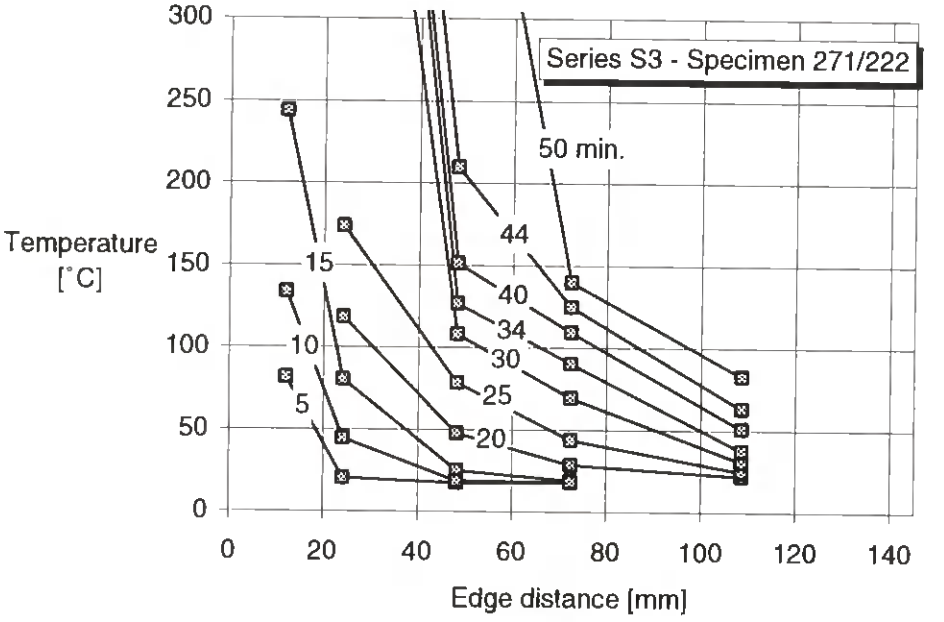

Figure 2.20: Example of temperature profiles along the vertical centre-line of the cross-section in series S3 (Specimens 222 and 271)

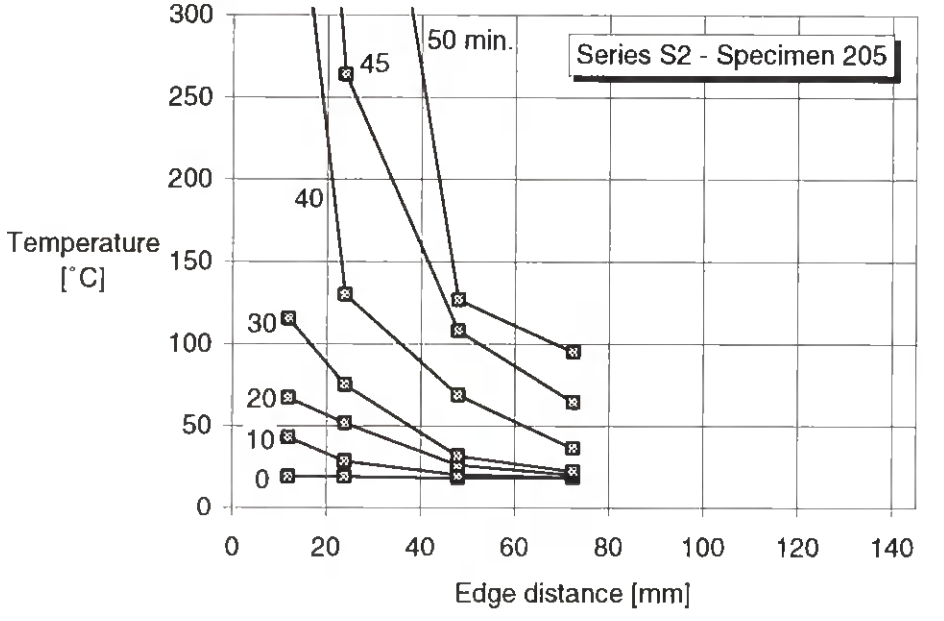

Figure 2.21: Example of temperature profiles along the vertical centre-line of the cross section in series S2 (Specimen 205)

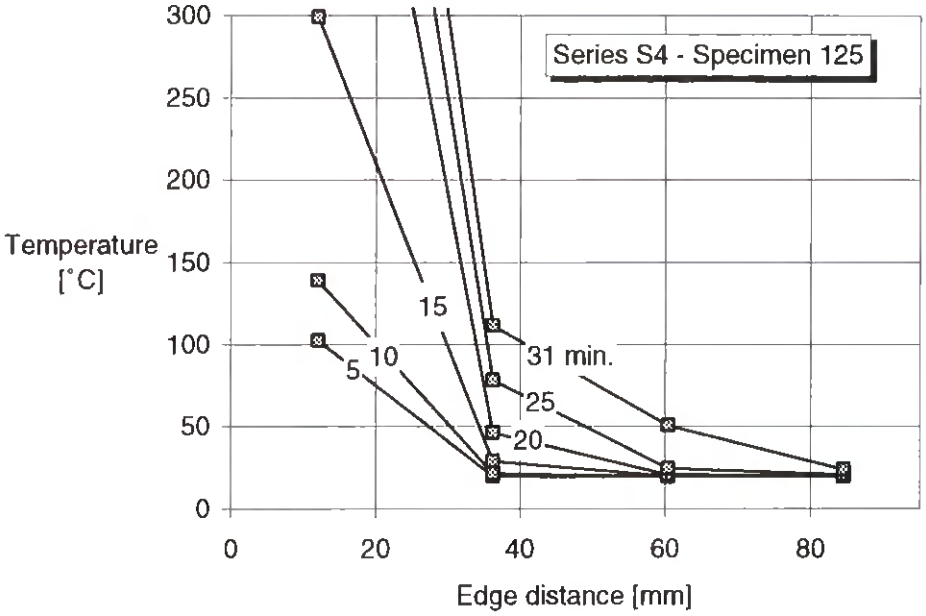

Figure 2.22: Example of temperature profiles along the vertical centre-line of the cross-section in series S4 (Specimen 125)

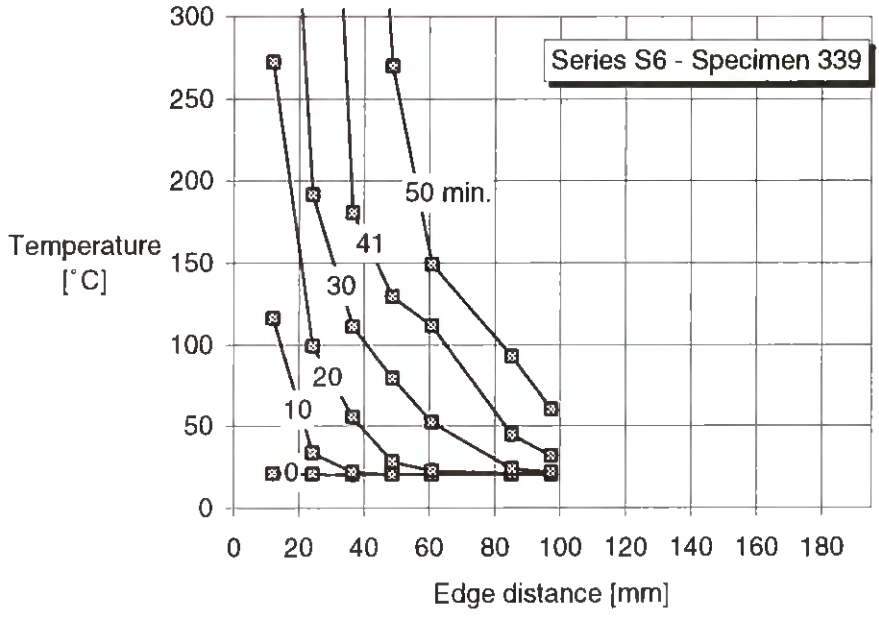

Figure 2.23: Example of temperature profiles along the vertical centre-line of the cross-section in series S3 (Specimen 339)

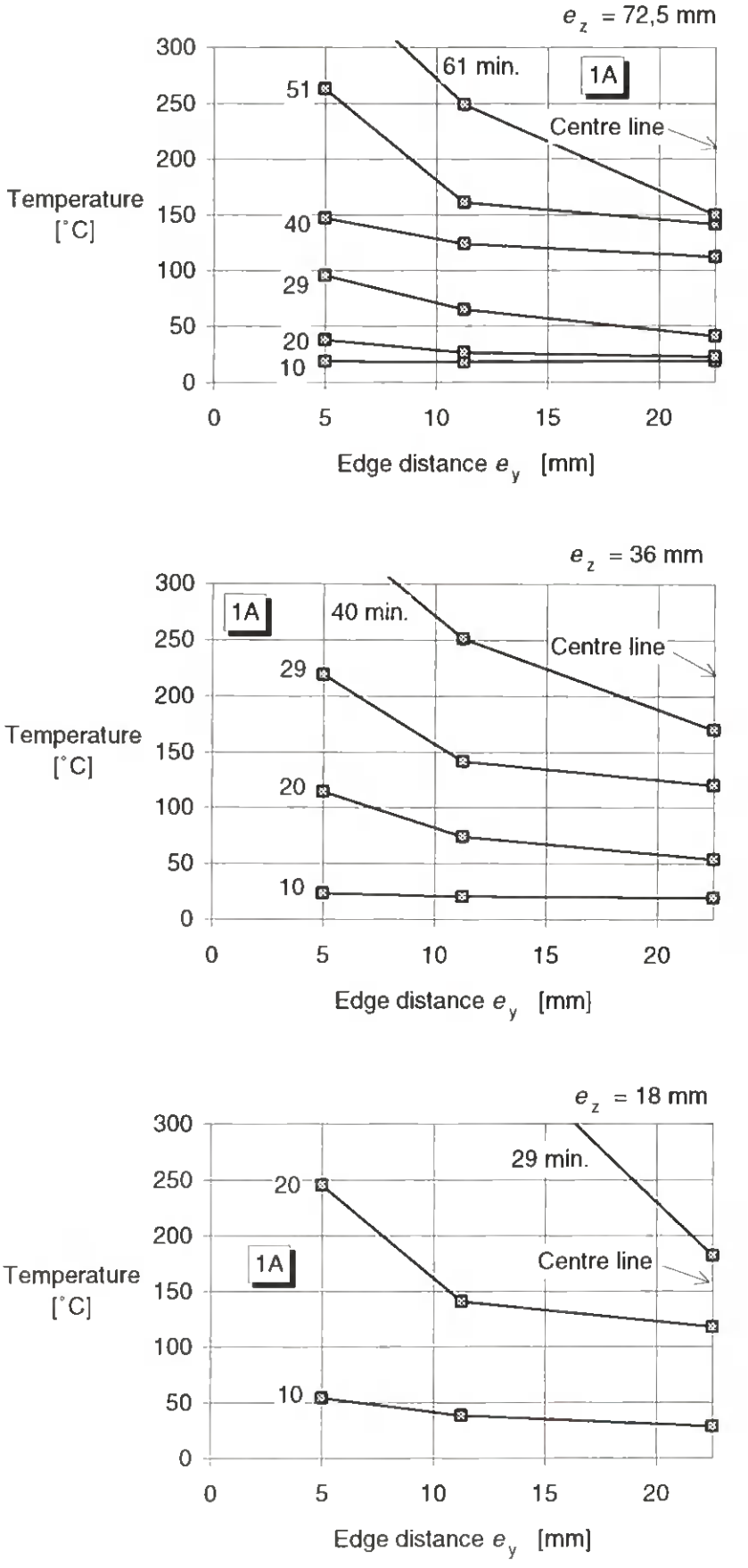

Figure 2.24: Temperature profiles at specific distances from exposed side of specimen 1A (series T)

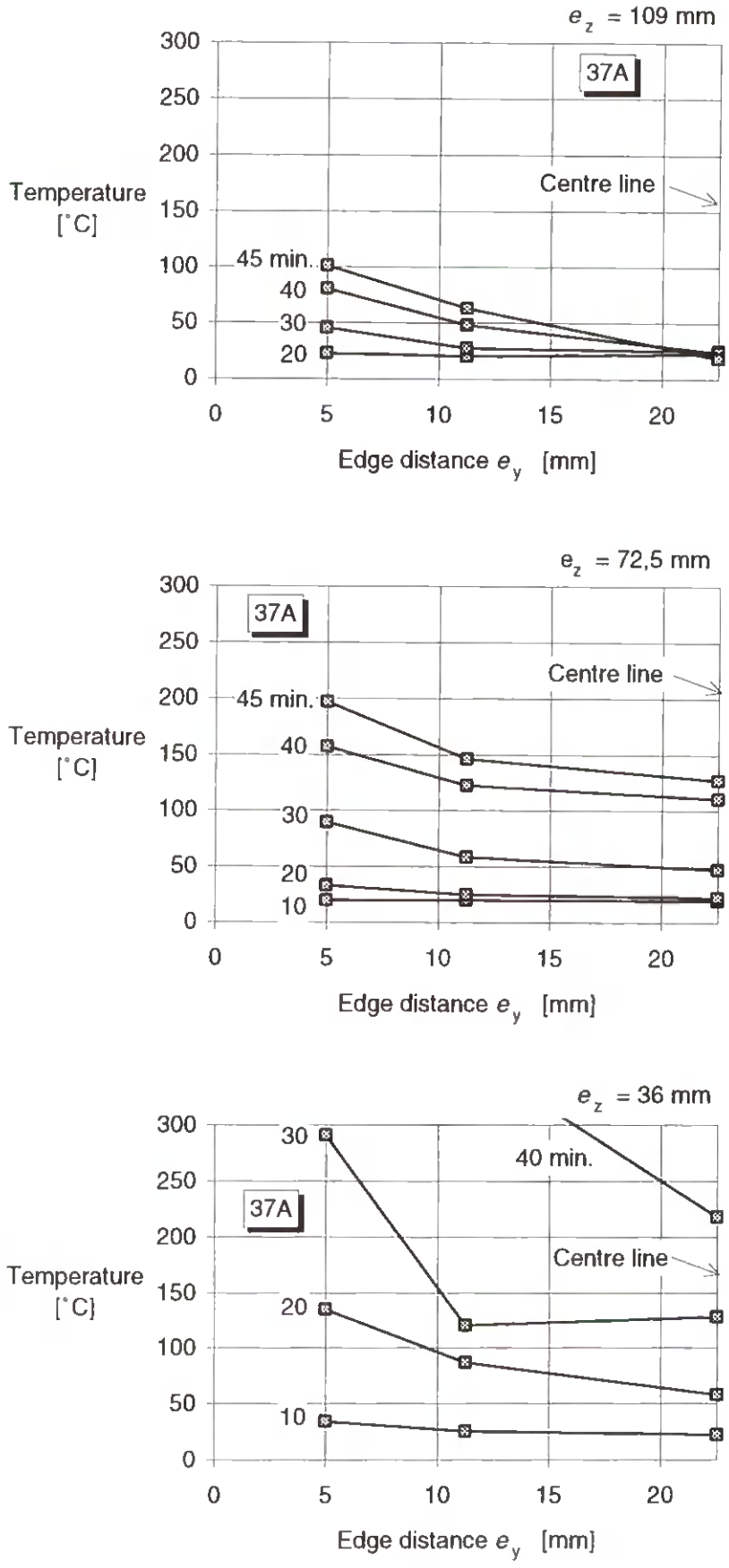

Figure 2.25: Temperature profiles at specific distances from exposed side of specimen 37A (series T)

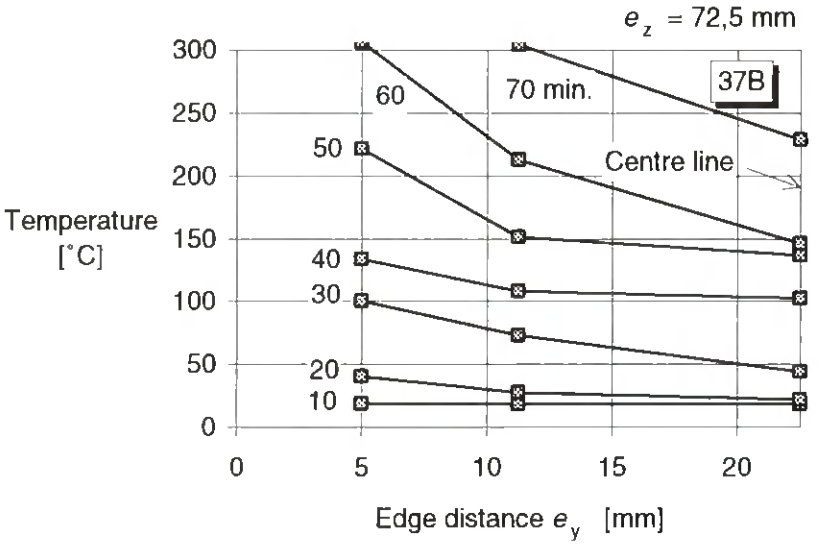

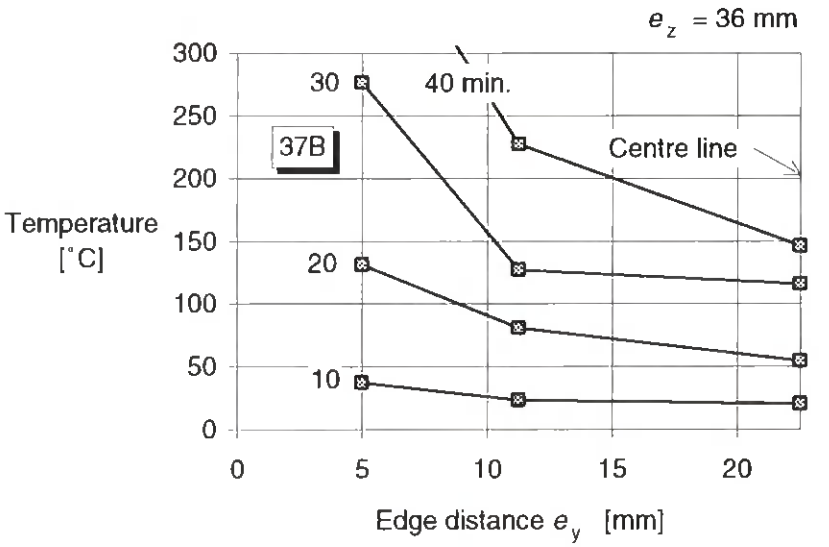

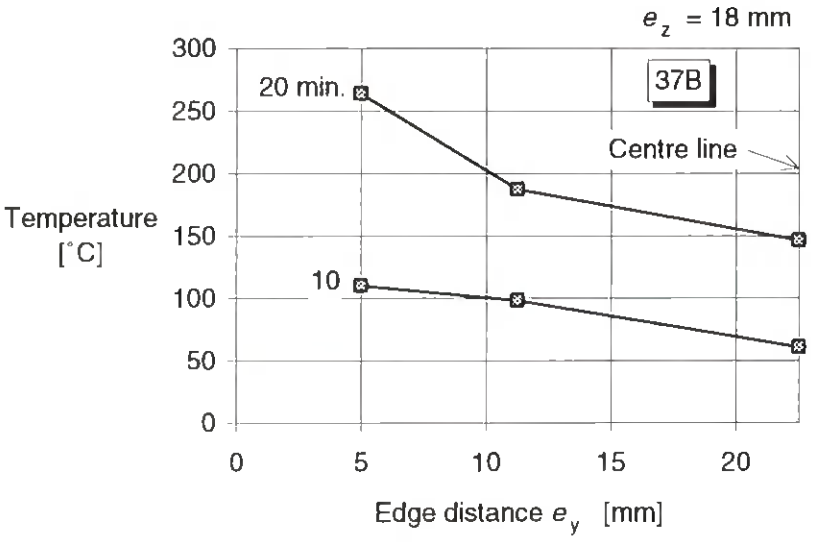

Figure 2.26: Temperature profiles at specific distances from exposed side of specimen 37B

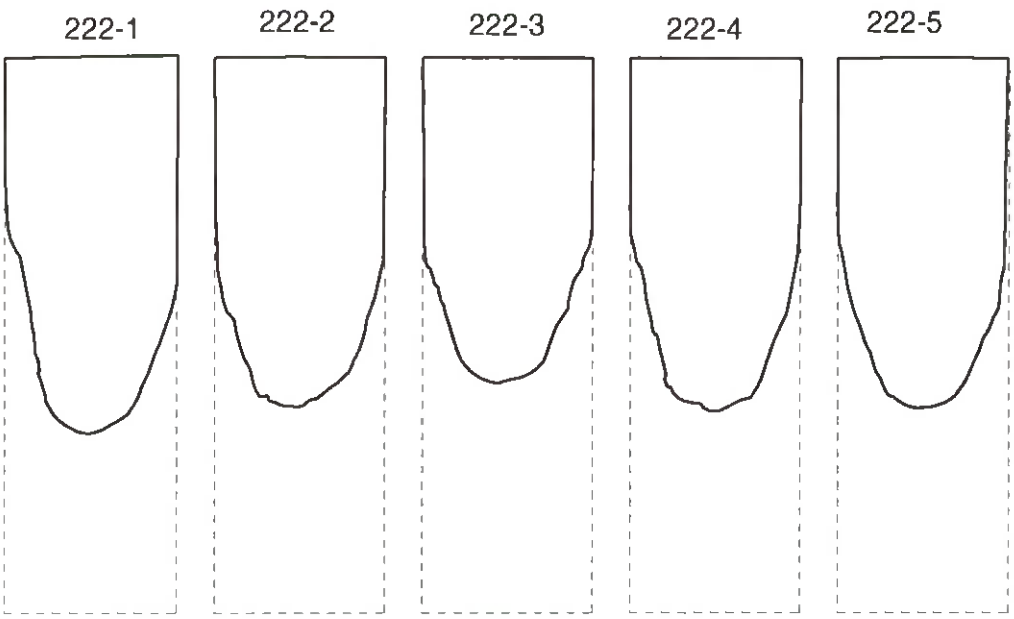

Figure 2.27: Example of residual cross section of member

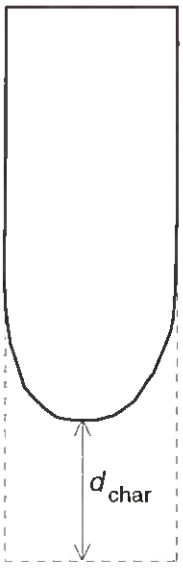

Figure 2.28: Definition of charring depth

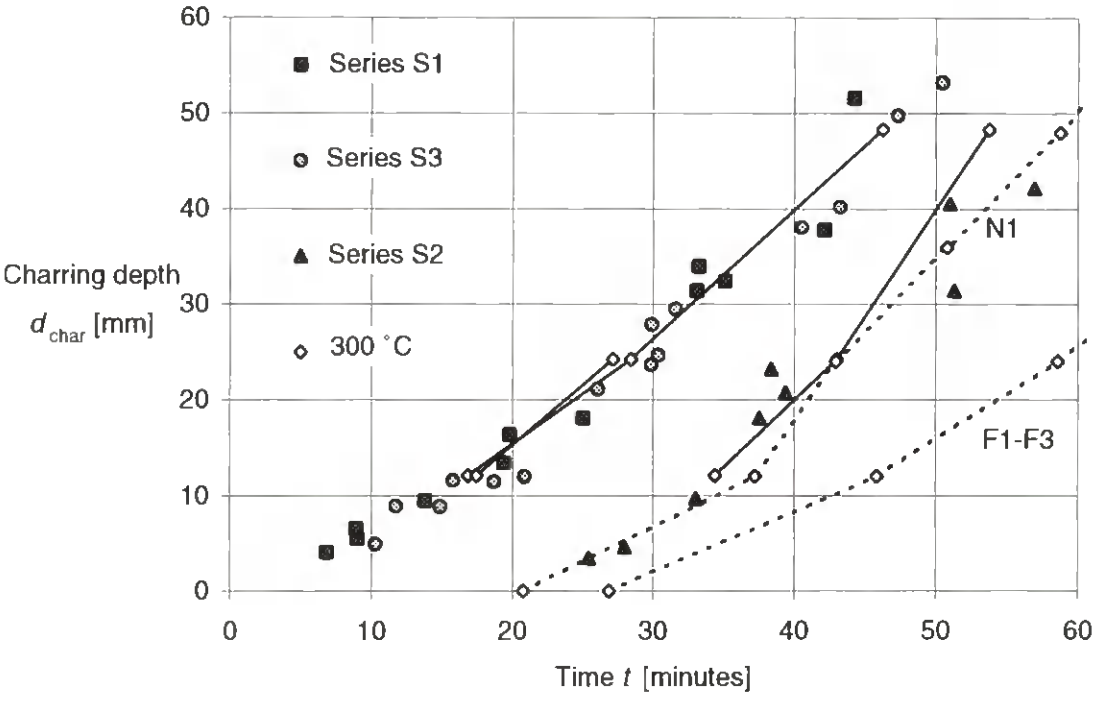

Figure 2.29: Charring depths near the vertical centre-line of the cross-section and position of the 300-degree isotherm in series S1-S3, and specimens N1 and F1-F3 of series T

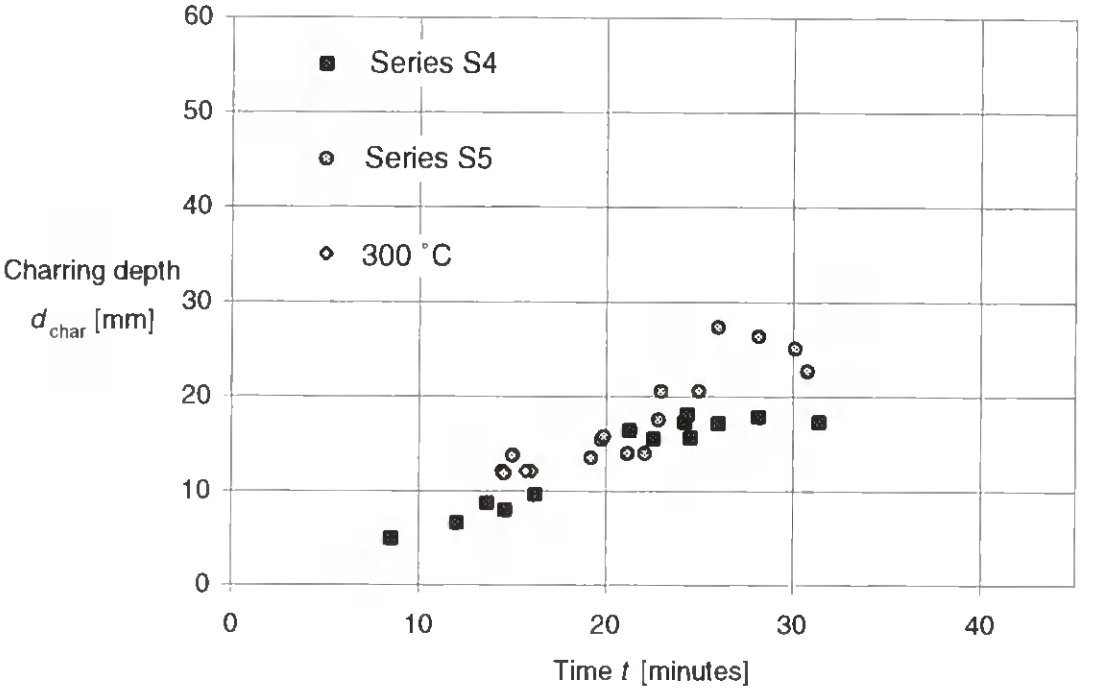

Figure 2.30: Charring depths near the vertical centre-line of the cross-section and position of the 300-degree isotherm in series S4 and S5

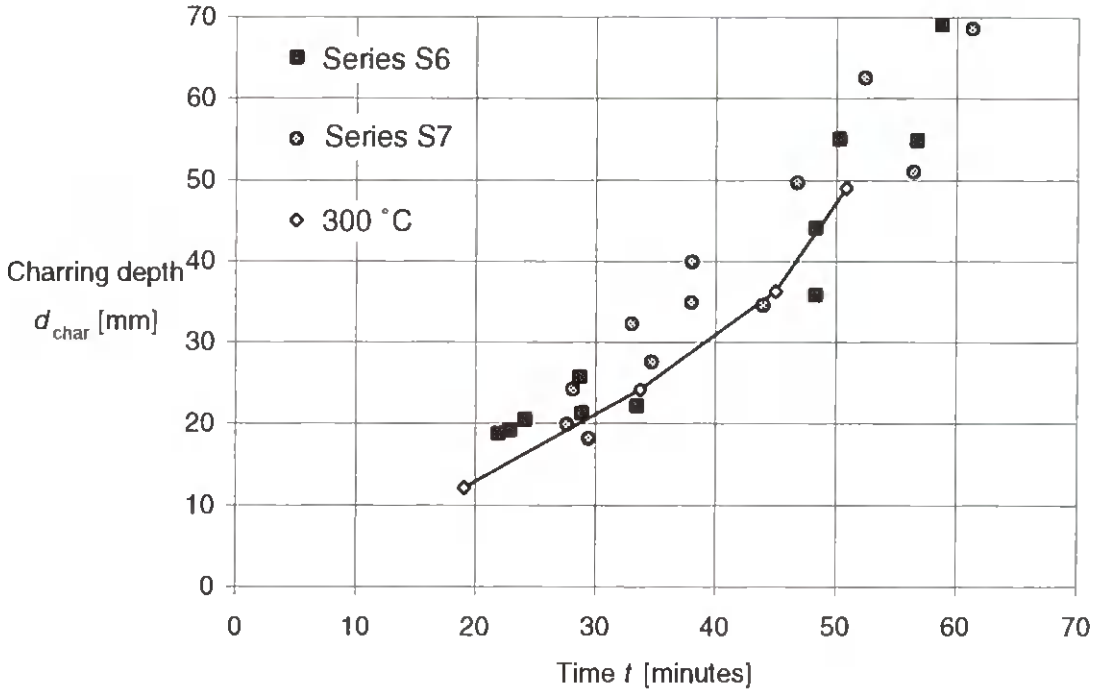

Figure 2.31: Charring depths near the vertical centre-line of the cross-section and position of the 300-degree isotherm in series S6 and S7

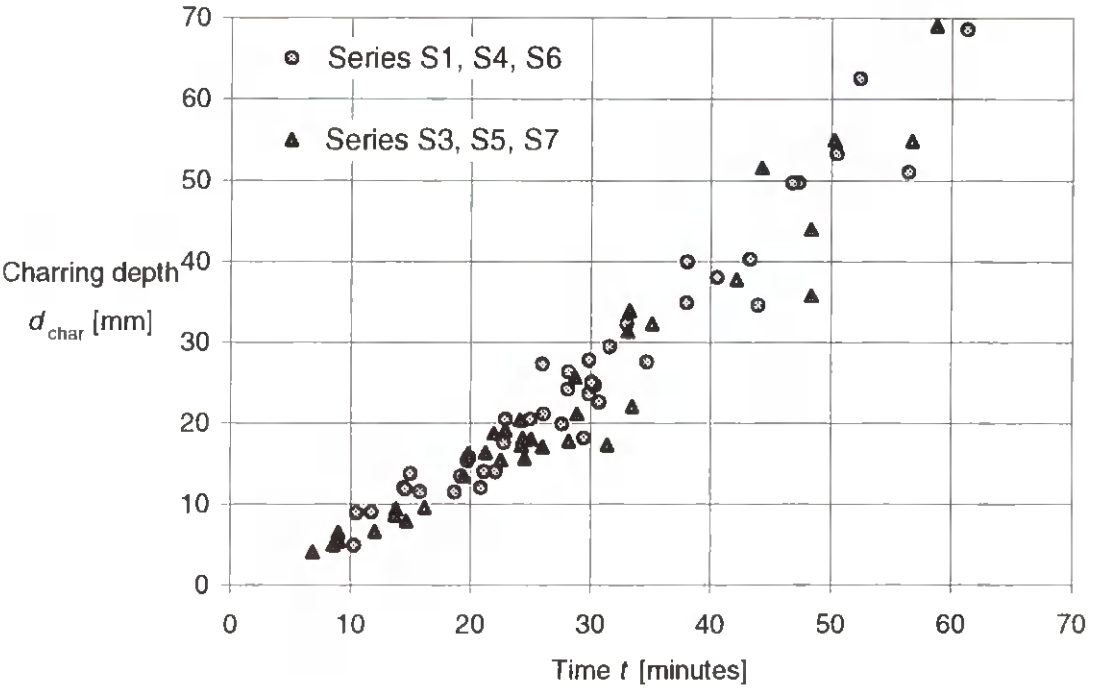

Figure 2.32: Charring depths near the vertical centre-line of the cross-section in all series

3 FIRE TESTING OF WALLS

3.1 MATERIAL - REFERENCE TESTS AT NORMAL TEMPERATURE

For the wall tests timber studs were chosen with a dimension of 45 mm × 145 mm and a length of 2410 mm. The timber was fairly free from knots as in the fire tests of members, see 2.1. The material was conditioned in a controlled climate chamber at 20 °C and 65 % RH. For each stud from the same piece of timber a small test specimen was cut and its dry density and moisture content were determined.

The modulus of elasticity in edgewise bending of each stud was determined in a series of reference tests at normal temperature. The span was 2310 mm and the specimen was acted upon by two equal forces at the third points. The load was applied in five steps such that the maximum mid-deflection was about 4 mm. The moduli of elasticity were determined using the most linear parts of the load-deflection curves. A plot of the modulus of elasticity versus dry density is shown in figure 3.1. The diagram also shows how the studs were distributed on the three walls W1-W3 such that the variation of these parameters was kept as small as possible. The material data for the studs are given in table 3.1.

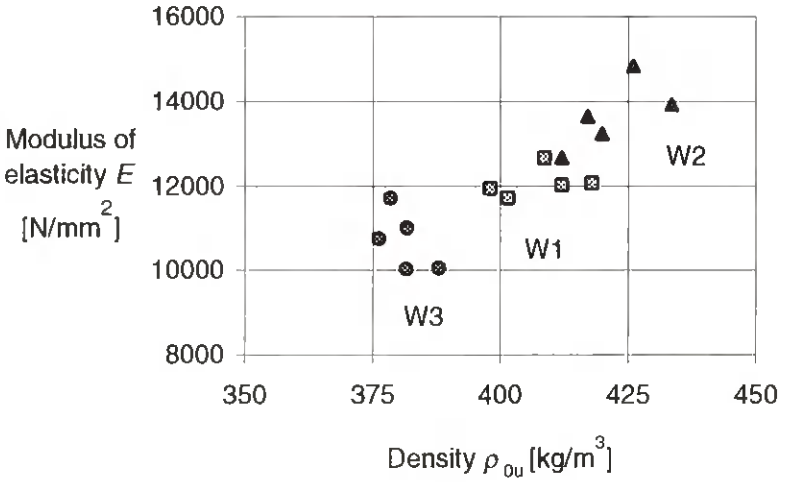

Figure 3.1: Modulus of elasticity of studs versus dry density - results from reference tests at normal temperature

3.2 TEST SPECIMENS AND TESTING EQUIPMENT

The full-scale fire tests were conducted at the Fire Technology Laboratory of the Technical Research Centre of Finland in Espoo. The fire tests were made with walls corresponding to test series S1 and S2, i.e. the specimen W1 was without a lining on the fire-exposed side, while in specimen W2 the studs were protected by gypsum plasterboard with a thickness of 12,5 mm as specified in 2.1. In specimen W3 the gypsum boards were replaced by gypsum plasterboard with improved core cohesion at high temperature with a thickness of 15 mm and a weight of 12,5 kg/m^2. These boards were produced by AB Gyproc, Sweden, and are marketed in Sweden as "Protect F". Hereinafter they are designated as "gypsum plasterboards type F" according to the classification system of prEN 520.

Table 3.1: Material properties of studs - results from reference tests at normal temperature

Test	Stud No.	Moisture content u	Dry density ρ_{0u}	Modulus of elasticity E	E/E_{mean}
		[%]	[kg/m^3]	[MPa]	
W1	337	13,4	402	11696	0,969
	301	14,3	398	11934	0,988
	331	14,0	412	12002	0,994
	367	14,3	418	12060	0,999
	302	13,5	409	12654	1,048
	Mean values		408	12069	
W2	360	13,9	412	12670	0,927
	323	14,0	420	13238	0,969
	308	13,6	417	13650	0,999
	318	13,4	434	13921	1,019
	340	13,7	426	14832	1,086
	Mean values		422	13662	
W3	304	13,0	379	11704	1,093
	364	13,4	382	11000	1,028
	317	13,7	376	10745	1,004
	305	13,2	388	10051	0,939
	352	13,1	382	10024	0,936
	Mean values		381	10705	

The same type of rock fibre insulation as specified in 2.1 was used.

The walls were 2,50 m high and 3,00 m wide, with five load bearing studs at 600 mm centres. Additionally, two non load-bearing studs were placed at the edges in order to achieve an equal load distribution on the load bearing studs and integrity of the wall at the edges. See figure 3.2. In the figure the stud numbers of the three walls are specified.

On the non fire-exposed side of the walls horizontal strips of gypsum boards were attached to the studs. The strips were 400 mm wide, except the strip at the top which was 500 mm wide. The board strips were jointed at stud B or D respectively with staggered arrangement of the boards. The board strips were fixed to the studs at the third points of the strip width. By the division into strips composite action of the gypsum boards was prevented, c.f. 2.3.

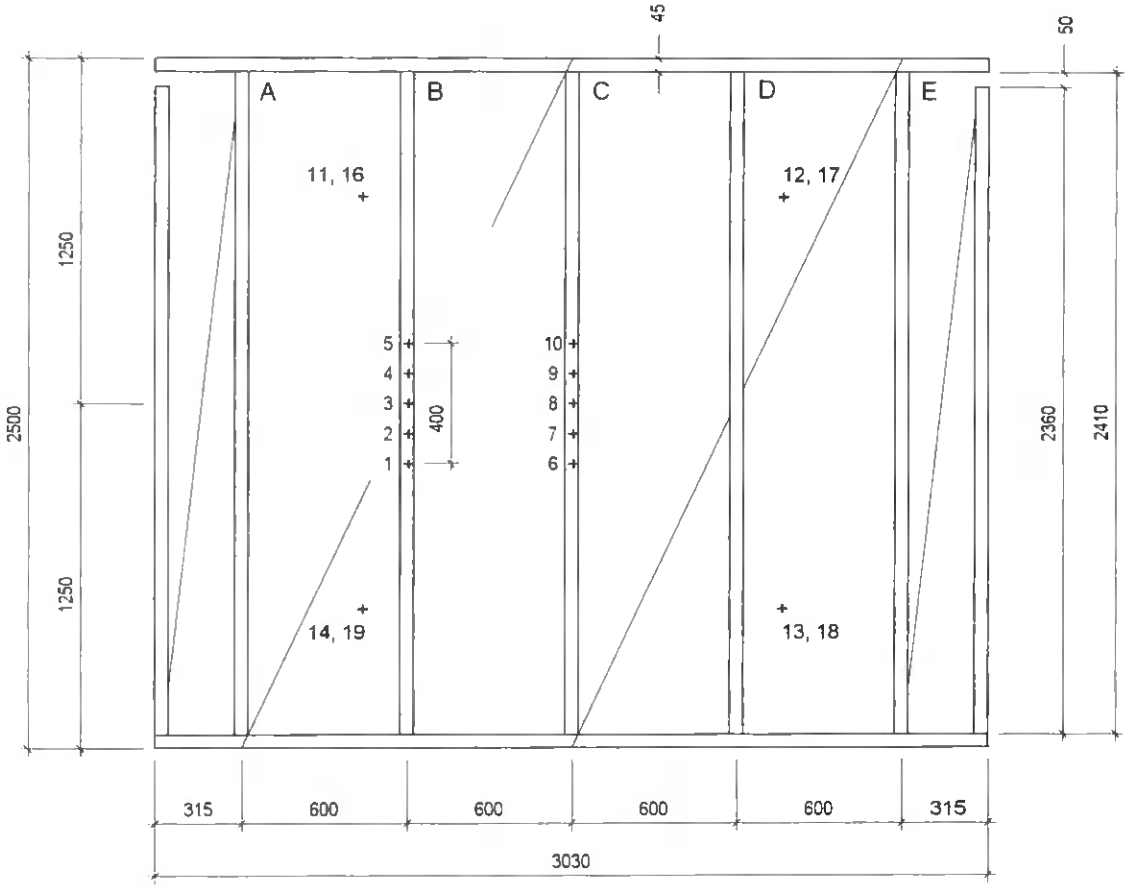

Dry density in kg/m^3

W1	367	337	301	302	331
W2	360	340	308	318	323
W3	252	304	317	305	364

Figure 3.2: Dimensions of wall assemblies W1-W3, arrangement of studs and arrangement gypsum plasterboards on fire-exposed side (W2 and W3). The position of studs and thermocouples is seen from the non-exposed side. The table below the figure shows the dry density of the studs in kg/m^3

On the fire-exposed side of the wall, in the case of specimen W2 and W3, the gypsum boards were 1200 mm wide and 2500 mm high. They were fixed to the timber frame using self-drilling screws with a length of 45 mm and a nominal diameter of 3,9 mm. The spacing of the screws was 200 mm along the edges and 300 mm along the intermediate studs B and C.

The opening of the oil-fired vertical furnace consisted of a water-cooled steel frame and at the lower support of a beam which was placed on two hydraulic jacks and movable in vertical direction. Between the supports and the sole plate and head plate respectively, 19 mm thick strips of silicate board were placed. The gap between the vertical edges of the wall and the steel frame were filled with rock fibre insulation.

At mid-height of the walls, on the non-exposed side, a wooden batten with a dimension of 30 mm H 45 mm and a length of 3 m was nailed to the load bearing studs. The purpose of this batten was to improve the bracing of the studs in their weak direction if the gypsum board strips should fail. By means of roller bearings at the ends of the batten, bracing forces could be taken by the steel frame without preventing lateral movement due to deflection of the wall.

3.3 LOCATION OF THERMOCOUPLES

Temperature measurements were made inside the studs as well as on both sides of the gypsum plasterboards on the non fire-exposed side of the wall. The position of the thermocouples in the studs can be seen from figures 3.2 and 3.3. Gauge points 11-15 are on the cavity side of the non-exposed gypsum plasterboard while gauge points 16-20 are on its exterior side.

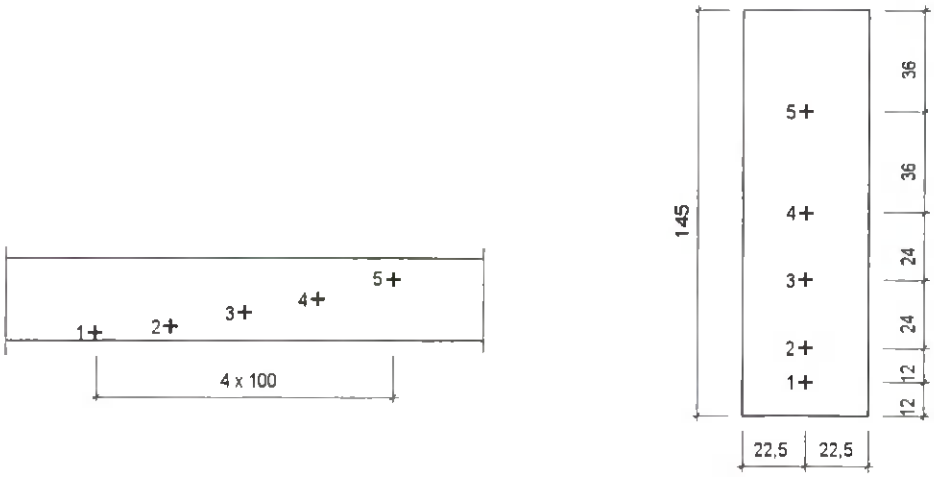

Figure 3.3: Position of thermocouples in the studs

3.4 TEST PROCEDURE

The walls were conditioned before the tests (20 °C/65 % RH). An axial force of 15 kN per stud was applied 30 minutes prior to the beginning of the fire test. The fire exposure was started and the temperature in the furnace was increased following the standard fire temperature-time curve according to ISO 834. The recorded temperature in the furnace and the pressure difference between the furnace and the test hall are shown in appendix B, figures B.2 and B.3. The applied load was held constant until failure occurred. After failure the oil burners were immediately turned off and the wall was unloaded. The specimen was then removed from the furnace and the fire in the wall was extinguished with water. The time between turning off the burner and extinguishing the fire in the studs was approximately 3 minutes. At heights of about 400, 800, 1250, 1700 and 2100 mm of the wall slices were cut out of the studs. The charcoal was then removed and the pieces put back into the climate chamber in order to be re-conditioned. Then the shape of the residual cross section was recorded by means of a digitizer.

3.5 RESULTS

3.5.1 TEST OBSERVATIONS

For observations during the fire tests, see Tables 3.2 - 3.4

Table 3.2: Observations during fire test of wall W1

Time in minutes	Observations
00:00	The test was started.
02:35 - 03.15	Ignition of the fire-exposed side of the wood studs
25:00	Deflection of the specimen becomes visible
40:00	Rate of deflection increases
49:30	Attachment of the gypsum board at the upper corner of the specimen fails and visible flames on the unexposed side
50:00	End of test

Table 3.3: Observations during fire test of wall W2

Time in minutes	Observations
00:00	The test was started
03:30	Ignition of the gypsum board lining paper
04:05	End of flaming
04:15	Vertical visible cracks on the fire-exposed gypsum boards
08:00	Plaster on the fire-exposed gypsum board joints begins to spall and fall down
16:30	Visible cracks on all fire-exposed boards
17:00 - 17:55	Ignition of the wood studs
25:30 - 38:30	Failure of the fire-exposed boards
32:30	Opening of gaps at the fire-exposed surface of horizontal insulation joints
34:00	Opening of gaps between mineral wool and studs on the fire-exposed side
40:00	Deflection of the specimen becomes visible
59:00	Loading could not follow deformation. Loading stopped
60:00	End of test

3.5.2 MECHANICAL PROPERTIES

During the fire tests the mid-deflection was recorded of the studs B, C and D, see figure 3.4. We can see that some difference exists between the deflections of the studs of one wall, but this difference does not correspond to the differences of the moduli of elasticity, c.f. the stud numbers in figure 3.2 and the data given in table 3.1.

The failure times of the walls, i.e. the time when the deflections-time curves are almost vertical, are the following:

W1: 50 minutes
W2: 59,5 minutes
W3: 75 minutes

Table 3.4: Observations during fire test of wall W3

Time in minutes	Observations
00:00	The test was started
04:05	Ignition of the gypsum board lining paper
04:25	End of flaming
07:30	Plaster on the fire-exposed board joints begins to spall and fall down
23:30	Small flame at fire exposed joint (stud C)
32:00	Curved shape of fire exposed boards between studs, short vertical cracks near studs
33:00	Flaming at the fire exposed side of the middle stud
45:00	Deflection of the specimen becomes gradually visible at the non-exposed side
51:00	Flaming at all vertical board joints of the fire exposed side
58:30	On the fire exposed side, opening of a board joint near the bottom of the middle stud
62:00	Large vertical crack in the fire exposed gypsum board between studs B and C, at the distance of 100 mm from stud B
63:15 - 69:00	Failure of the fire-exposed boards
67:00	Opening of gaps of horizontal insulation joints at the fire-exposed surface
73:00	Opening of gap between mineral wool and stud E on the fire exposed side
74:00	Loading could not follow deformation. Loading stopped.
75:00	End of test

We can see that the difference between failure times of the walls W1 and W2 is 9,5 minutes, due to the effect of the fire protection of the lining of gypsum plasterboard on the fire-exposed side, while in wall W3 the time to failure is increased by 25 minutes due to the effect of the gypsum plasterboard of type F.

The mean of the deflections of the studs B, C and D was calculated and the time difference t_{pr} was determined for equal mean deflections of the walls W1 and W2, and the walls W1 and W3 respectively. The time difference t_{pr}, i.e. the protective effect of the gypsum boards, is the horizontal distance between the deflection curves in figure 3.4. Plots of t_{pr} versus time t_1 for wall W1 are shown in figure 3.5. For comparison, the relationship between t_{pr} and failure time according to figure 2.18 is also shown in the diagram.

For wall W2 we get a difference of 12,4 minutes for a time of 45 minutes and of 15,1 minutes for a time of 30 minutes. These values are in the same order of magnitude as obtained by comparison of the corresponding regression curves for load ratio versus failure time, and of the effect of the protective gypsum boards on the charring depth as shown in figure 2.29. In wall W3 the effect of fire protection of the gypsum plasterboard of type F reaches its maximum after about 40 minutes.

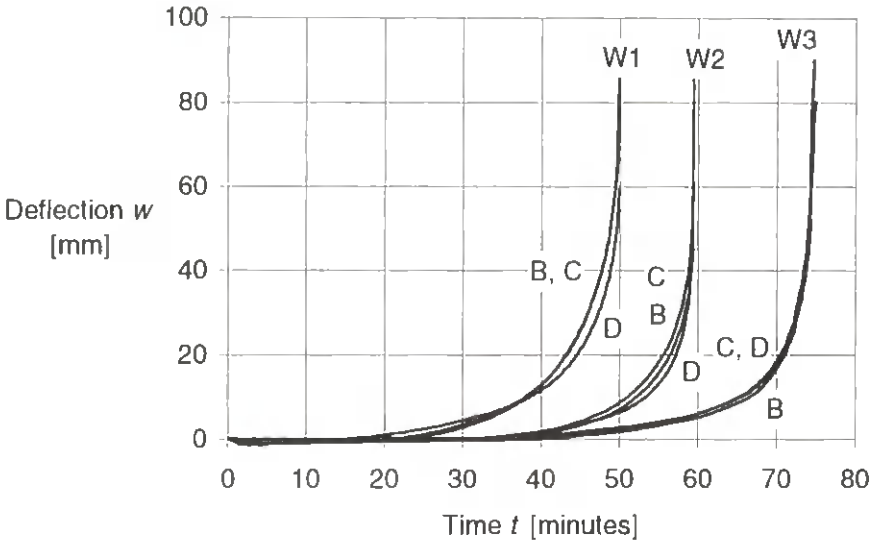

Figure 3.4: Mid-deflection versus time of studs B, C and D

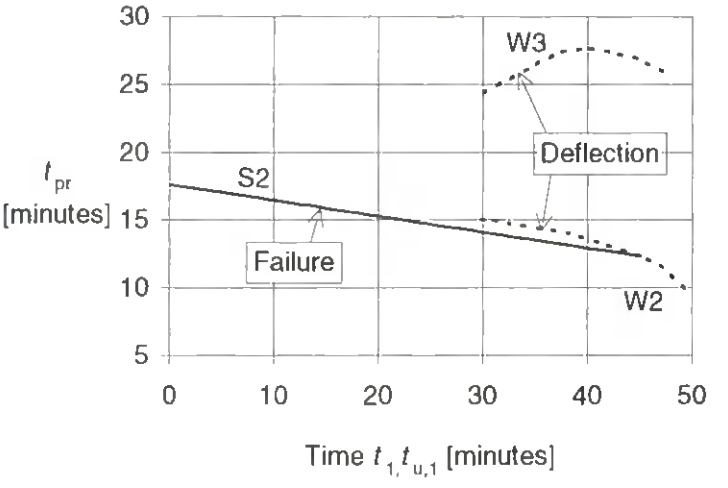

Figure 3.5: The effect of fire-protective plasterboard in tests W2 and W3 versus time for unprotected construction. The curve for series S2 is taken from Figure 2.18

3.5.3 TEMPERATURE MEASUREMENTS

3.5.3.1 Temperature in the studs

Plots of temperature versus time are shown in figure 3.6. The curve numbers refer to gauge points according to figures 3.2 and 3.3. The fire protecting effect of the gypsum boards attached to the walls W2 and W3 can be seen comparing the pairs of curves with numbers 1 and 6, 2 and 7, 3 and 8. Due to the opening of the joint between the gypsum boards at stud C, the temperature rise is greater at this stud than at stud B which is behind the vertical centre line of one of the boards. At the gauge points 3, 4, 8 and 9 a sudden rise of temperature occurs when the gypsum boards of type F begin to fall down, see table 3.4. Using these recorded temperatures, temperature profiles along the centre line of the cross section of the studs B and C were determined and plotted for some time values, see figures 3.7-3.8. For studs B of the

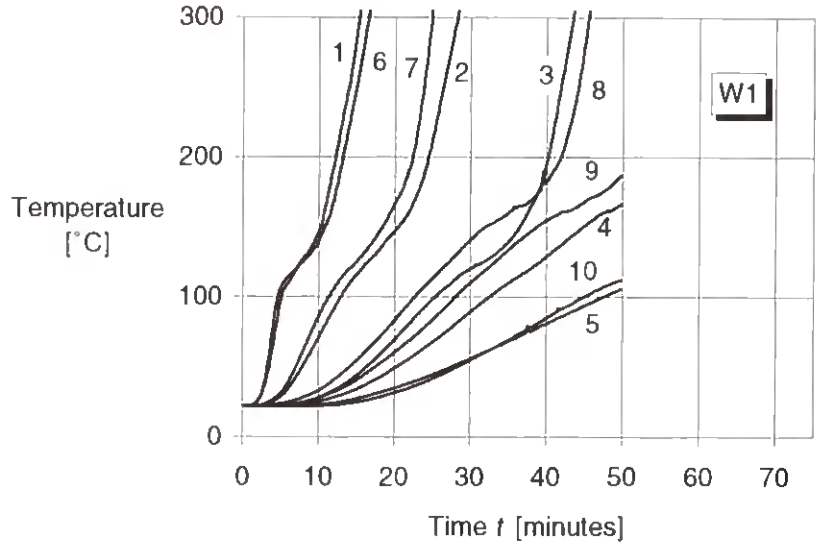

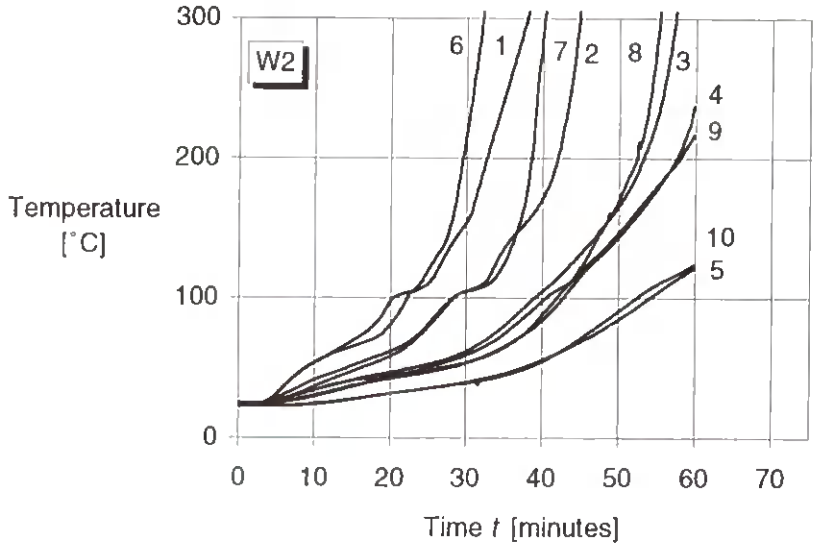

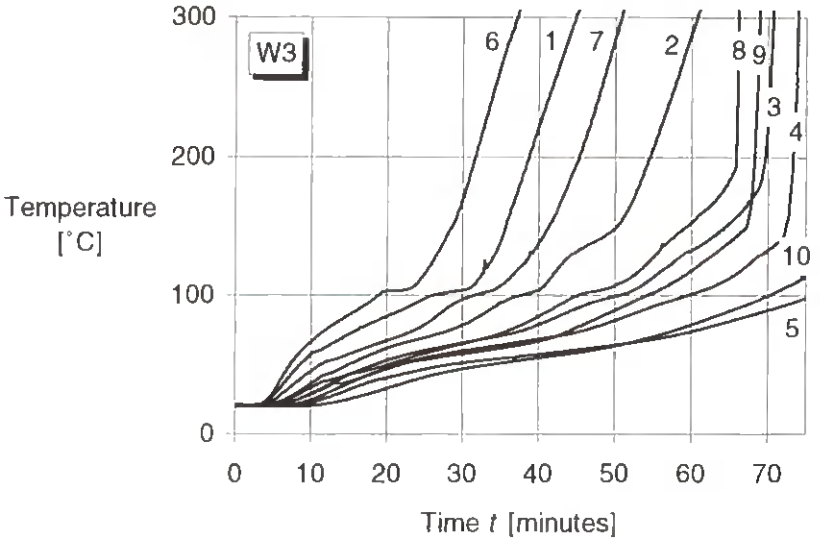

Figure 3.6: Temperature versus time in the studs B and C. The curve numbers refer to gauge points according to figures 3.2 and 3.3

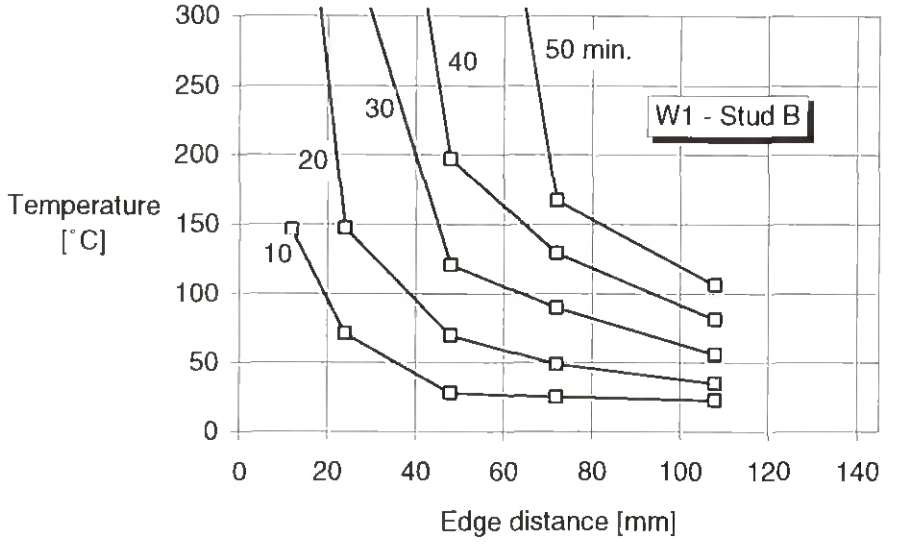

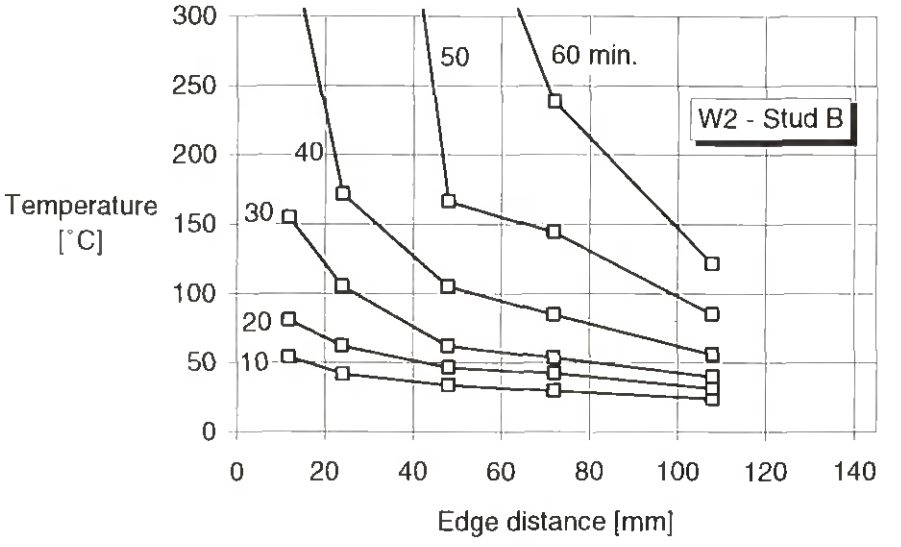

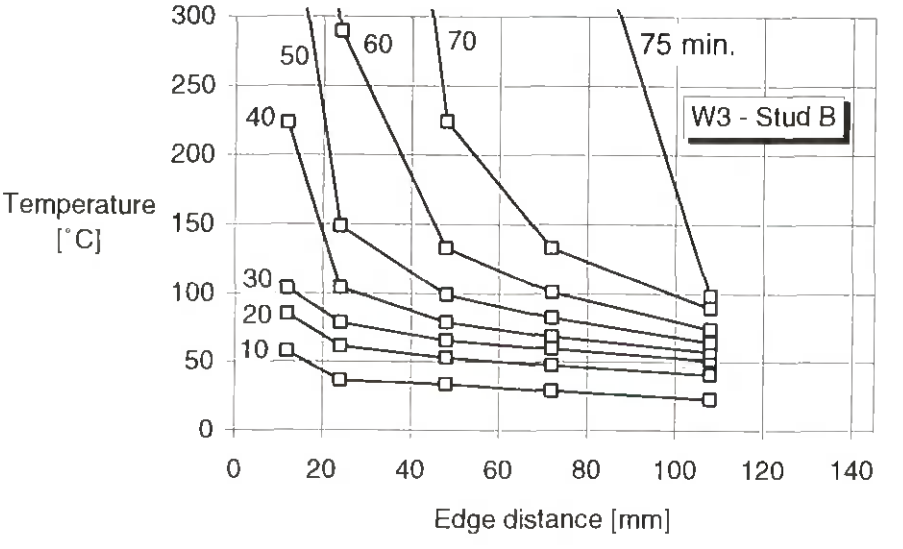

Figure 3.7a-c : Temperature profiles along the centre line of the cross-section of stud B

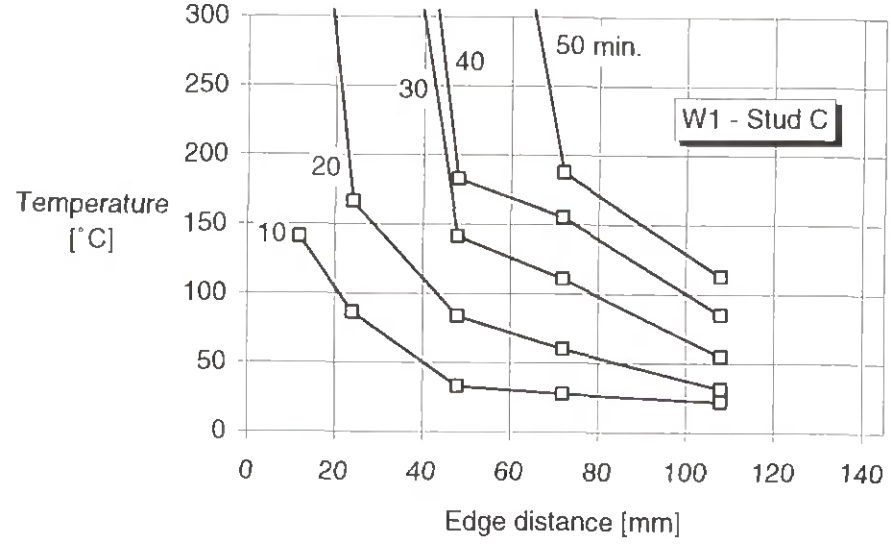

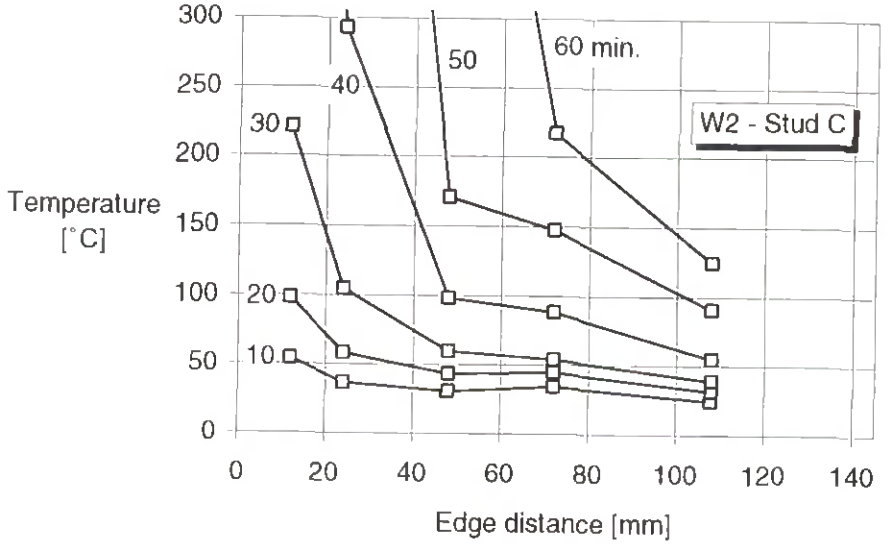

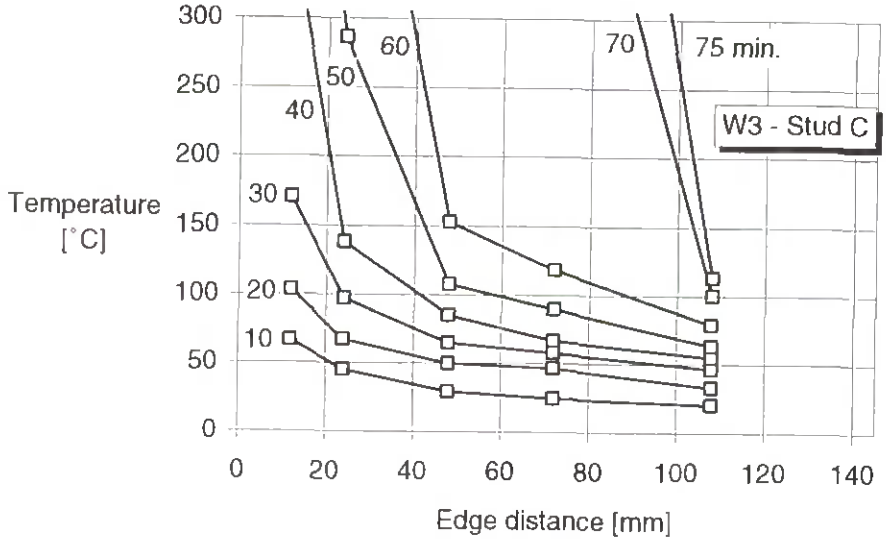

Figure 3.7d-f : Temperature profiles along the centre line of the cross-section of stud C

walls W1 and W2 the temperature profiles are very similar to the corresponding temperature profiles of series S2 and S3, see 2.20 and 2.21. From figure 3.7e and f we can see that the temperature profiles change very fast after 60 minutes, first at stud C and then at stud B, when the gypsum boards of type F begin to fall down. It is of interest to compare the temperature at time of failure, see figure 3.8. While the temperature profiles are of about the same shape in the walls W1 and W2, e.g. the rise of temperature from 100 to 300 / C occurs within a distance of about 45 mm, in wall W3 the corresponding rise of the temperature occurs within a distance of between 10 and 20 mm. The temperature at gauge points 5 and 10 at a distance of 109 mm from the original edge is not much influenced by the total failure of the gypsum board.

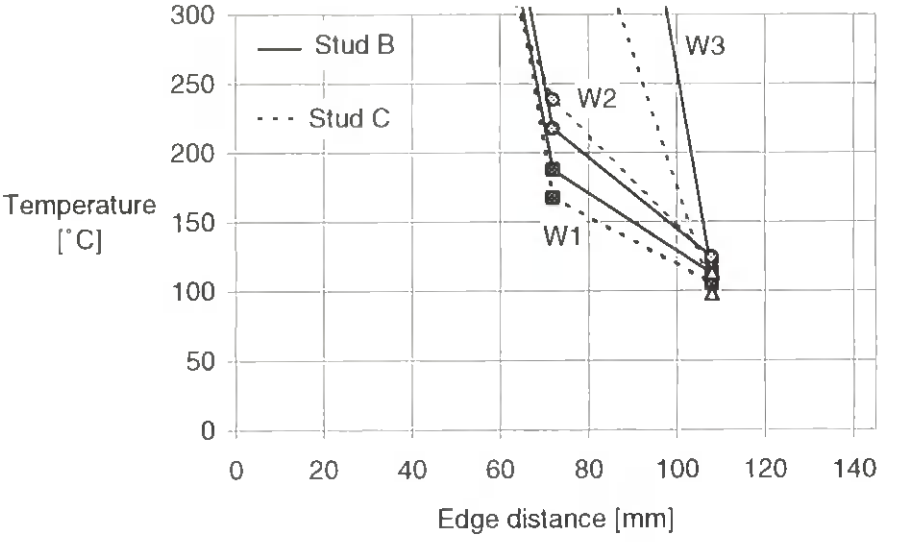

Figure 3.8: Temperature profiles along the centre-line of the cross-section at failure

3.5.3.2 Temperature between the studs

Plots of temperature versus time recorded at both sides of the gypsum boards on the unexposed side of the wall are shown in figure 3.9. The curve numbers refer to gauge points according to figures 3.2 and 3.3. At walls W2 and W3 a sudden temperature rise is observed after 6 to 7 minutes due to the ignition and burning of the paper facing of the gypsum boards, see Tables 3.3 and 3.4.

In figure 3.10 mean values of temperatures recorded at gauge points 11-15 and 16-20 respectively are plotted as a function of time. Comparing the temperature recorded at the inner side of the gypsum boards of the walls, we get the protective effect of the gypsum boards in the walls W2 and W3 in relation to the unprotected wall W1, see figure 3.11 where the curves are plotted as bold curves. For comparison, the curves of figure 3.5 are added as dotted lines. We can see that the fire protective effect of the gypsum boards is different with respect to the chosen criterion, but at the time of failure of the wall this difference is very small.

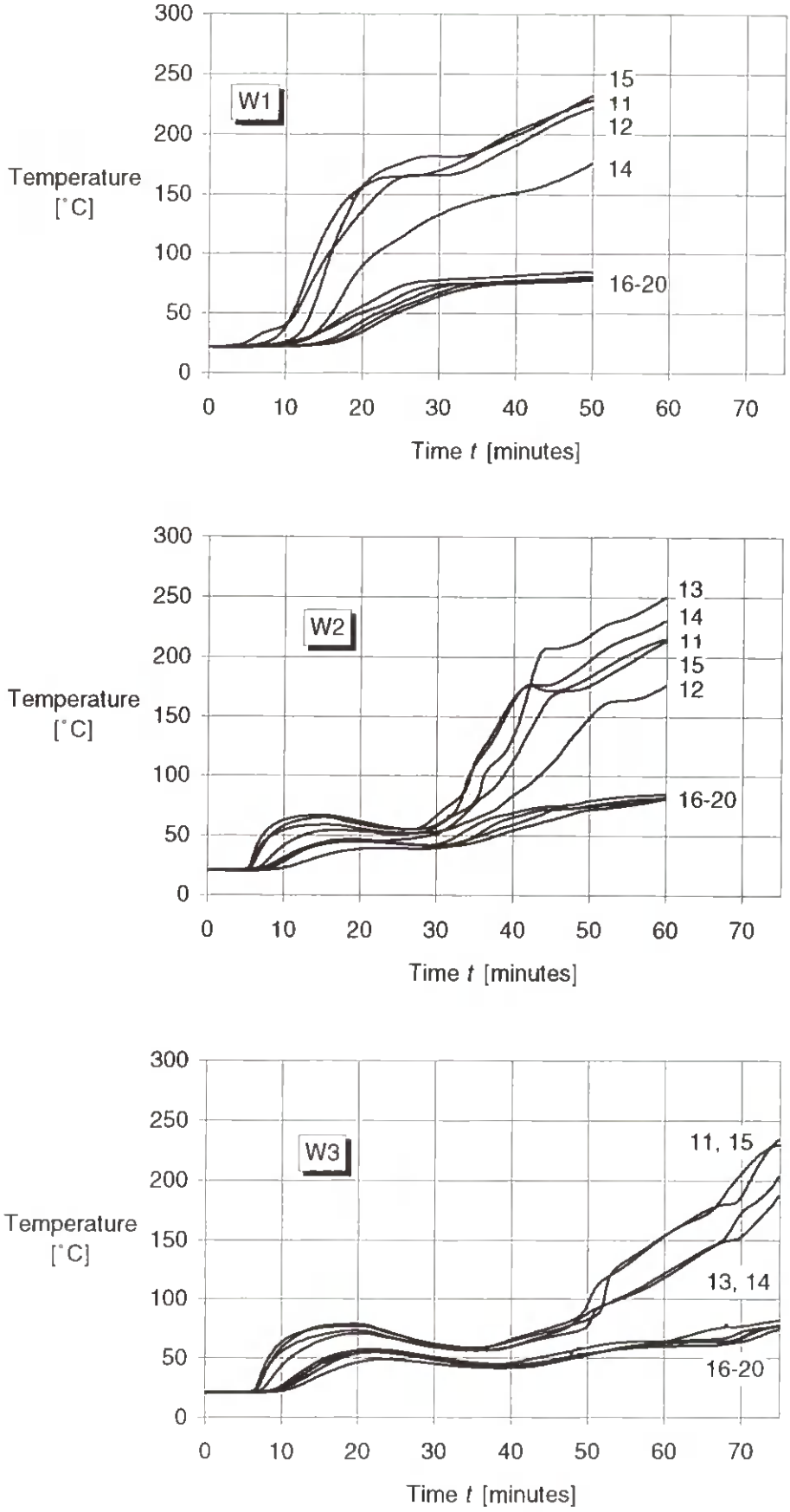

Figure 3.9: Temperature versus time measured between the studs on both sides of gypsum plasterboard on the unexposed side of the wall

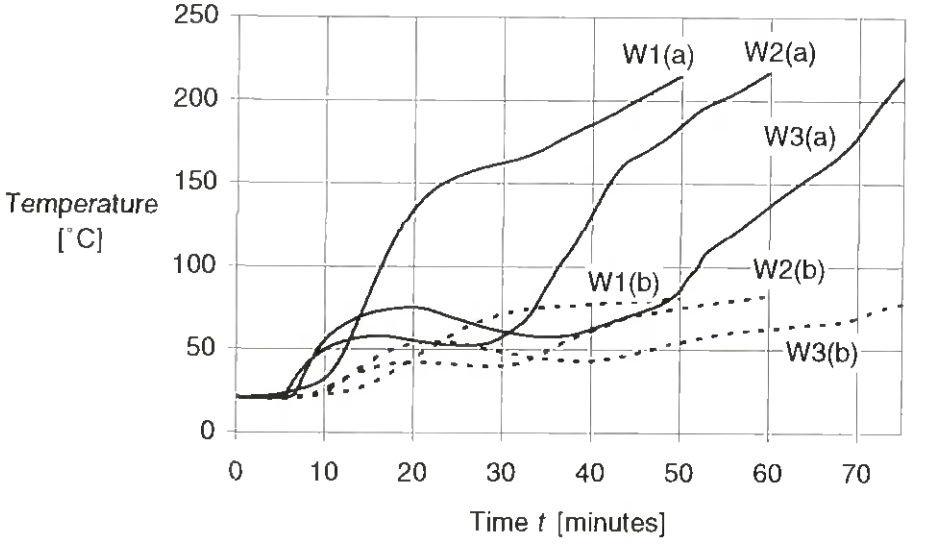

Figure 3.10: Averaged values of temperature versus time on cavity side (gauge points 11-15, curves a) and exterior side of non exposed side of gypsum plasterboard (gauge points 16-20, curves b) of walls W1-W3

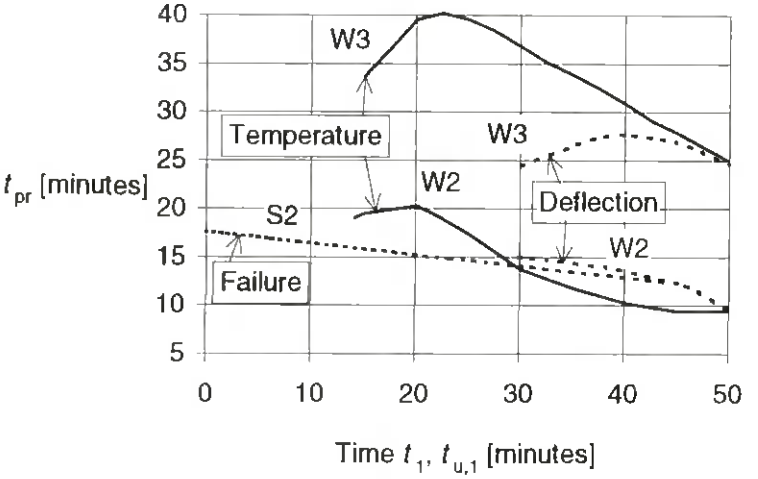

Figure 3.11: The effect of the fire protective gypsum plasterboard on the temperature recorded at gauge points 11-16, deflections, and failure times of series S2

3.5.4 CHARRING DEPTHS

Some of the recorded residual cross sections of wall W3 are shown in Appendix C, figure C.6. The minimum charring depths were determined, see figure 2.28, and are shown in figure 3.12 for positions at different distances x from the lower support of the walls. There exists a considerable scatter of the results along the studs and between the studs, but the order of magnitude is about the same for the three walls. For each of the walls the mean charring depth was determined, see table 3.5. The mean values of the three walls are very close. The total deviation from the total mean is not greater than two percent. A conclusion is that the charring depth is the main parameter for the failure of the walls. Due to the load sharing effect of the wall the failure load and the time to failure is apparently not much affected, even though there is a considerable difference of charring depths in the different studs.

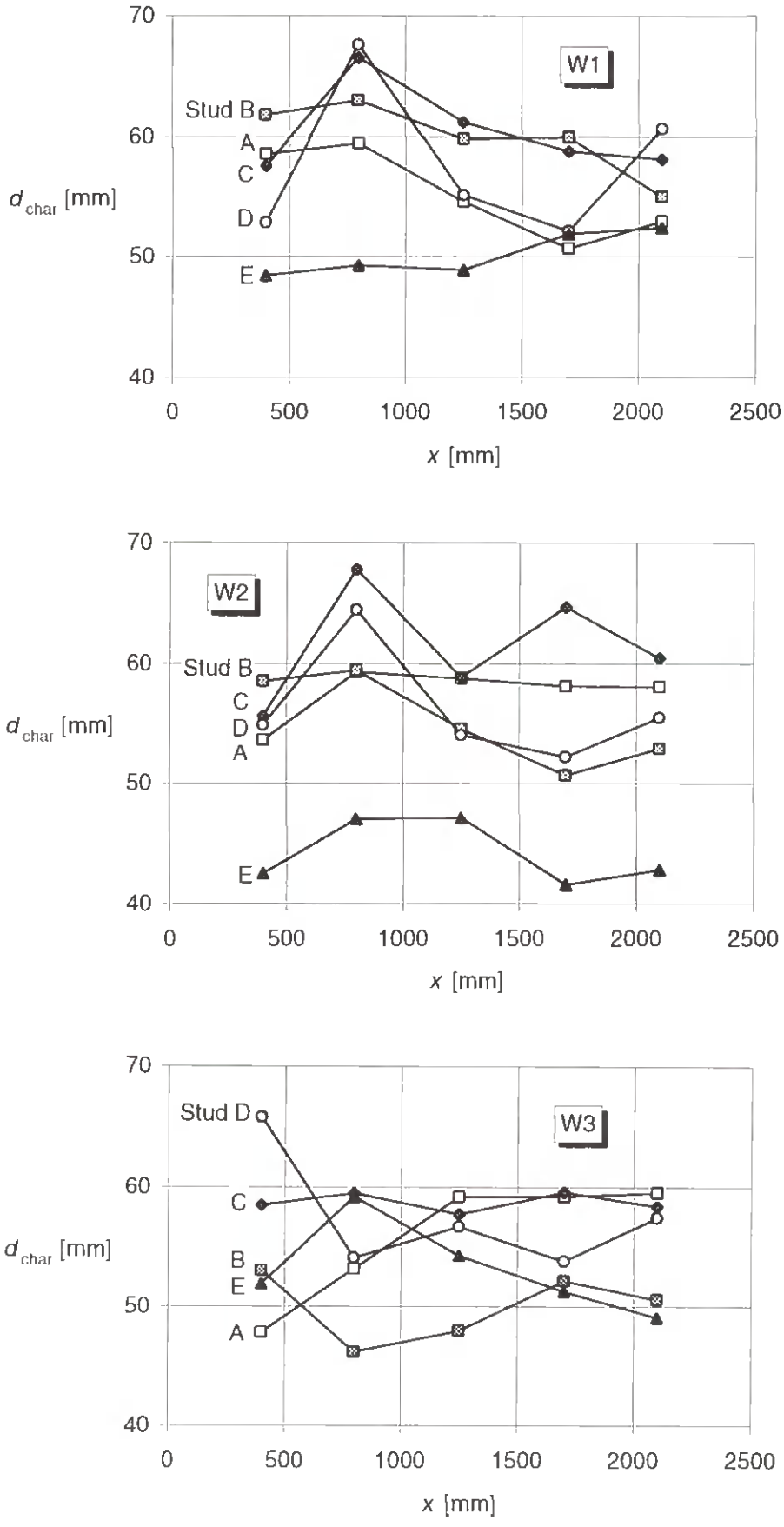

Figure 3.12: Charring depths near the centre-line of the cross-section at different heights of the walls

Table 3.5: Mean charring depths in walls W1-W3

	Mean charring depth d_{char} [mm]	Relative charring depth $\frac{d_{char}}{55,55}$
W1	56,68	1,020
W2	54,93	0,989
W3	55,05	0,991
W1-W3	55,55	1,000

In the same way as described in 2.7.4, the charring depths are also presented as the position of the 300 degree isotherm, see figure 3.13. We can see that curves for the wall W1 agree well with the curves obtained from series S1 and S2. The effect of the gypsum board joint at stud C can be seen from the curves for the walls W2 and W3. Due to the opening of the joints the charring depth is greater at stud C than at stud B which is placed behind the gypsum board. The curve obtained for series S2 agrees fairly well with the curves for W2. We can see that the charring depth obtained in small-scale tests agrees well with those recorded in the full-scale tests. In the case of wall W3, in the final stage of the test, the position of the 300 degree isotherm does not agree with the charring depths recorded after failure, see table 3.5 and figure 3.12. Since this discrepancy occurs at both studs B and C, it could be argued that the thermocouples were not in the position as given in figure 3.3. Assuming that the thermocouples were attached at edge distances of 12, 24, 36, 48 and 60 mm we would get results with better agreement with the recorded charring depths.

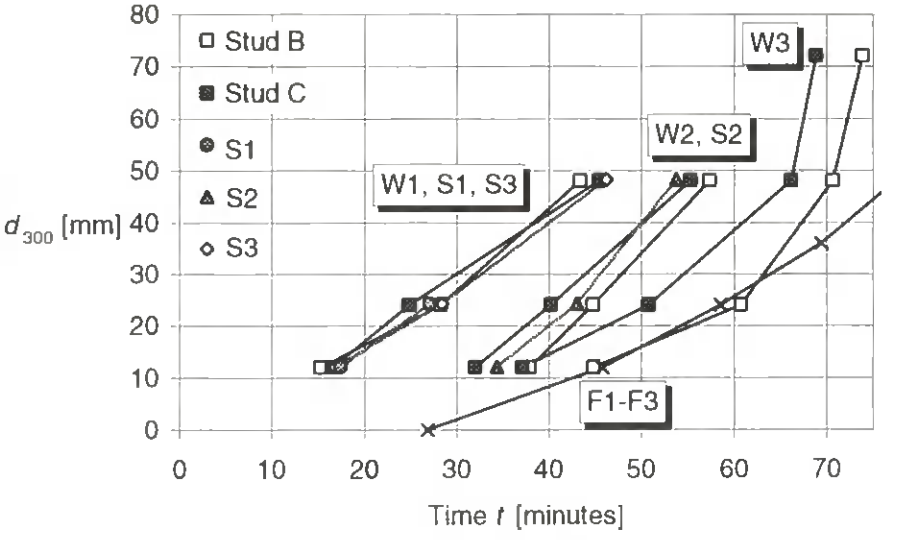

Figure 3.13: Position of the 300-degree isotherm at centre line of cross section in the walls W1-W3, members of series S1-S3 and specimens F1-F3

The effect of the protective gypsum boards on the delay of charring is shown in figure 3.14. Because of the joint of the boards at stud C, the lag of charring at stud C is about two third of the lag at stud B.

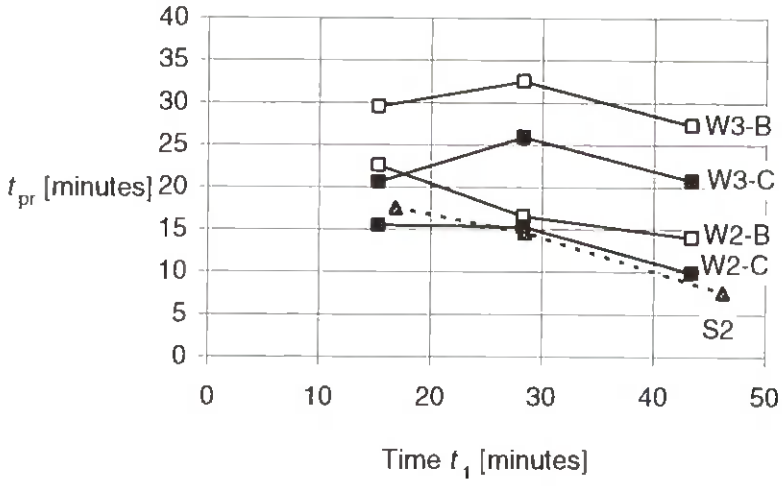

Figure 3.14: The effect of the fire protective gypsum board on the position of the 300-degree isotherm in studs B and C

4 ANALYTICAL MODEL

4.1 GENERAL

The residual cross sections as shown in Appendix C are far too complicated to be used in practical design. In König (1991) different approaches to modelling the members in bending were discussed. It was shown that the residual cross section could be replaced by a rectangular cross section in calculation. Such simplification is in line with rules given in Eurocode 5, Part 1.2. In the code strength and stiffness parameters are reduced by multiplying with a modification factor for fire $k_{mod,f}$. In the following simplified expressions are derived for the determination of the charring depth and the reduction of strength and stiffness parameters.

4.2 BENDING STRENGTH

From the recorded residual cross sections the areas, section moduli and second moments of area were determined. An equivalent residual cross section with the original width of 45 mm was defined such that it has the same section modulus as the real residual cross section. The width b_f of this cross section was equal to the original width of 45 mm and the depth determined as

$$h_f = h - d_{char,n} \tag{4.1}$$

where h is the original depth of the cross section and $d_{char,n}$ is the notional charring depth, see figure 4.1. In figure 4.2 the ratio of the notional charring depth and the minimum charring depth d_{char} is shown as a function of the minimum charring depth which is measured at the centre line of the cross section as shown in figure 2.28. For small charring depths this ratio is greater than for large ones when the minimum charring depth itself is influenced by the charring from the sides.

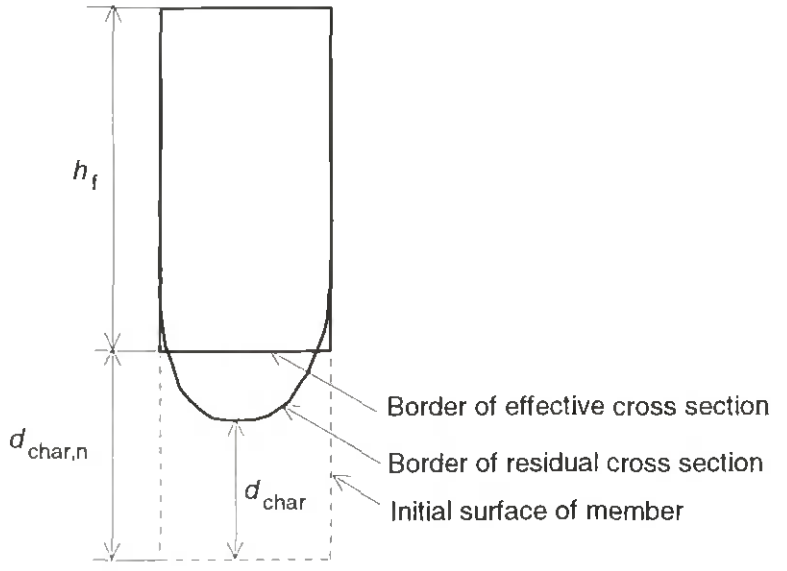

Figure 4.1: Definition of effective and residual cross section

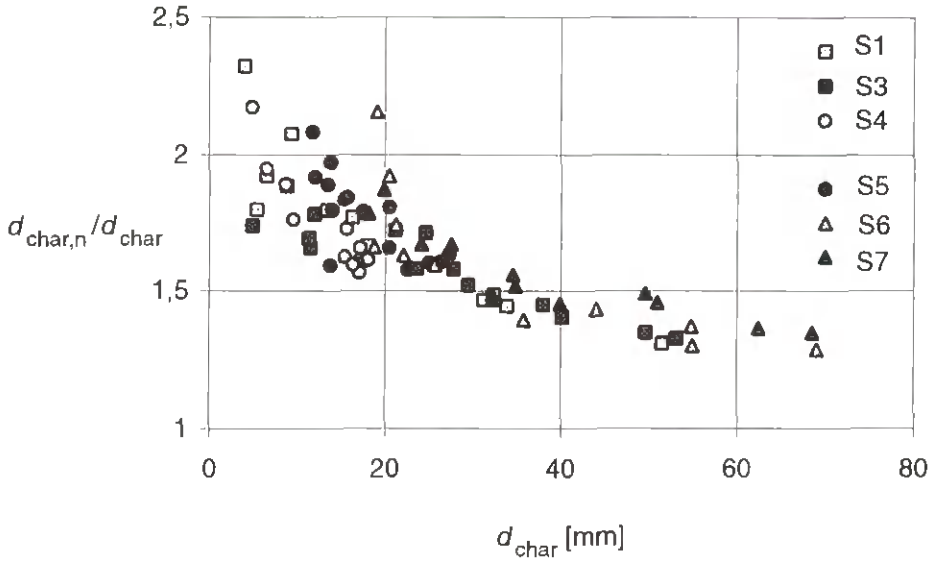

Figure 4.2: Ratio of notional and minimum charring depth versus notional charring depth

From the designer's viewpoint it is desirable that the charring rate is constant with time. While the relationship between the real charring depth and time is non-linear, (see figure 2.31), the plot of the notional charring depth versus time shown in figure 4.3 is approximately linear due to the fact that the minimum charring depth is smaller in the beginning (see figure 2.31).

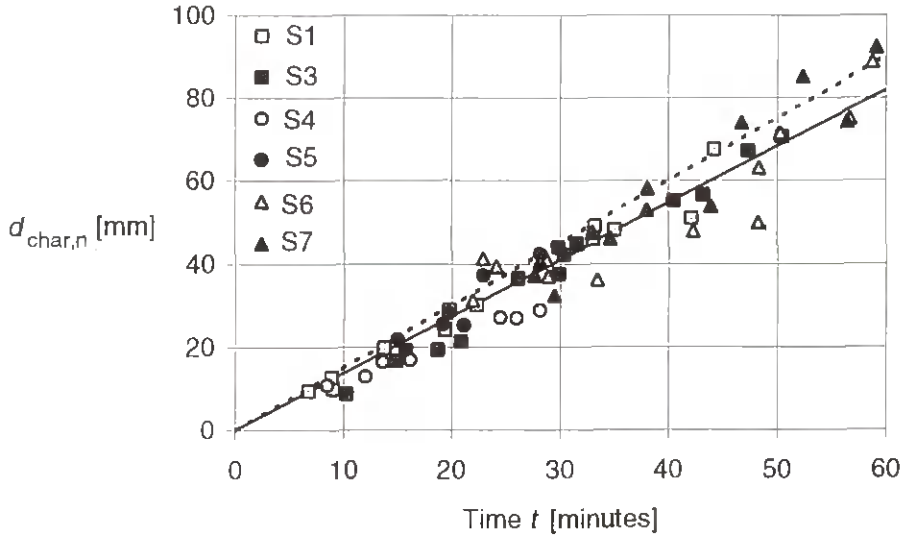

Figure 4.3: Notional charring depth versus time

The regression line is described by

$$d_{char,n} = 1{,}365\, t \tag{4.2}$$

For design the dotted line described by the expression

$$d_{char,n} = 1{,}5\, t \tag{4.3}$$

should be used. The notional charring rate to be used is therefore β_0 = 1,5 mm/minute.

For each specimen of series S1 and S3 to S7 the reduction of the bending strength was determined as

$$k_{\mathrm{mod,f}} = \frac{M_{\mathrm{f}}}{M_0}\frac{W_0}{W_{\mathrm{f}}} \tag{4.4}$$

where

M_{f} Bending moment capacity in the fire test
M_0 Predicted bending moment capacity at normal temperature
W_{f} Section modulus of residual cross section
W_0 Section modulus of original section

The results show a considerable scatter, see figure 4.4. One of the reasons is the scatter of results from reference tests at normal temperature (see figure 2.1), which influences the accuracy of the predicted values of M_0. For each group of series S1/S4/S6 and S3/S5/S7 regression lines are determined by linear regression under the condition that the modification factor is unity when the charring depth is zero. The regression lines are described by the

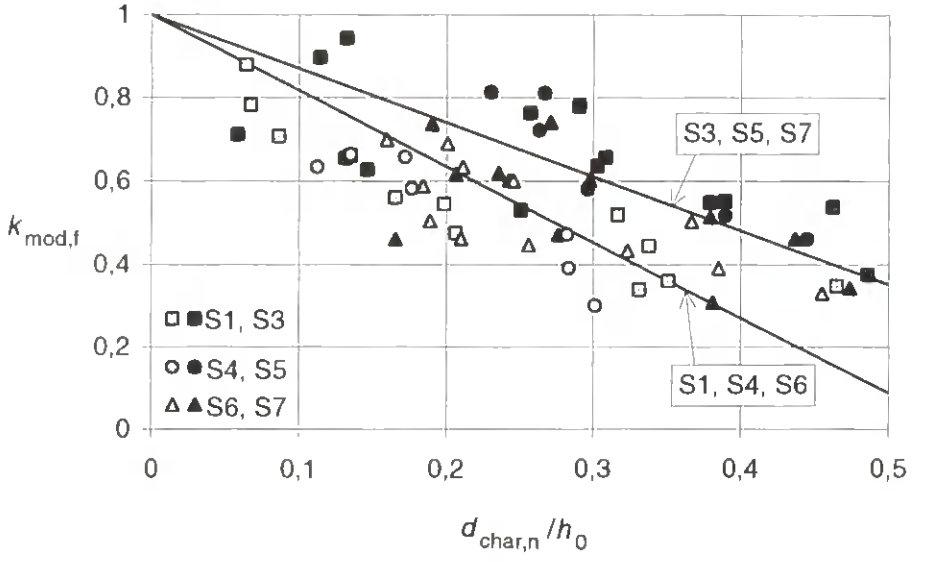

Figure 4.4: Modification factor for fire versus notional charring depth ratio

following expressions:

$$k_{\mathrm{mod,f}} = 1 - 1{,}825\frac{d_{\mathrm{char,n}}}{h} \tag{4.5}$$

when the fire exposed side is in compression, and

$$k_{\mathrm{mod,f}} = 1 - 1{,}3\frac{d_{\mathrm{char,n}}}{h} \tag{4.6}$$

when the fire exposed side is in tension.

4.3 FLEXURAL STIFFNESS

From the designer's viewpoint it is desirable that the same charring rate is used when the section modulus and the flexural stiffness is calculated. Thus, instead of calculating another notional charring depth which gives the same second moment of area of the residual cross section, the same notional charring rate as obtained in 4.2, equations (4.2) or (4.3), should be used. With the following modification factor

$$k_{\text{mod,f}} = 1 - 2{,}1\frac{d_{\text{char,n}}}{h} \tag{4.7}$$

for series S1, S4 and S6 and

$$k_{\text{mod,f}} = 1 - 1{,}1\frac{d_{\text{char,n}}}{h} \tag{4.8}$$

for series S3, S5 and S7 we get fits of the experimental relationships between the flexural stiffness ratio and time. See figures 4.5 and 4.6. We can see that the agreement of the calculated curves is fairly good if we consider experimental curves for load ratios between 0,1 and about 0,3. In normal fire design practice load levels would be of this order of magnitude. Equations (4.7) and (4.8) can thus be used for different member depths.

4.4 WALL STUDS

König and Källsner (1988) presented two models which take into account the partial clamping of the stud ends. When the stud is deflecting, due to the rotation of the stud ends, the loading point of the axial force is moving towards the edge on the unexposed side of the member. In one of the models the end surfaces were idealized as being shaped as convex cylindric surfaces, thus allowing the stud to roll on the support plate. See figure 4.7. The radius of the cylindrical end surface is dependant on the stiffness of the sole and head plate perpendicular to grain. It was obtained from tests at normal temperature where the charring was simulated by means of removing layers of the studs by planing.

The relationship of the mid-deflection of the studs of wall W1 was calculated, using the stiffness properties presented by König and Källsner (1988), the modulus of elasticity given in Table 3.1, the charring depth according to Equation (4.2) and the modification factor for fire according to Equation (4.8). See figure 4.8, curve (a). We can see that the time of failure is predicted fairly well, while the calculated deflection is much smaller than the experimental data. A possible conclusion is that the stiffness of the foundation was smaller in the fire test than assumed due to the influence of the elevated temperature on the modulus of elasticity perpendicular to grain of the sole and head plate. By increasing the stiffness of the foundation a better agreement was achieved, see curve (c). In these calculations modification factors obtained from series S3, S5 and S7 were used, i.e. the fire exposed side was in tension. If we use the modification factor according to Equation (2.7) for series S1, S4 and S6 the time of failure is underestimated, see curve (b). The reason is that the influence of creep which occurs in parts of the cross section is less when the stud is loaded in axial direction and more similar to the conditions when the member is in bending and its fire exposed side is in tension.

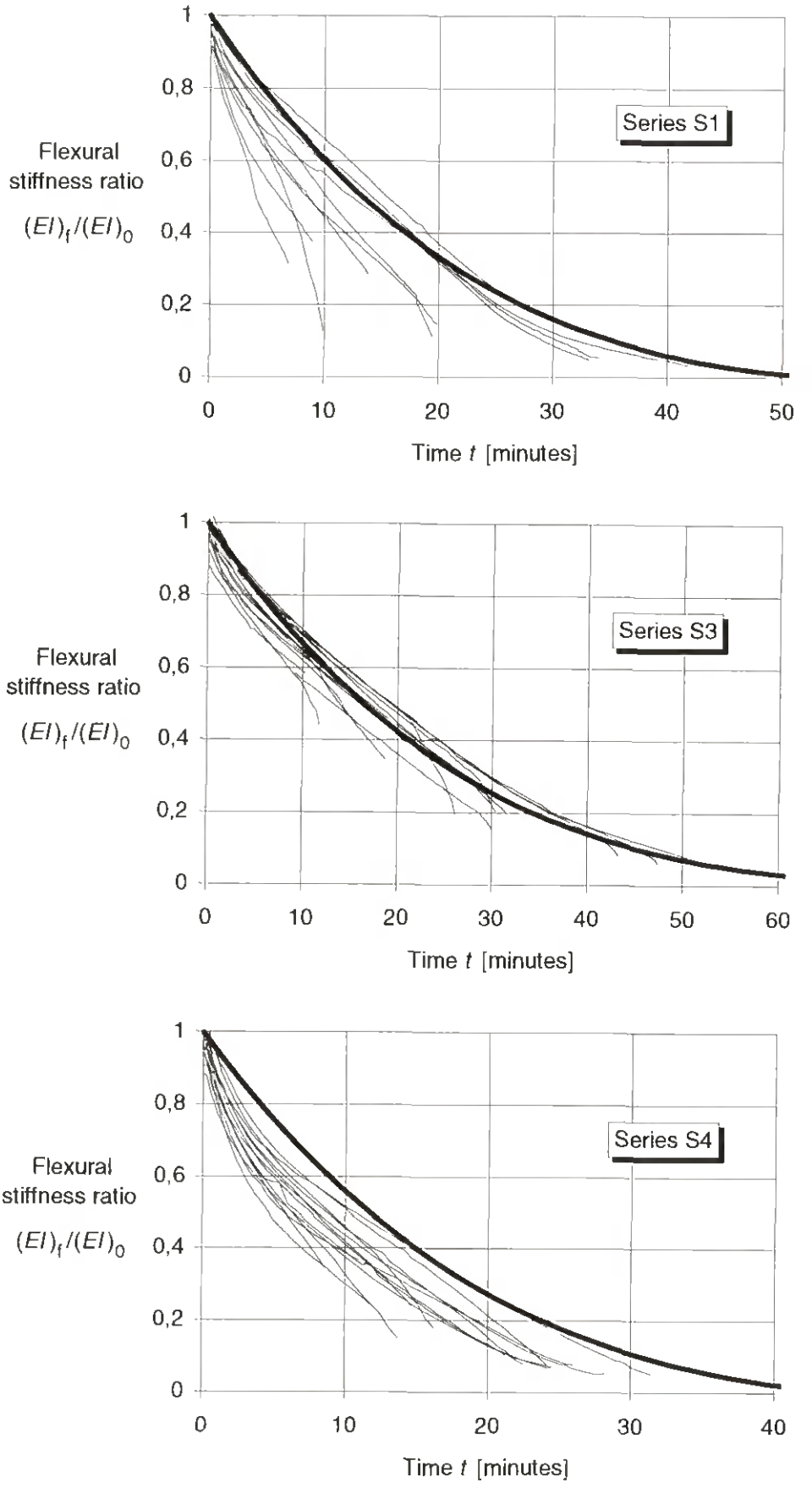

Figure 4.5: Flexural stiffness ratios versus time in series S1, S3 and S4 - comparison of model and test results

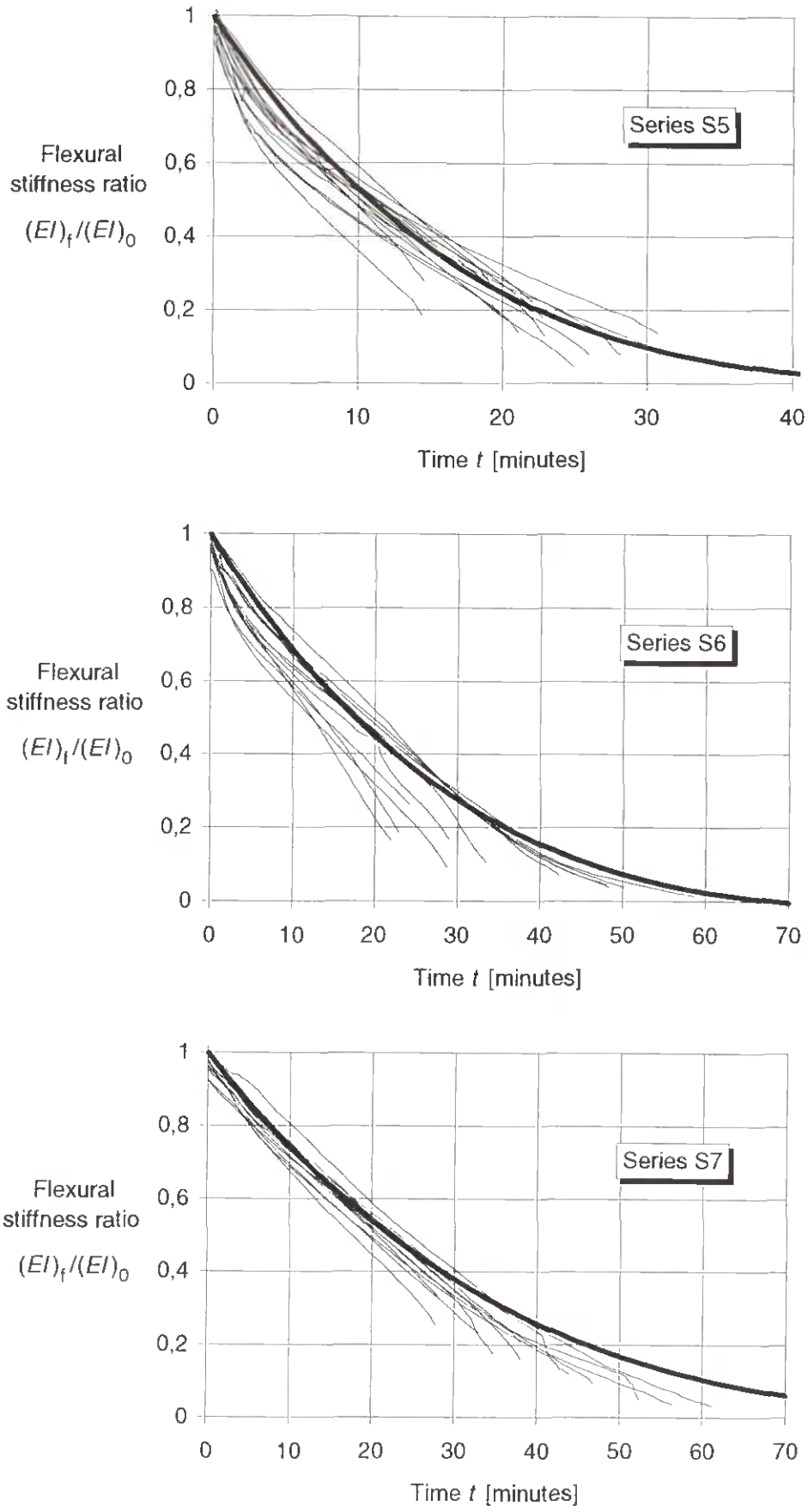

Figure 4.6: Flexural stiffness ratios versus time in series S1, S3 and S4 - comparison of model and test results

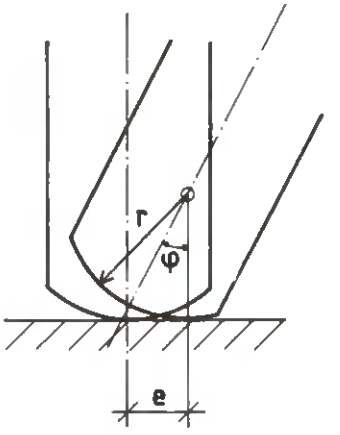

Figure 4.7: Modelling of stud end by means of cylindrical surface

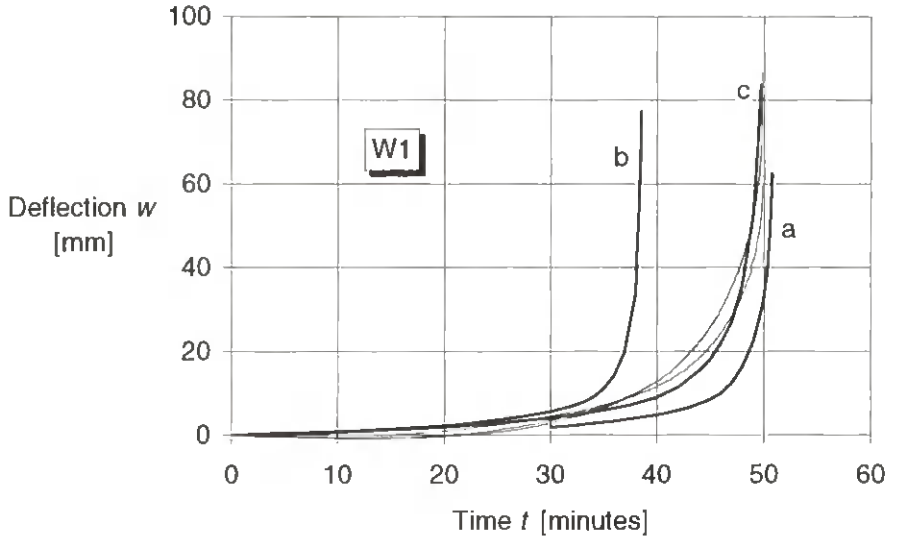

Figure 4.8: Comparison of calculated deflections (bold lines) of studs of wall W1 with test results

In practical design the designer wants to know the failure time and the failure load. In order to avoid the use of the complicated analytical model used in the calculation of the curves (a) to (c), the following simplifications were made: 1) The end supports of the studs are assumed to be hinged, 2) the axial load is assumed to be centric. Using the column buckling formulae according to Eurocode 5, Part 1-1 (ENV 1995-1-1) we obtain the relationship between failure load and time to failure, i.e. the fire resistance, shown in figure 4.9. In this calculation the compressive strength of the timber was put equal to 40 N/mm^2 , obtained from the assumption that the ratio of the modulus of elasticity and compressive strength in the direction of the grain is 300. The agreement with the experimental failure time of 50 minutes for an axial load of 15 kN is good. In reality, and in the analytical model, the effect of load eccentricity due to the charring on one side is compensated by the fact that the loading point is moving towards the edge of the stud.

Figure 4.9: Example of relationship between load bearing capacity of stud and fire resistance (time to failure)

5 CONCLUSIONS

From this investigation the following conclusions can be drawn:

- Traditionally, fire testing of wall and floor assemblies has been made by performing full-scale tests. In this investigation we demonstrate that small-scale testing can be an effective method in studying the behaviour of load bearing fire-exposed walls and floors. This method has the advantage that the influence of specific parameters on the total behaviour can be studied separately, e.g. the properties of timber with respect to charring and loss of strength, and the effect of fire protective claddings. There is, of course, a limitation of using small-scale tests, since some materials behave differently, e.g. gypsum plasterboards. Their full-scale effect should be investigated separately, and the results of small-scale testing corrected correspondingly.

- Traditionally, in fire testing of loaded structures, the load is applied at least 30 minutes prior to the fire test (ISO 834) and kept constant during the whole fire test. In practice it would often be desirable to use the possibility of varying the load during the fire test, in order to be able to get failure at a specified time. A test procedure could be that a load level is chosen in order to prevent premature failure, e.g. failure before a target fire resistance is reached. In the last stage of the fire test the applied load is increased in order to provoke failure at the target time, or as immediately as possible after that time. It is shown that the influence of a variable load during the fire test on the results is small and should be disregarded in practice. One should keep in mind that even in fire testing with a constant load the strain rate is different from zero, since the residual cross section is decreasing and the stress-strain curve of the material is in the case of compression pronounced non-linear.

- The fire resistance is dependent on the applied load, i.e. the load in relation to the load-bearing capacity at normal temperature

- The charring rate is independent of the state of stress

- The charring depth can be defined as the location of the 300-degree isotherm.. It would be practical to use this definition in test standards for the determination of charring rates.

- The conditions of charring and strength of a fire exposed members which are partially protected by rock fibre insulation can be described in a simplified analytical model even though the shape of the residual cross section is irregular and the internal stress distribution in the residual cross section is dependant on the state of stress on the fire exposed side. The model is such that the real residual cross section is replaced by a rectangular cross section, and the reduction of strength and stiffness properties is given by simple expressions.

- Calculating the failure load of a wall stud, the following simplified assumption may be made: the complicated conditions at the stud ends are replaced by hinged supports, the axial load is centric and the imperfections of the stud is the same as at normal temperature design.

- The contribution to fire resistance by the fire protective gypsum plasterboards varies with time.

6 REFERENCES

EN 408, Timber structures - Test methods - Structural timber and glued laminated timber. Determination of some physical and mechanical properties

ENV 1995-1-2: 1994, Eurocode 5, Design of timber structures, Part 1.2, General rules - Structural fire design

Glos, P. & Henrici, D., 1990, "Festigkeit von Bauholz bei hohen Temperaturen". Institut für Holzforschung der Universität München, München

Hadvig, S., 1981, "Charring of wood in building fires". Technical University of Denmark, Lyngby

Hall, G.S., 1968, "Fire resistance tests of laminated timber beams". Trada Research Report WT/RR/1, High Wycombe

Hao, H.C. & White, R. H., 1992, "Burning rate of solid wood measured in a heat release rate calorimeter". Fire and Materials, Vol. 16, 197-206

ISO 834-1975, Fire-resistance tests - Elements of building construction.

König, J., 1988, "The structural behaviour of axially loaded wood studs exposed to fire on one side". Swedish Inst. for Wood Techn. Res., Report No. I 8808057, Stockholm

König, J. & Källsner, B., 1988, "The influence of the support conditions on the load bearing capacity of axially loaded wood studs under simulated fire conditions". Proceedings of the 1988 International Conference on Timber Engineering, Seattle

König, J. & Norén, J., 1991, "Fire tests on timber frame members under pure bending". 1991 International Timber Engineering Conference, London

König, J., 1991, "Modelling the effective cross section of timber frame members exposed to fire". CIB-W18A Meeting Twenty-four, Oxford

Meyer-Ottens, C., 1979, "Feuerwiderstandsdauer unbekleideter hoher Rechteckbalken aus Brettschichtholz". Published in Forschungsbeiträge für die Baupraxis, Karl Kordina zum 60. Geburtstag gewidmet. Wilhelm Ernst & Sohn, Berlin

Mikkola, E., 1990, "Charring of wood". VTT - Technical Research Centre of Finland, Espoo

Norén, J., 1988, "Failure of structural timber when exposed to fire". Proceedings of the 1988 International Conference on Timber Engineering, Seattle

Östman, B., König, J. & Norén, J, 1994, "Contribution to fire resistance of timber frame assemblies by means of fire protective boards". 3rd International Fire and Materials Conference, Washington DC

prEN 520, Gypsum plasterboards - Specifications - Test methods, Draft standard

Schaffer, E. L., 1967, "Charring rate of selected woods - transverse to grain". Forest Products Laboratory, Madison

APPENDIX A - TEST RESULTS - REFERENCE TEST SERIES R1-R3

Table A1: Test results of reference tests - Series R1 (45 mm × 145 mm)

Specimen No.	Moisture content u	Dry density ρ_{0u}	Bending strength f_m	Regression line	Regression coefficient r^2
	[%]	[kg/m^3]	[MPa]		
254	13,0	324	51,7		
257	13,9	355	55,5		
206	14,1	369	47,6		
221	14,1	369	43,8		
215	13,9	374	41,1		
235	14,1	388	62,6	$f_m = 0{,}138\ \rho_{0u}$	0,42
229	14,3	422	60,4		
203	14,8	442	60,1		
267	14,0	452	67,9		
244	14,5	459	66,1		
213	14,5	462	53,8		
246	14,7	473	63,3		

Table A2: Test results of reference tests - Series R2 (45 mm × 95 mm)

Specimen No.	Moisture content u	Dry density ρ_{0u}	Bending strength f_m	Regression line	Regression coefficient r^2
	[%]	[kg/m^3]	[MPa]		
105	13,6	472	63,4		
110	13,3	426	59,8		
112	13,8	413	58,4		
126	13,6	432	68,5		
127	13,5	405	62,5		
129	13,8	389	65,4		
133	13,6	480	72,9	$f_m = 0{,}158\ \rho_{0u}$	0,29
136	13,8	488	76,2		
137	13,9	455	79,1		
140	13,4	408	70,9		
141	13,6	441	73,3		
142	13,6	436	77,2		
145	13,5	488	77,4		

Table A3 Test results of reference tests - Series R3 (45 mm × 195 mm)

Specimen No.	Moisture content u	Dry density ρ_{0u}	Bending strength f_m	Regression line	Regression coefficient r^2
	[%]	[kg/m^3]	[MPa]		
355	14,1	500	62,6		
369	14,0	480	72,5		
358	13,6	470	56,8		
328	14,5	440	55,6		
310	14,5	436	61,2		
361	14,1	424	57,6		
348	14,0	419	52,3		
319	13,8	413	59,2	$f_m = 0{,}135\ \rho_{0u}$	0,51
329	13,2	409	55,1		
370	14,2	403	61,4		
314	12,8	403	56,7		
366	13,5	388	49,5		
372	12,6	378	48,1		
313	13,3	368	52,7		
312	12,5	358	50,7		

APPENDIX B - TEMPERATURE AND PRESSURE-TIME CURVES OF FURNACE

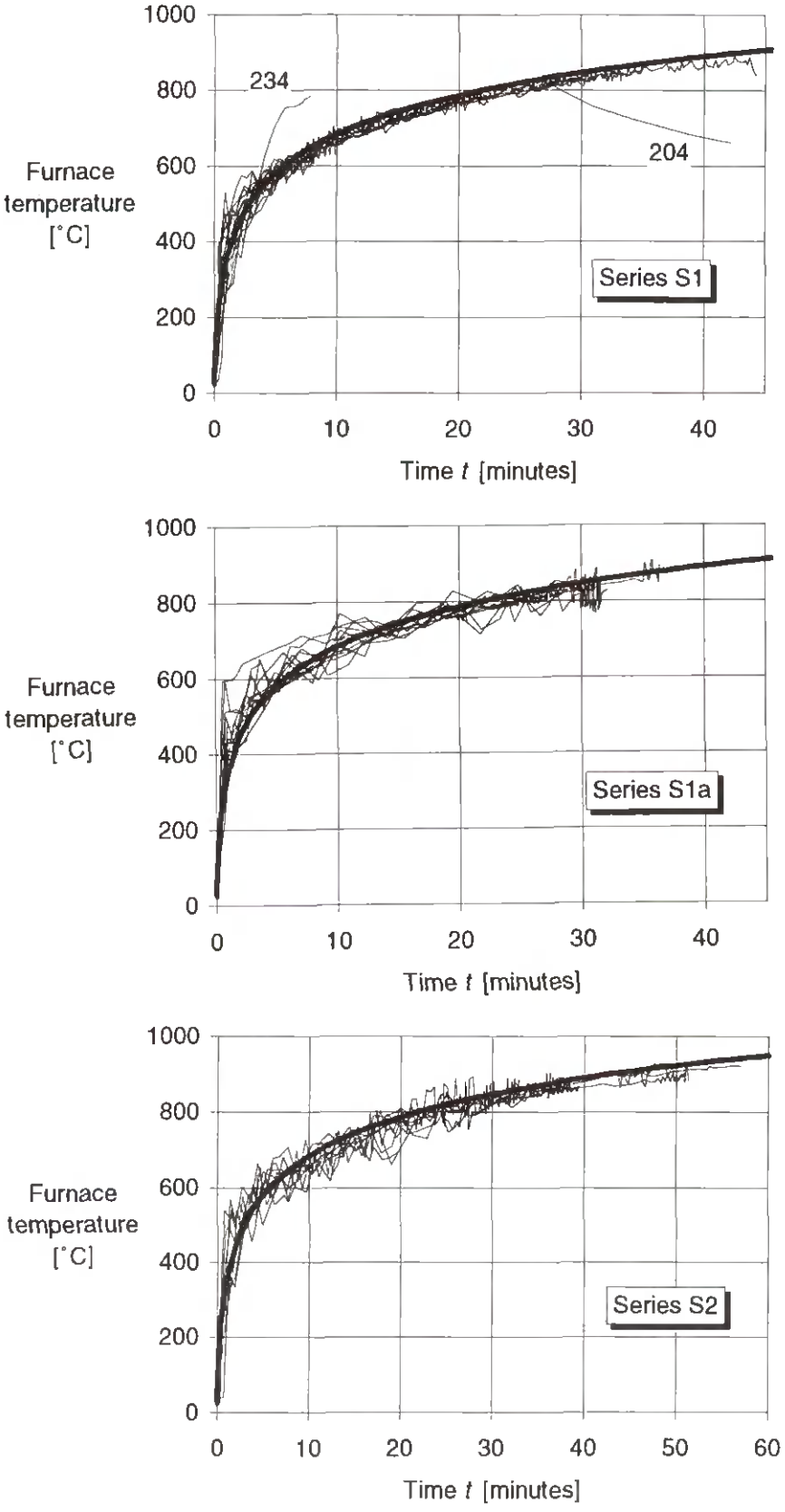

Figure B.1: Furnace temperature in small-scale tests, series S1, S1a and S2

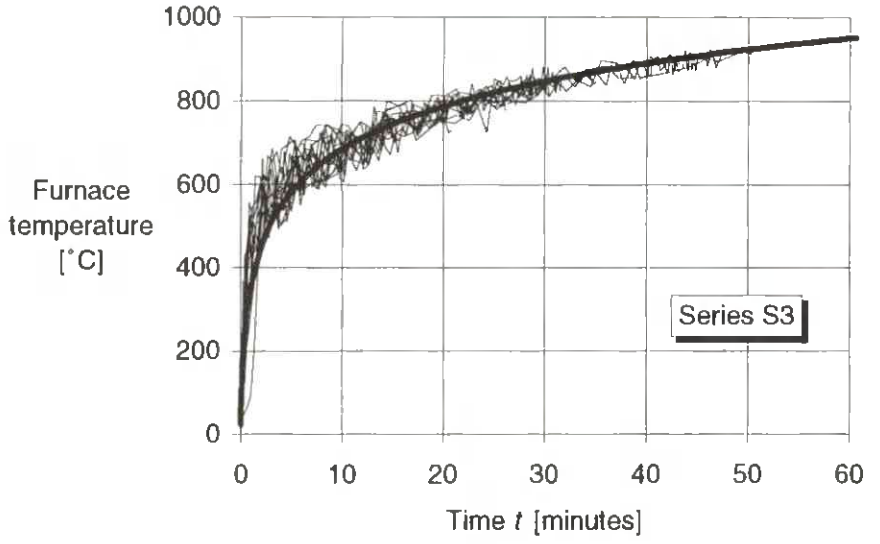

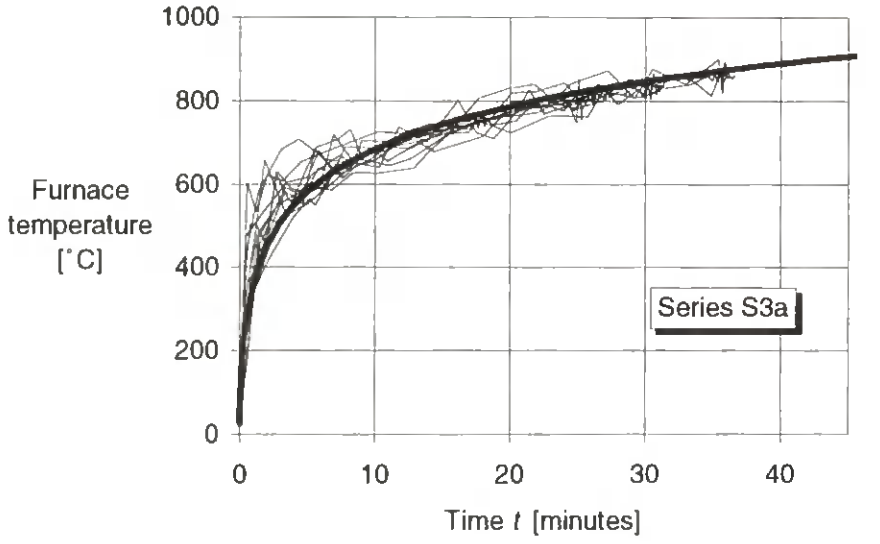

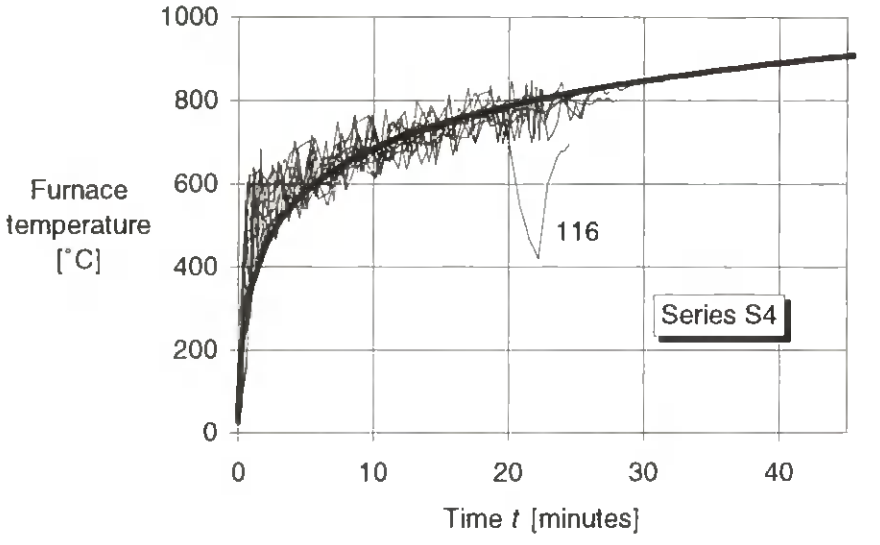

Figure B.2: Furnace temperature in small-scale tests, series S3, S3a, and S4

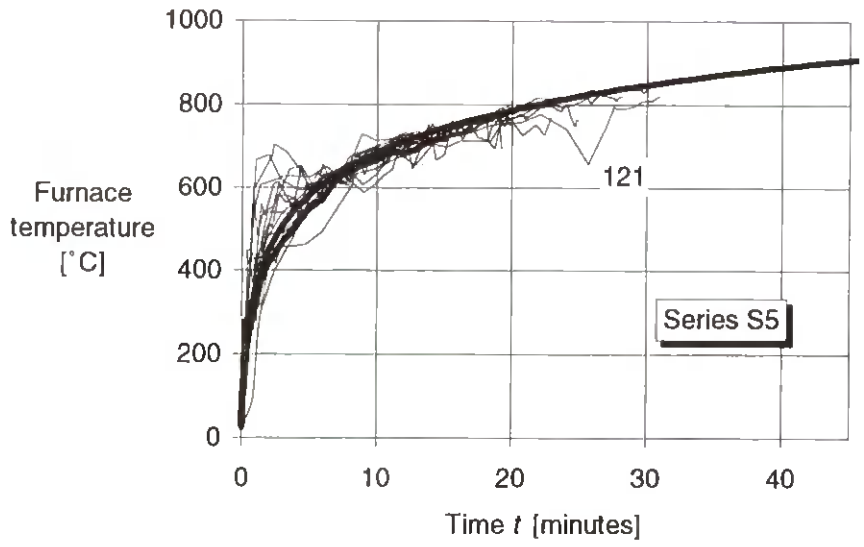

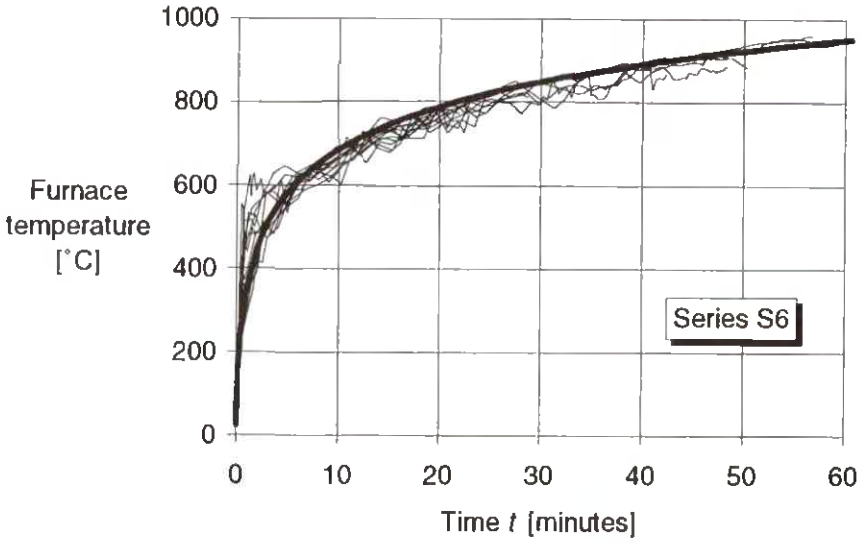

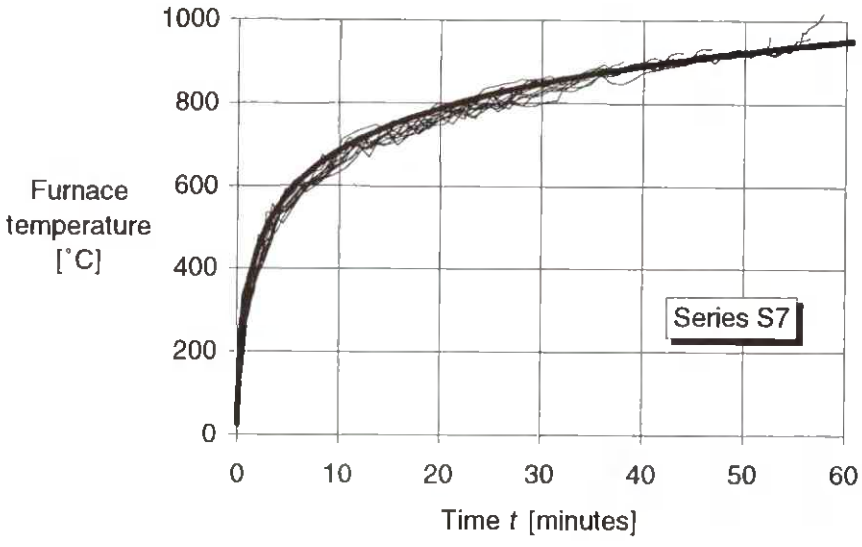

Figure B.3: Furnace temperature in small-scale tests, series S5, S6 and S7

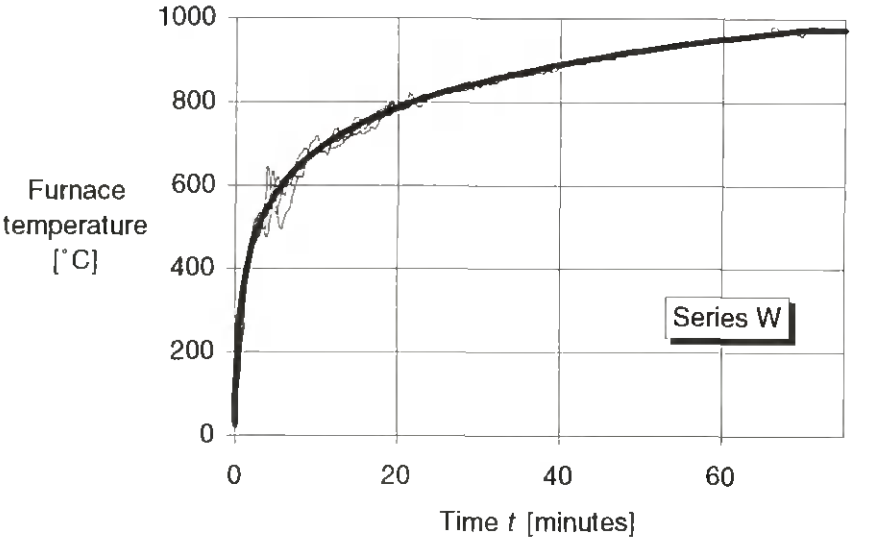

Figure B.2: Furnace temperature in full-scale wall tests

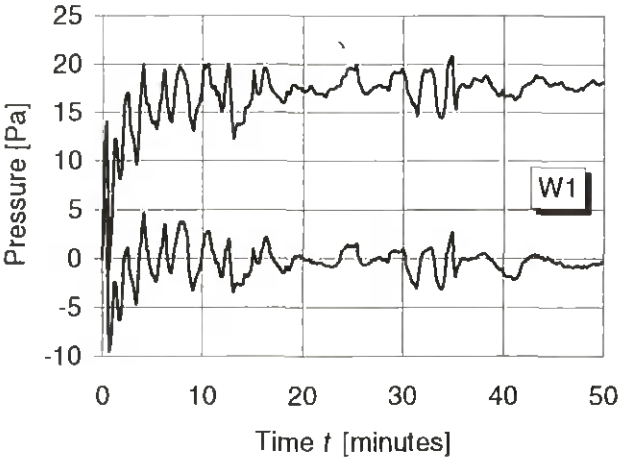

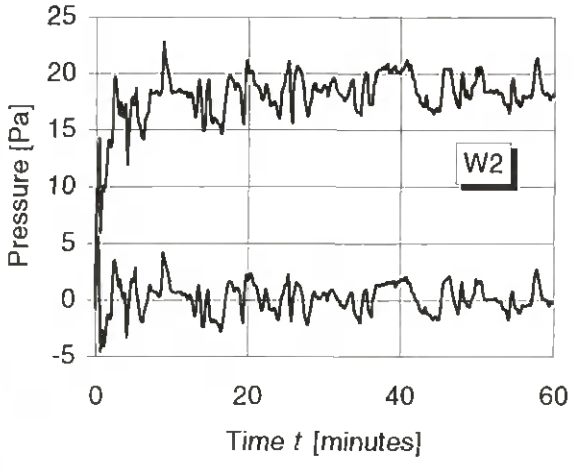

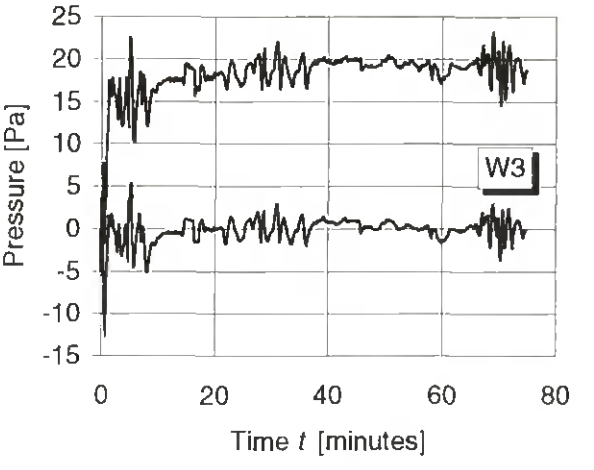

Figure B.4: Pressure difference between furnace and test hall at levels of 500 and 2500 mm in full-scale wall tests

APPENDIX C - RESIDUAL CROSS SECTIONS

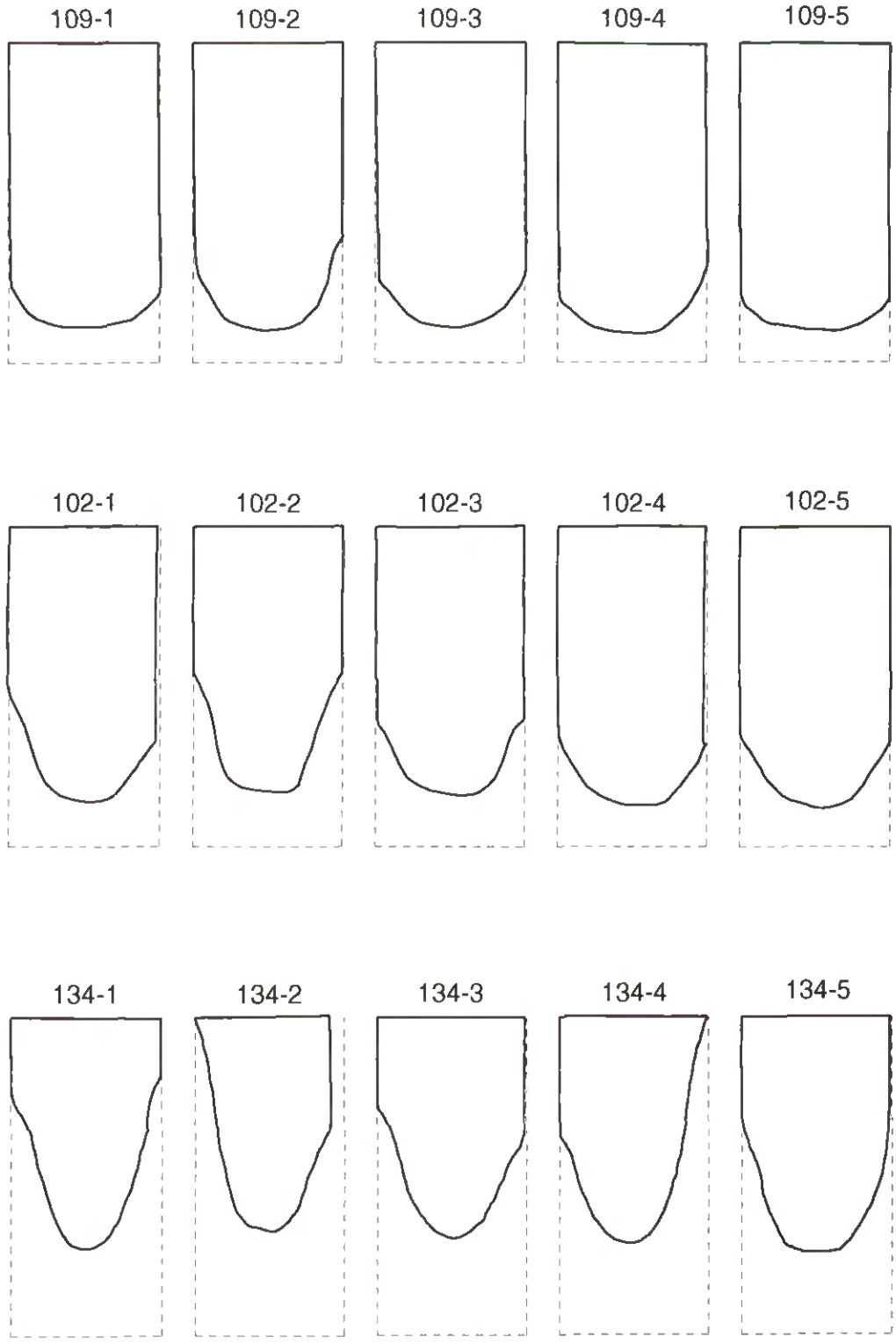

Figure C.1: Residual cross-sections of members with an original dimension of 45 mm × 95 mm

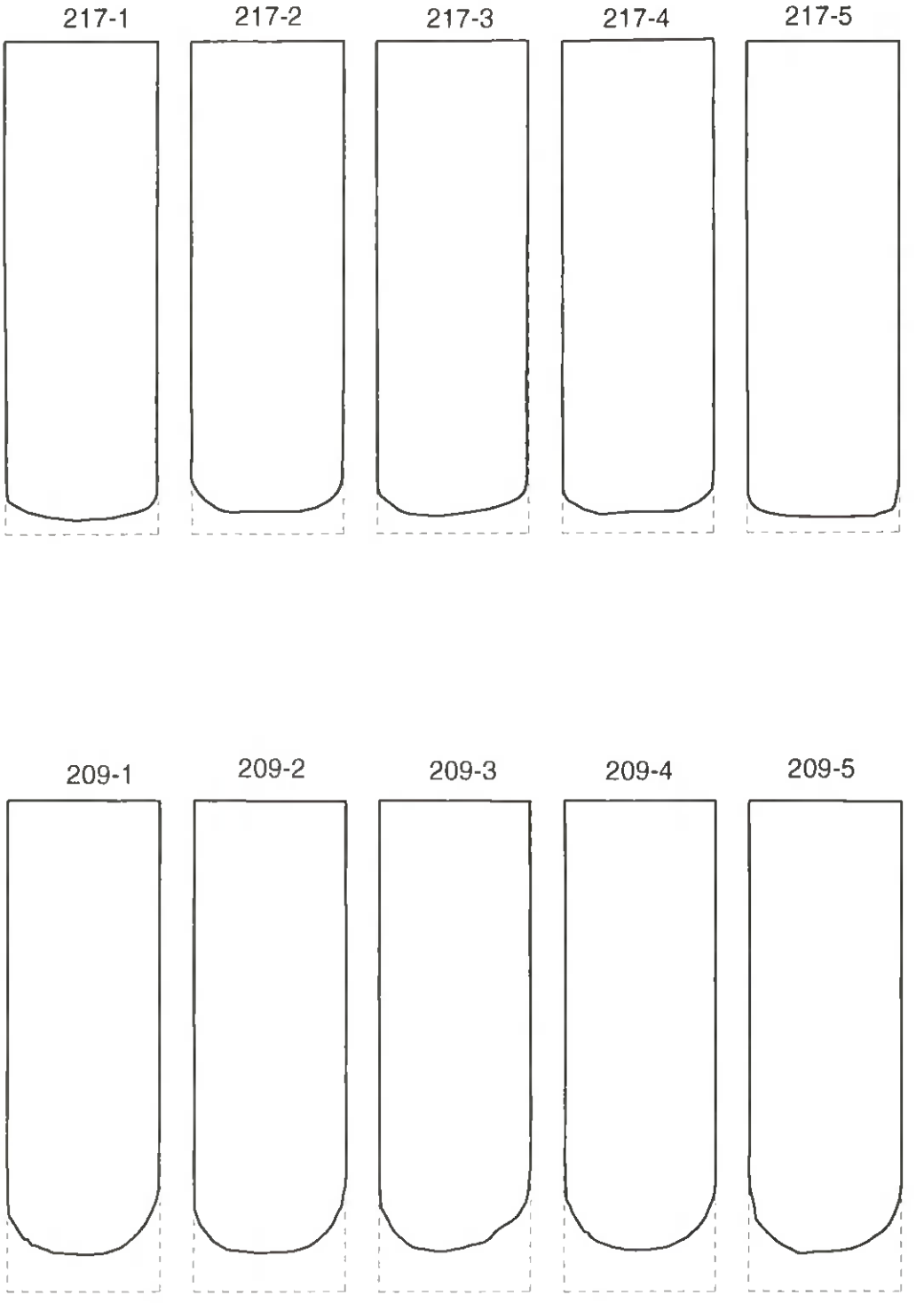

Figure C.2: Residual cross-sections of members with an original dimension of 45 mm × 145 mm

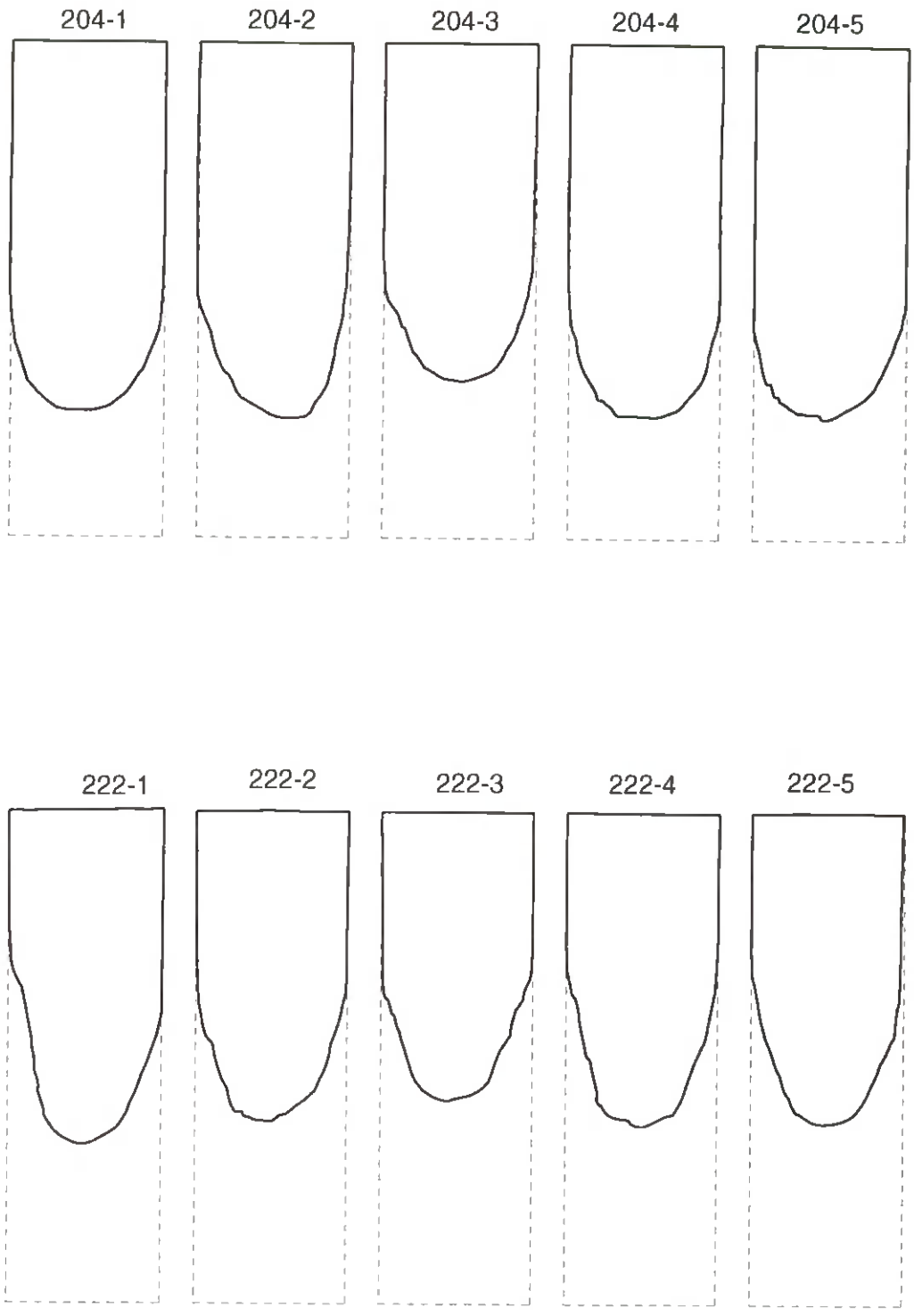

Figure C.3: Residual cross-sections of members with an original dimension of 45 mm × 145 mm

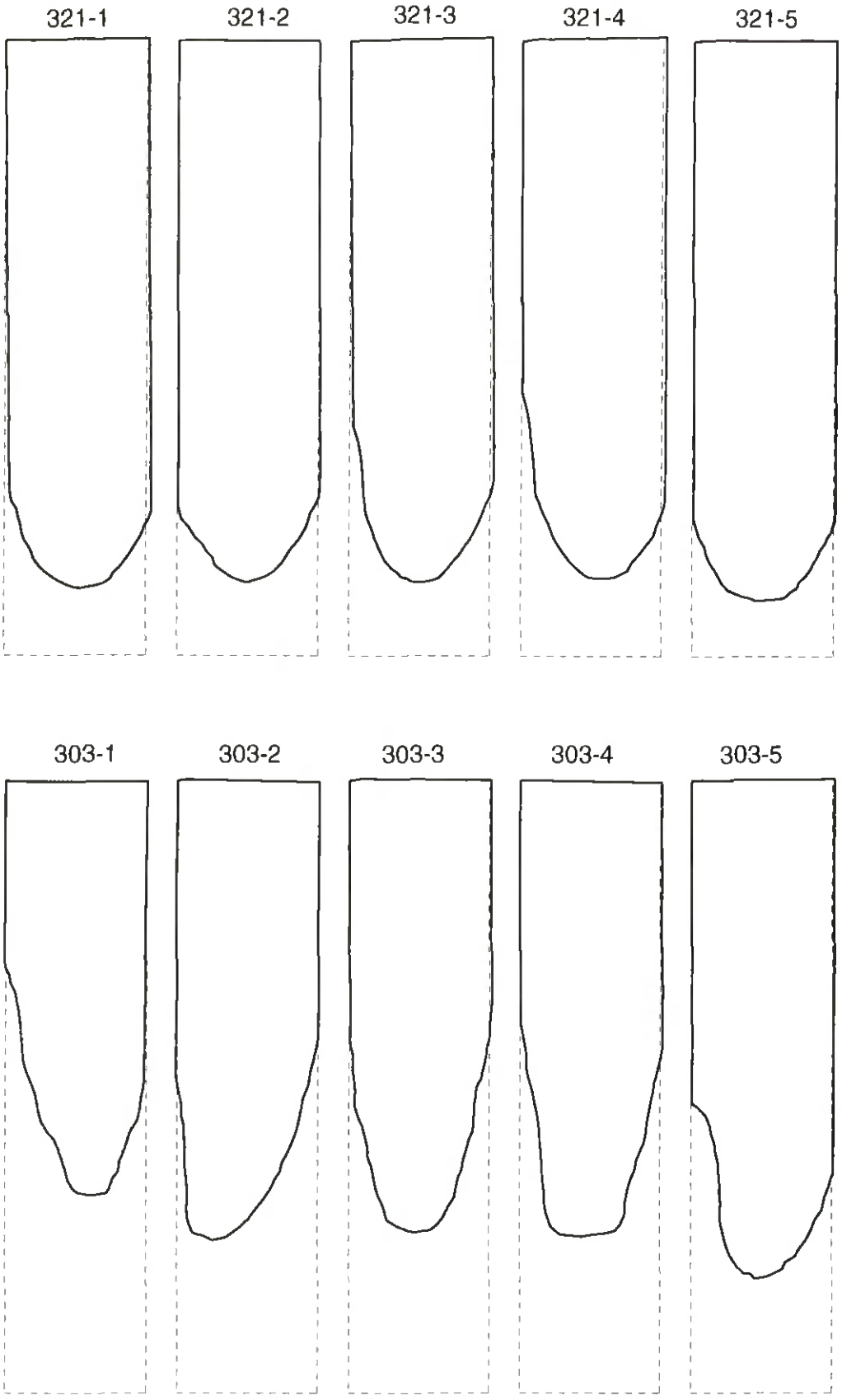

Figure C.4: Residual cross-sections of members with an original dimension of 45 mm ×195 mm

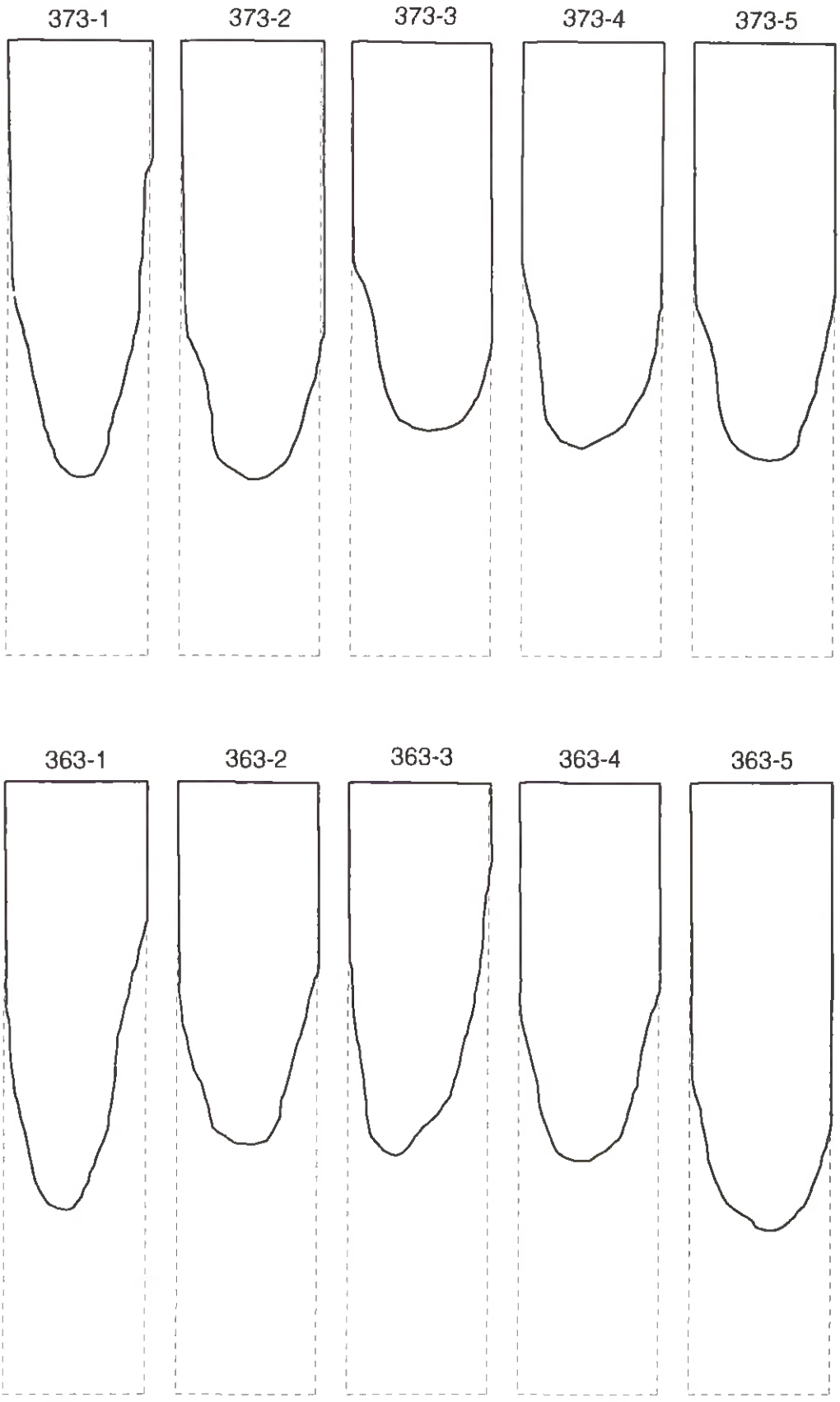

Figure C.5: Residual cross-sections of members with an original dimension of 45 mm × 95 mm

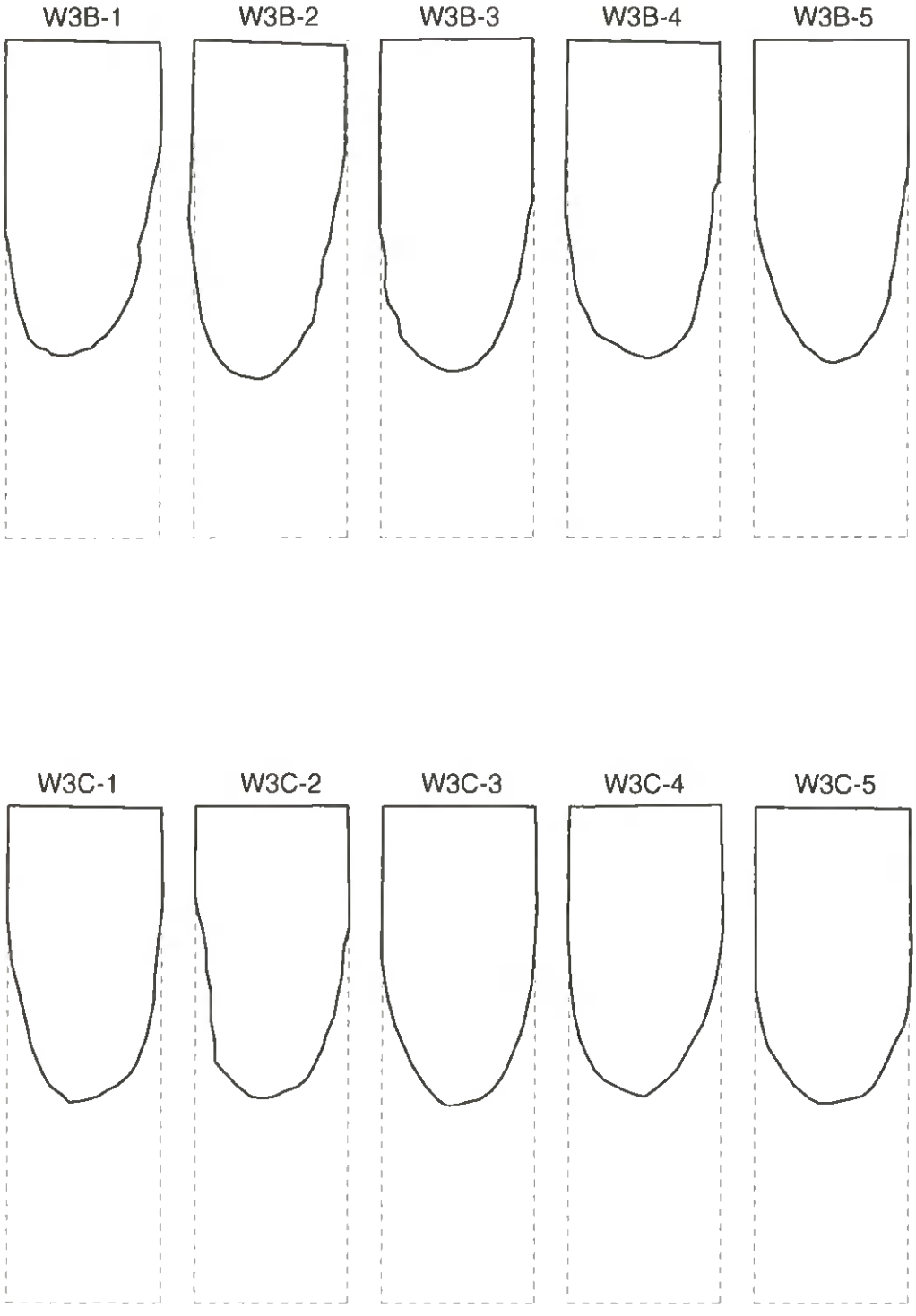

Figure C.6: Residual cross-sections of studs B and C of wall W3 with an original dimension of 45 mm × 95 mm

APPENDIX D - TEST RESULTS - MECHANICAL PROPERTIES

Table D1: Test results - Mechanical properties of series S1

Specimen No.	Moisture content u	Dry density ρ_{0u}	Load ratio M_f/M_0	Time to failure t_u
	[%]	[kg/m^3]		[minutes]
268	13,2	431	0,769	6,9
225	13,3	422	0,680	9,1
266	13,1	372	0,590	9,0
256	13,3	398	0,494	13,8
219	13,5	463	0,390	19,4
232	14,0	456	0,349	19,9
243	13,8	463	0,298	22,4
255	13,6	439	0,242	33,1
210	13,6	423	0,194	33,3
204	13,6	396	0,151	42,2
248	13,9	423	0,151	35,1
211	13,7	382	0,099	44,3

Table D2: Test results - Mechanical properties of series S1a

Specimen No.	Moisture content u	Dry density ρ_{0u}	Initial load ratio M_f/M_0	Load ratio at failure M_f/M_0	Time to failure t_u
	[%]	[kg/m^3]			[minutes]
201	13,3	442	0,10	0,293	31,43
228	13,8	379	0,15	0,245	30,57
212	13,4	424	0,15	0,330	27,18
15	14,4	391	0,10	0,240	24,97
16	14,5	437	0,10	0,336	26,07
22	14,0	419	0	0,299	31,23
26	14,5	337	0,10	0,225	29,65
27	14,4	369	0,10	0,328	20,48
30	14,7	470	0,10	0,364	32,13
8	14,0	367	0	0,231	31,53
21	14,6	426	0	0,285	26,83
29	14,4	393	0	0,187	36,43
33	14,4	380	0	0,270	27,35

Table D3: Test results - Mechanical properties of series S2

Specimen No.	Moisture content u	Dry density ρ_{0u}	Load ratio M_f/M_0	Time to failure t_u
	[%]	[kg/m^3]		[minutes]
237	14,0	465	0,400	37,52
253	14,1	363	0,294	38,35
260	14,0	435	0,502	33,02
258	13,7	420	0,101	56,97
224	14,3	437	0,490	27,97
205	14,1	476	0,202	51,33
230	14,2	377	0,127	51,00
231	14,0	393	0,298	39,40
202	14,3	424	0,602	25,43

Table D4: Test results - Mechanical properties of series S3

Specimen No.	Moisture content u	Dry density ρ_{0u}	Load ratio M_f/M_0	Time to failure t_u
	[%]	[kg/m^3]		[minutes]
209	14,1	453	0,493	15,82
217	14,0	399	0,629	10,32
271	14,0	414	0,708	18,73
236	13,9	402	0,155	47,37
238	12,9	324	0,545	11,78
245	14,1	413	0,703	14,93
252	14,1	378	0,313	31,62
263	14,0	420	0,420	29,88
247	14,0	373	0,309	29,93
208	13,7	406	0,211	40,55
240	14,0	432	0,391	30,40
262	13,6	392	0,297	26,13
222	13,6	409	0,099	50,48
249	14,0	424	0,205	43,27
265	14,0	461	0,457	20,88

Table D5: Test results - Mechanical properties of series S3a

Specimen No.	Moisture content u	Dry density ρ_{0u}	Initial load ratio M_f/M_0	Load ratio at failure M_f/M_0	Time to failure t_u
	[%]	[kg/m^3]			[minutes]
216	14,1	421	0	0,261	36,20
227	14,0	451	0,25	0,602	18,30
270	14,0	394	0,15	0,262	28,50
9	14,5	365	0,15	0,390	25,42
31	14,3	394	0,10	0,357	30,67
2	14,4	448	0,10	0,195	36,02
32	14,7	373	0,10	0,255	35,82
34	14,5	473	0,10	0,322	30,97
36	14,7	406	0,10	0,385	26,50
17	14,5	467	0	0,247	36,63
24	14,7	377	0	0,211	31,13
25	14,5	453	0	0,416	27,65
38	14,1	448	0	0,264	26,37

Table D6: Test results - Mechanical properties of series S4

Specimen No.	Moisture content u	Dry density ρ_{0u}	Load ratio M_f/M_0	Time to failure t_u
	[%]	[kg/m^3]		[minutes]
125	13,8	487	0,096	31,38
104	14,1	483	0,285	22,55
146	14,0	475	0,146	28,18
132	13,9	463	0,142	24,23
109	13,9	454	0,394	16,23
116	14,0	446	0,200	24,53
130	13,2	437	0,498	8,58
107	13,5	429	0,450	13,68
114	13,9	412	0,142	24,37
111	13,8	409	0,242	26,02
122	13,8	401	0,496	12,07
144	14,0	369	0,246	21,28

Table D7: Test results - Mechanical properties of series S5

Specimen No.	Moisture content u	Dry density ρ_{0u}	Load ratio M_f/M_0	Time to failure t_u
	[%]	[kg/m^3]		[minutes]
106	14,0	509	0,290	22,10
118	13,9	484	0,236	22,83
124	13,8	478	0,192	22,97
148	13,8	467	0,142	28,18
149	13,4	462	0,481	15,05
121	13,5	450	0,190	30,78
117	14,3	443	0,391	21,17
108	13,8	439	0,099	30,12
134	14,0	428	0,147	26,02
139	13,5	424	0,287	19,78
102	14,0	421	0,436	19,23
119	13,9	412	0,115	25,00
123	14,1	407	0,289	14,50
101	13,4	400	0,334	19,92
138	13,4	368	0,374	14,60

Table D8: Test results - Mechanical properties of series S6

Specimen No.	Moisture content u	Dry density ρ_{0u}	Load ratio M_f/M_0	Time to failure t_u
	[%]	[kg/m^3]		[minutes]
325	13,2	509	0,199	50,30
315	13,6	480	0,247	48,33
357	13,0	472	0,391	33,47
345	13,6	451	0,341	42,35
336	12,4	446	0,148	56,72
351	13,0	421	0,098	58,73
343	13,0	410	0,493	21,97
377	13,0	406	0,439	24,13
330	12,5	398	0,198	48,35
320	13,1	382	0,289	28,73
321	13,2	375	0,331	28,92
306	14,1	332	0,394	22,90

Table D9: Test results - Mechanical properties of series S7

Specimen No.	Moisture content u	Dry density ρ_{0u}	Load ratio M_f/M_0	Time to failure t_u
	[%]	[kg/m^3]		[minutes]
311	13,0	479	0,246	43,97
341	13,4	451	0,394	38,03
335	12,0	442	0,117	56,45
373	12,4	425	0,146	52,40
316	13,3	411	0,297	38,08
363	12,3	414	0,095	59,10
374	12,2	410	0,362	34,72
324	12,4	407	0,345	33,03
303	12,7	399	0,198	46,78
334	12,0	398	0,320	29,50
347	12,2	392	0,482	27,67
375	11,9	383	0,388	28,13

APPENDIX E - TEST RESULTS - TEMPERATURE MEASUREMENTS

In the following temperature-time relationships at gauge points in the timber members are shown for specimens in series S1 - S6. For identification of specimens and series see appendix D.

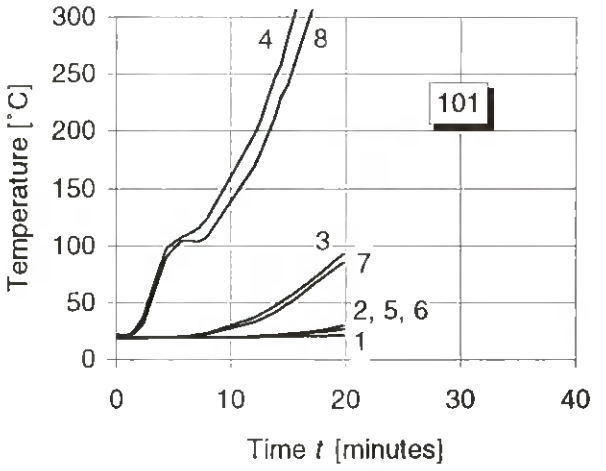

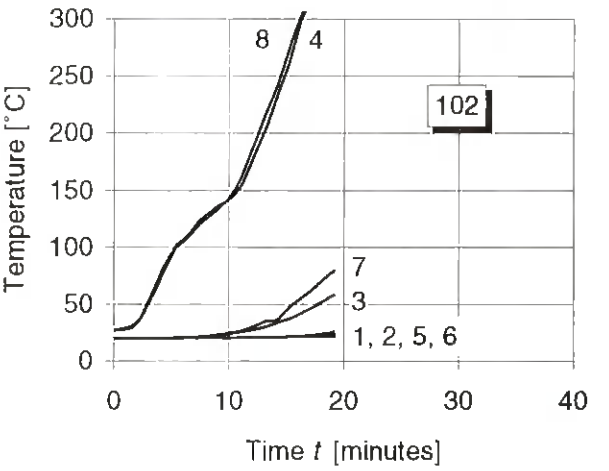

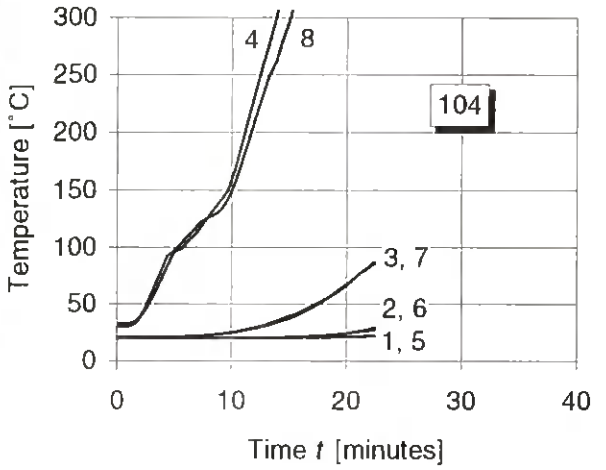

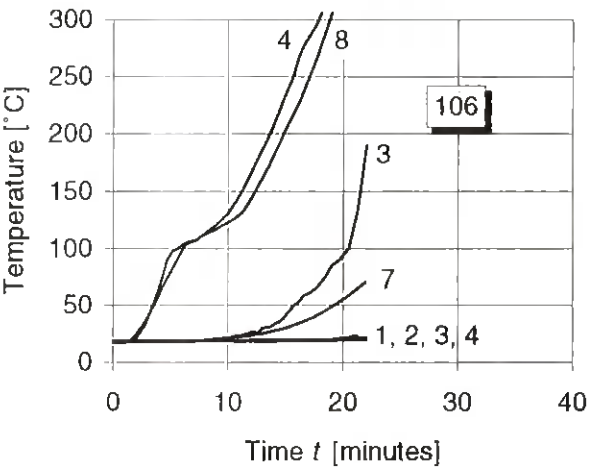

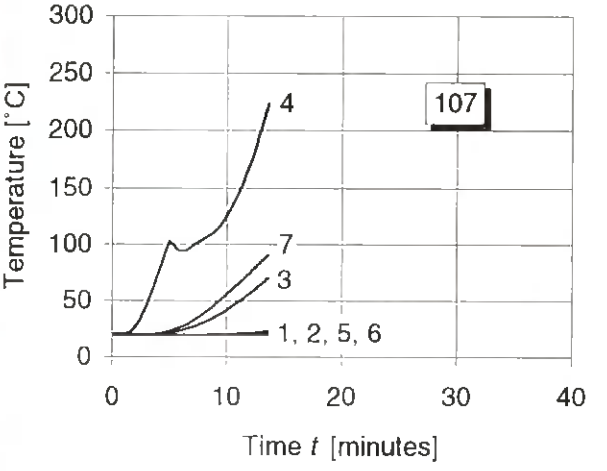

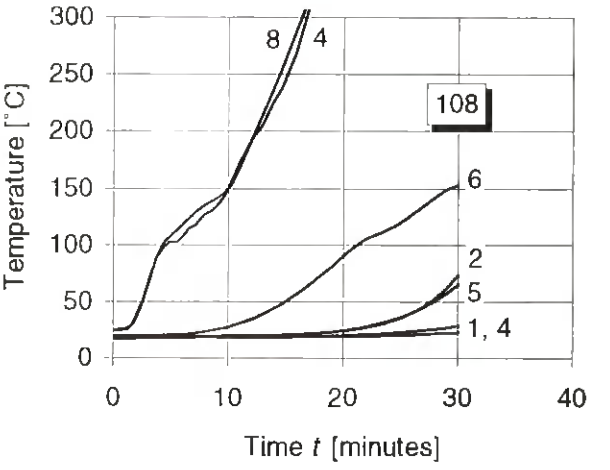

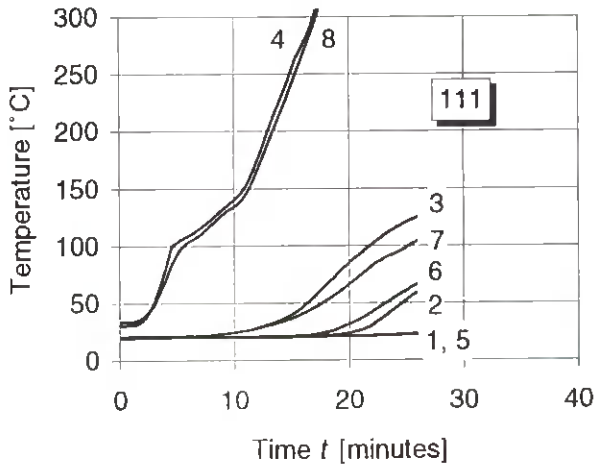
Temperature [°C]
300
250
200
150
100
50
0
0
10
20
30
40
Time t [minutes]
111
4
8
3
7
6
2
1, 5

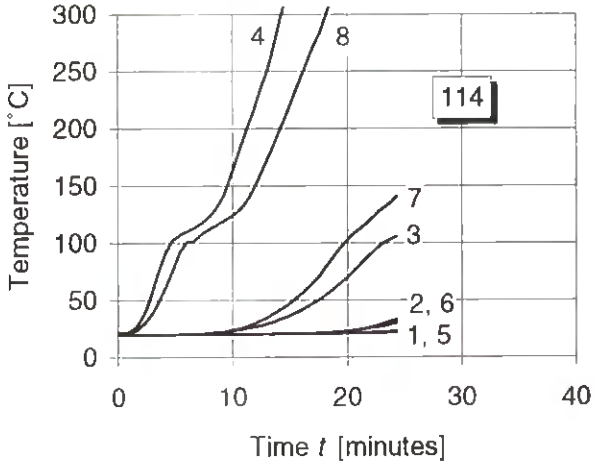
Temperature [°C]
300
250
200
150
100
50
0
0
10
20
30
40
Time t [minutes]
114
4
8
7
3
2, 6
1, 5

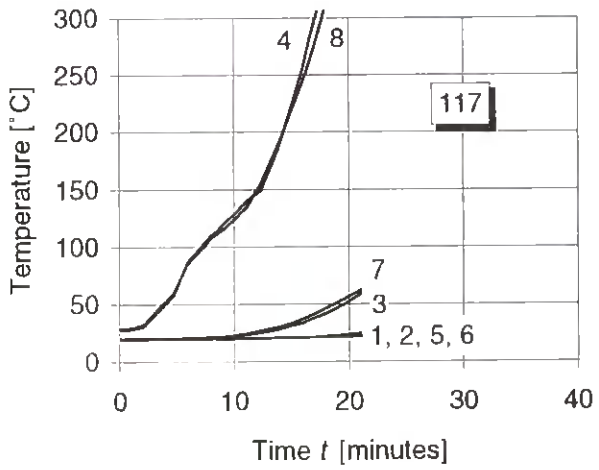
Temperature [°C]
300
250
200
150
100
50
0
0
10
20
30
40
Time t [minutes]
117
4
8
7
3
1, 2, 5, 6

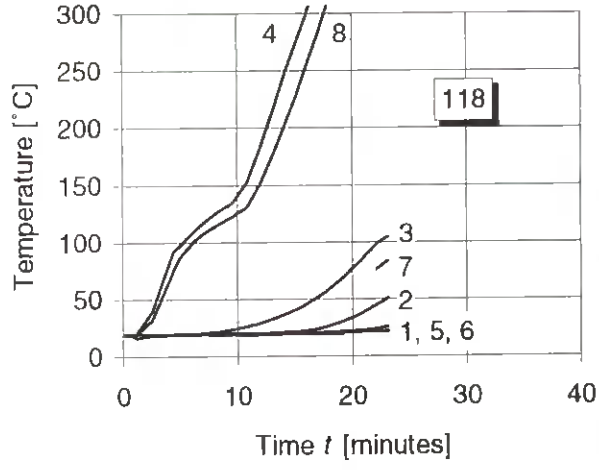
Temperature [°C]
300
250
200
150
100
50
0
0
10
20
30
40
Time t [minutes]
118
4
8
3
7
2
1, 5, 6

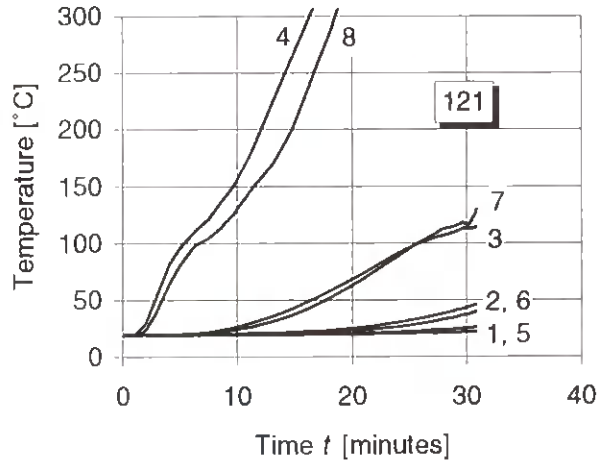
Temperature [°C]
300
250
200
150
100
50
0
0
10
20
30
40
Time t [minutes]
121
4
8
7
3
2, 6
1, 5

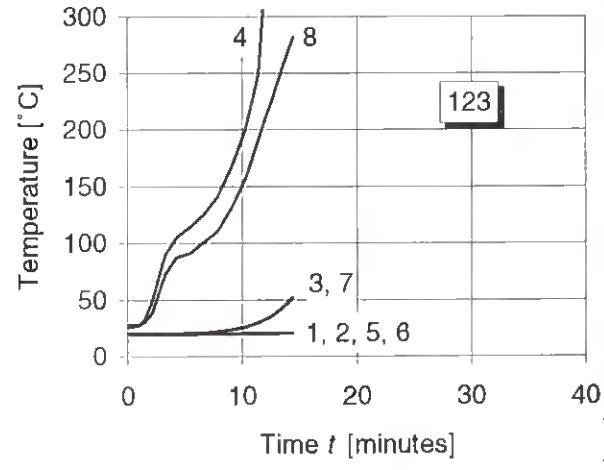
Temperature [°C]
300
250
200
150
100
50
0
0
10
20
30
40
Time t [minutes]
123
4
8
3, 7
1, 2, 5, 6

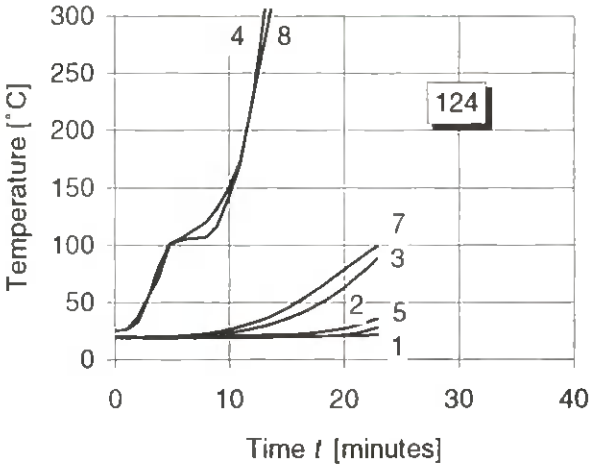
Temperature [°C]
300
250
200
150
100
50
0
0
10
20
30
40
Time t [minutes]
124
4
8
7
3
2
5
1

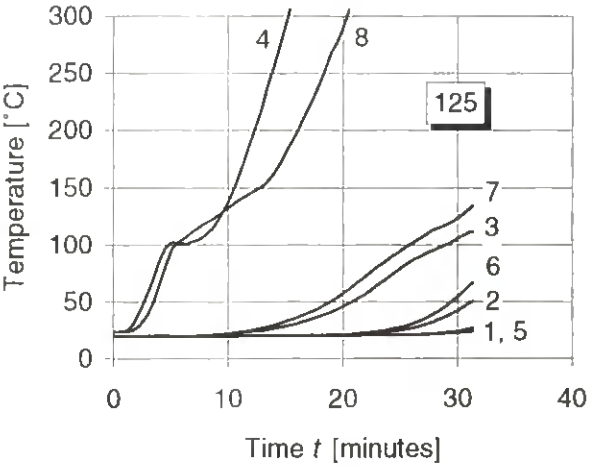
Temperature [°C]
300
250
200
150
100
50
0
0
10
20
30
40
Time t [minutes]
125
4
8
7
3
6
2
1, 5

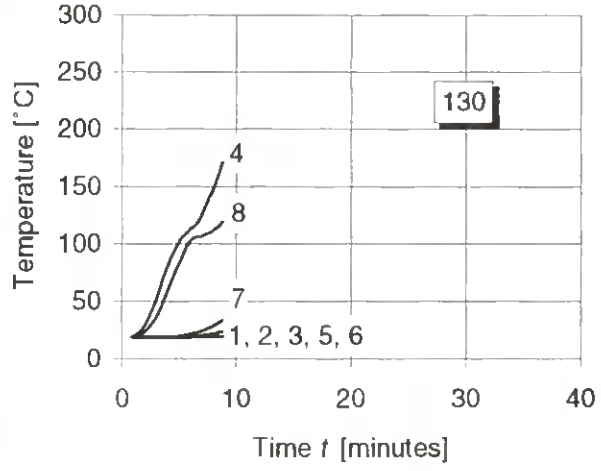
Temperature [°C]
300
250
200
150
100
50
0
0
10
20
30
40
Time t [minutes]
130
4
8
7
1, 2, 3, 5, 6

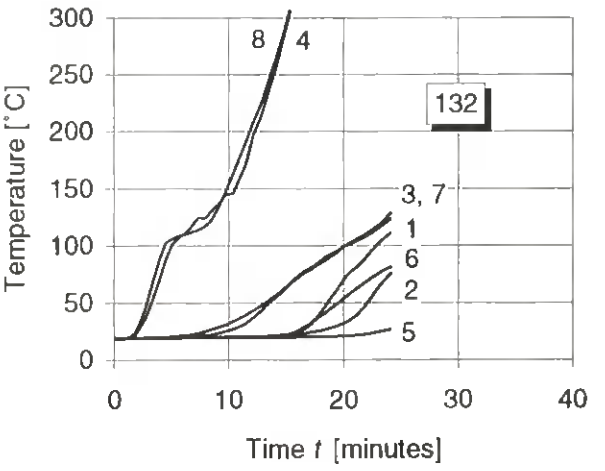
Temperature [°C]
300
250
200
150
100
50
0
0
10
20
30
40
Time t [minutes]
132
8
4
3, 7
1
6
2
5

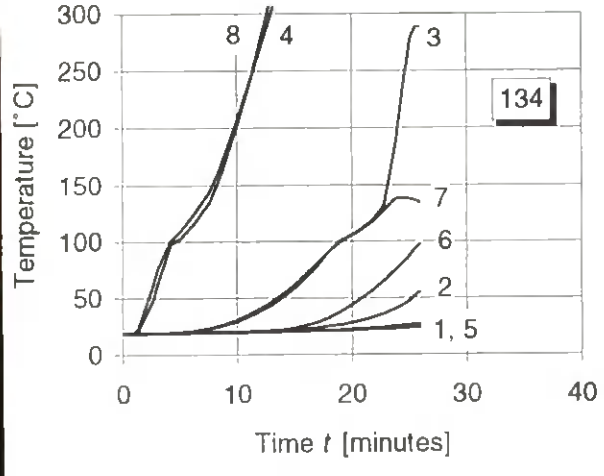
Temperature [°C]
300
250
200
150
100
50
0
0
10
20
30
40
Time t [minutes]
134
8
4
3
7
6
2
1, 5

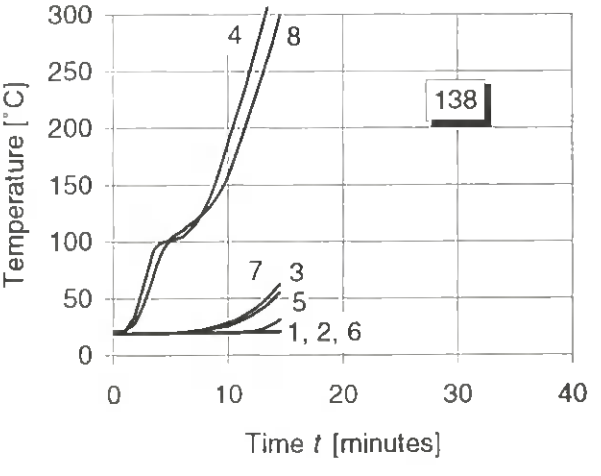
Temperature [°C]
300
250
200
150
100
50
0
0
10
20
30
40
Time t [minutes]
138
4
8
7
3
5
1, 2, 6

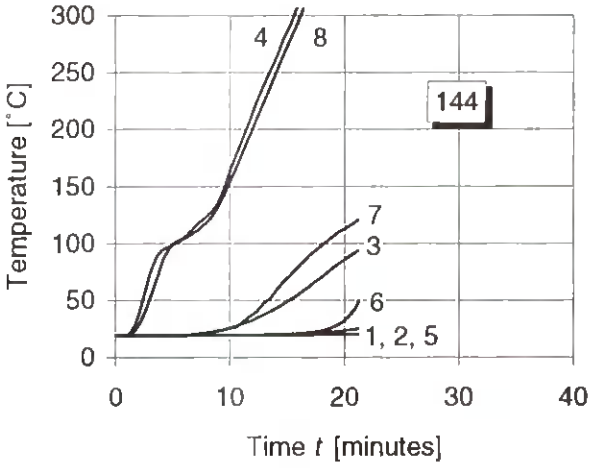
144
Temperature [°C]
Time t [minutes]
4
8
7
3
6
1, 2, 5

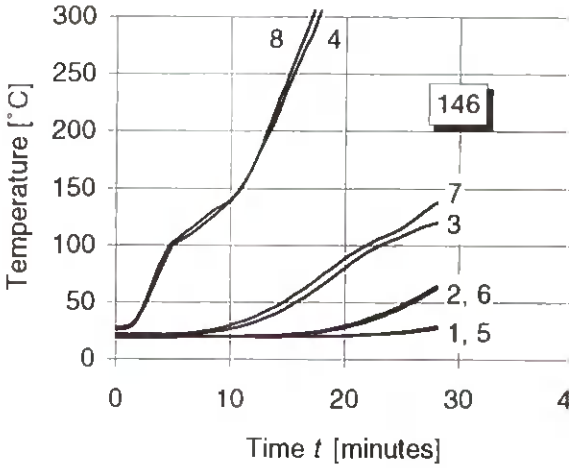
146
Temperature [°C]
Time t [minutes]
8
4
7
3
2, 6
1, 5

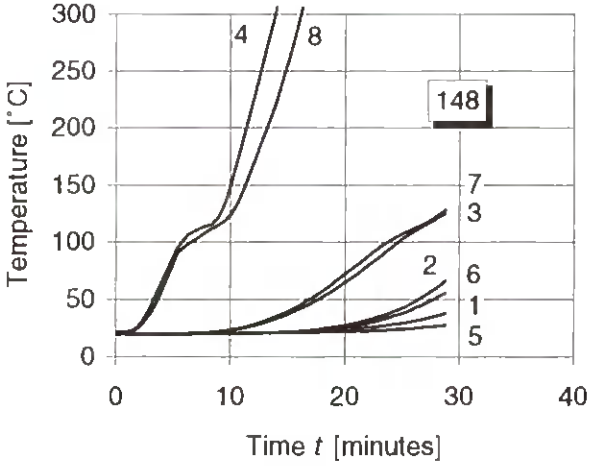
148
Temperature [°C]
Time t [minutes]
4
8
7
3
2
6
1
5

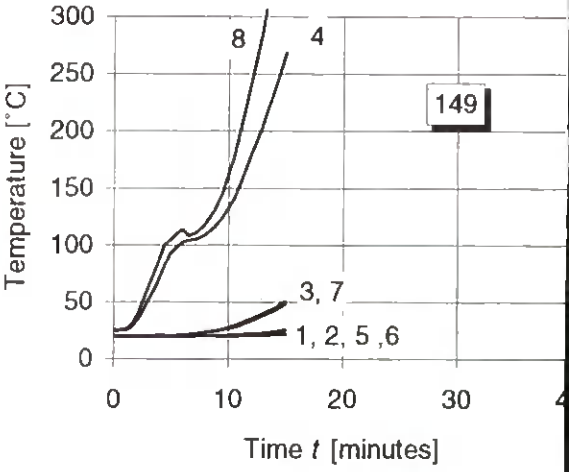
149
Temperature [°C]
Time t [minutes]
8
4
3, 7
1, 2, 5 ,6

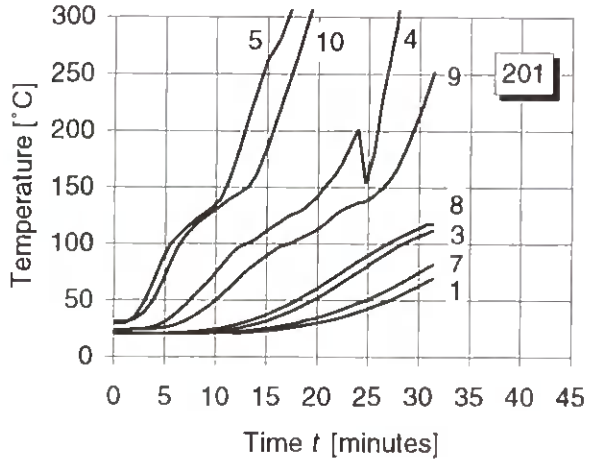
201
Temperature [°C]
Time t [minutes]
5
10
4
9
8
3
7
1

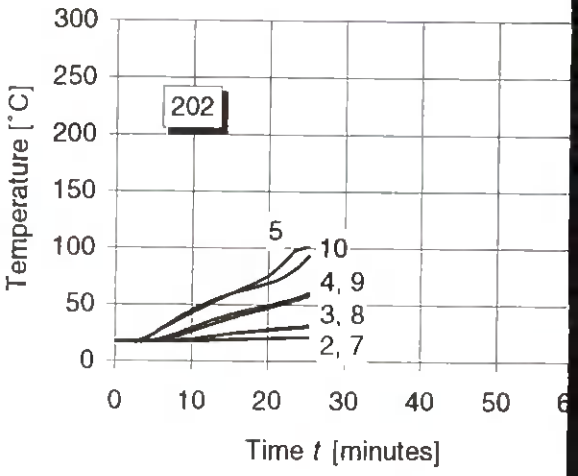
202
Temperature [°C]
Time t [minutes]
5
10
4, 9
3, 8
2, 7

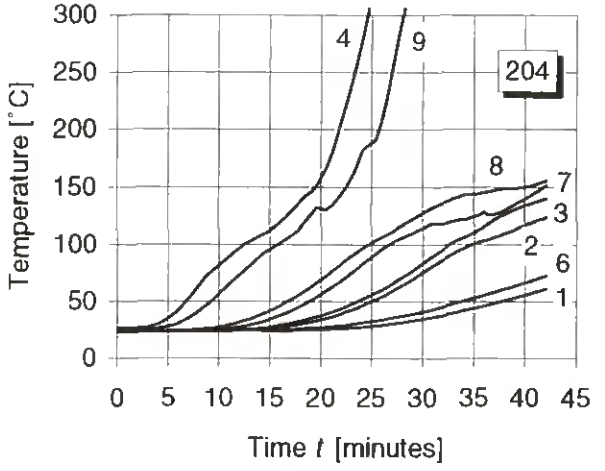
Temperature [°C]
300
250
200
150
100
50
0
0 5 10 15 20 25 30 35 40 45
Time t [minutes]
204
4
9
8
7
3
2
6
1

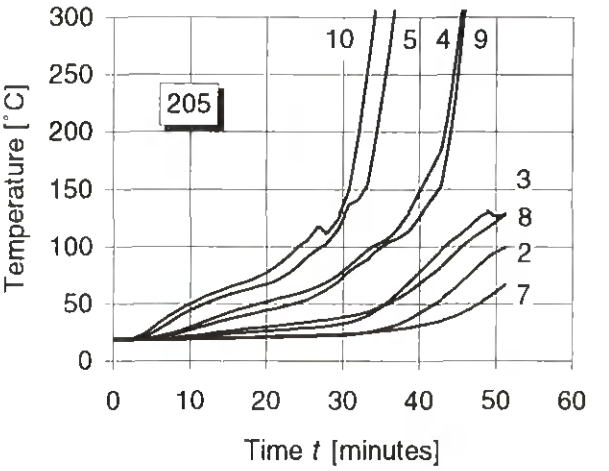
Temperature [°C]
300
250
200
150
100
50
0
0 10 20 30 40 50 60
Time t [minutes]
205
10
5
4
9
3
8
2
7

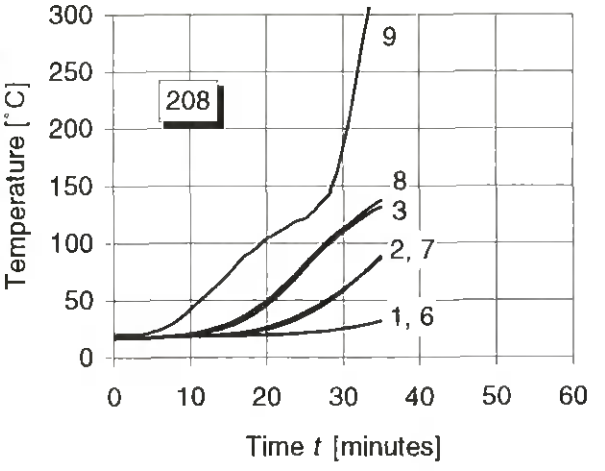
Temperature [°C]
300
250
200
150
100
50
0
0 10 20 30 40 50 60
Time t [minutes]
208
9
8
3
2, 7
1, 6

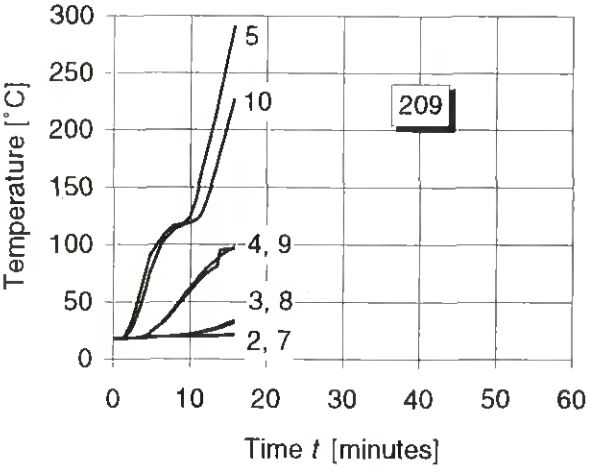
Temperature [°C]
300
250
200
150
100
50
0
0 10 20 30 40 50 60
Time t [minutes]
209
5
10
4, 9
3, 8
2, 7

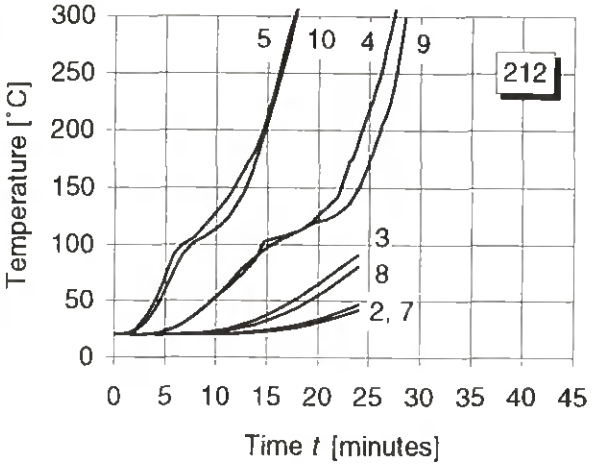
Temperature [°C]
300
250
200
150
100
50
0
0 5 10 15 20 25 30 35 40 45
Time t [minutes]
212
5
10
4
9
3
8
2, 7

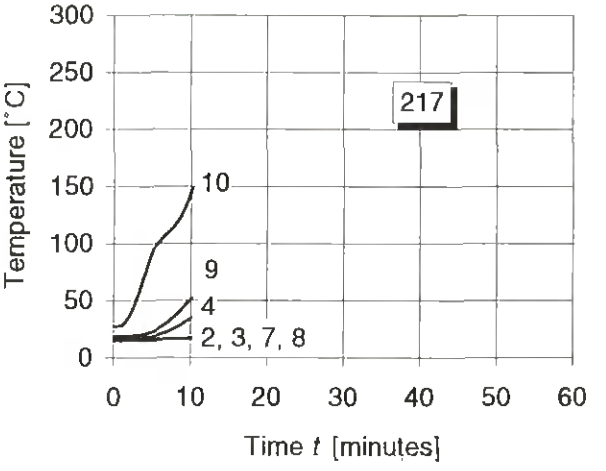
Temperature [°C]
300
250
200
150
100
50
0
0 10 20 30 40 50 60
Time t [minutes]
217
10
9
4
2, 3, 7, 8

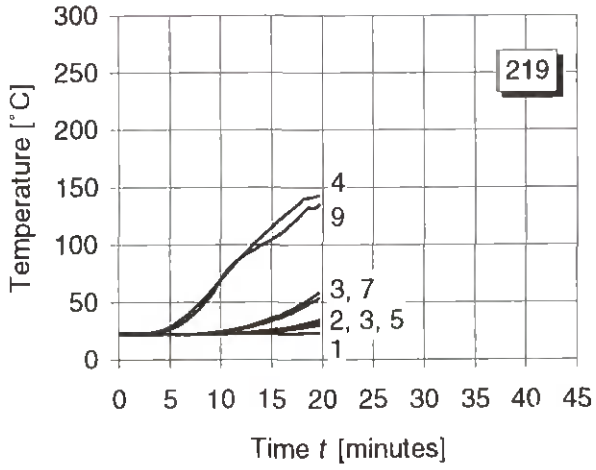
219
Temperature [°C]
Time t [minutes]
4
9
3, 7
2, 3, 5
1

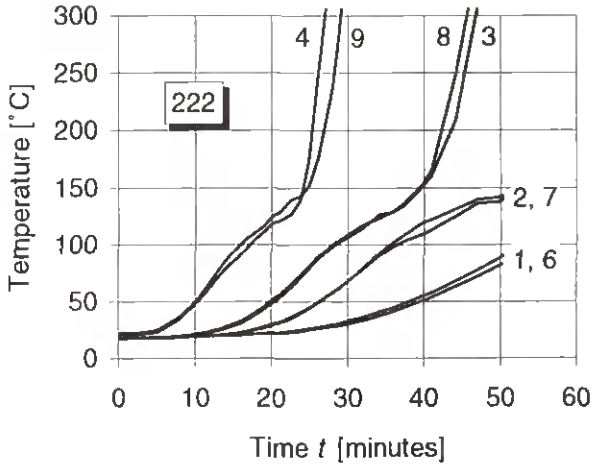
222
Temperature [°C]
Time t [minutes]
4
9
8
3
2, 7
1, 6

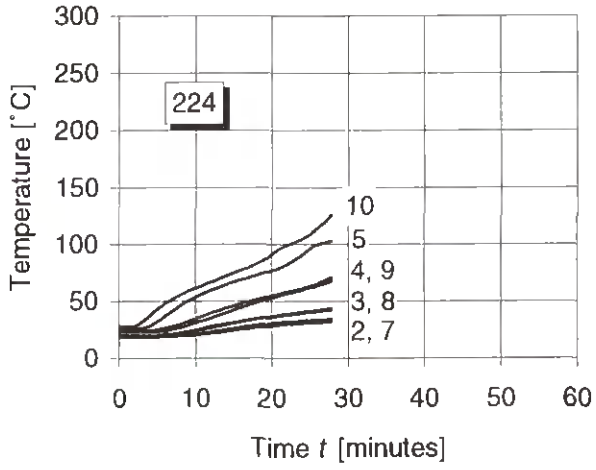
224
Temperature [°C]
Time t [minutes]
10
5
4, 9
3, 8
2, 7

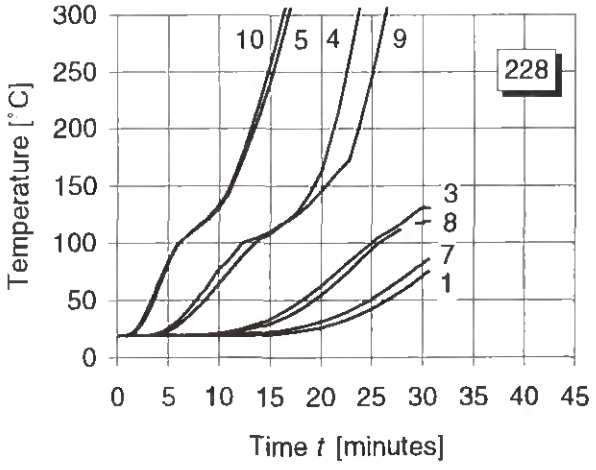
228
Temperature [°C]
Time t [minutes]
10
5
4
9
3
8
7
1

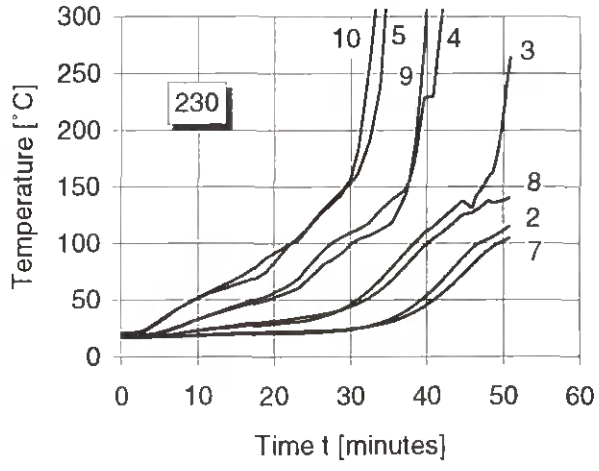
230
Temperature [°C]
Time t [minutes]
10
5
4
3
9
8
2
7

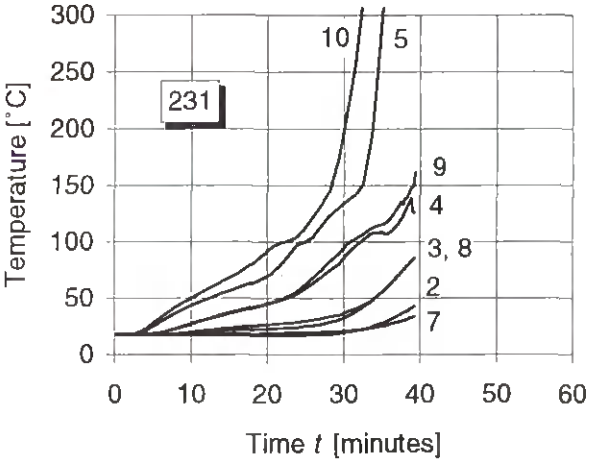
231
Temperature [°C]
Time t [minutes]
10
5
9
4
3, 8
2
7

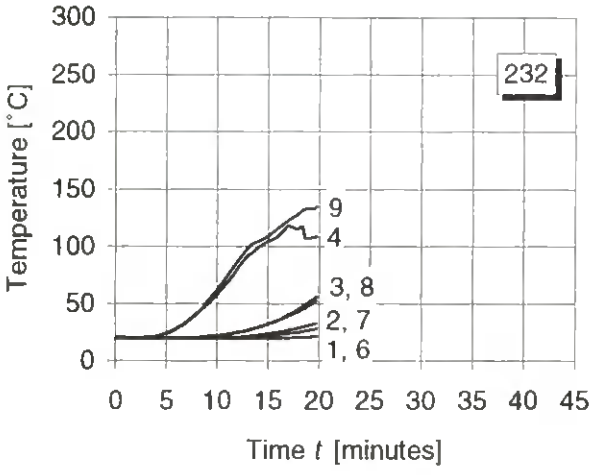
232
Temperature [°C]
Time t [minutes]
9
4
3, 8
2, 7
1, 6

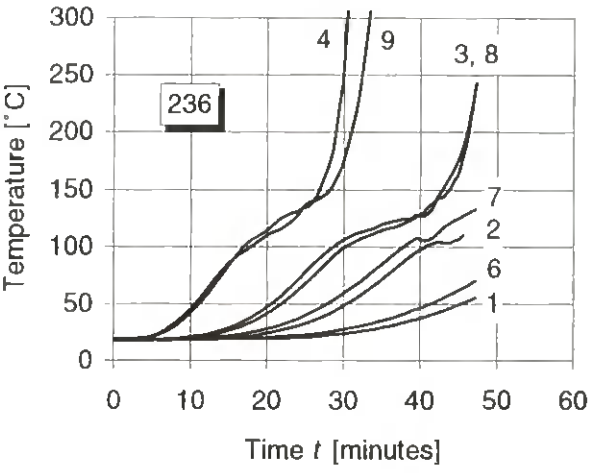
236
Temperature [°C]
Time t [minutes]
4
9
3, 8
7
2
6
1

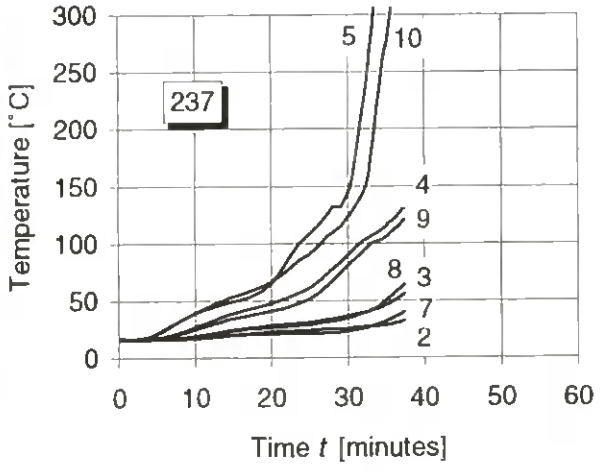
237
Temperature [°C]
Time t [minutes]
5
10
4
9
8
3
7
2

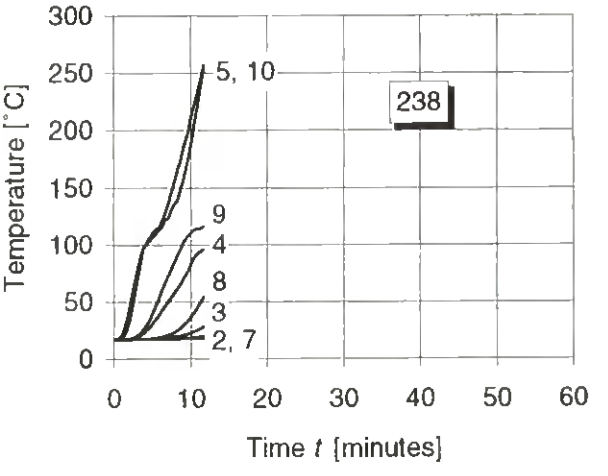
238
Temperature [°C]
Time t [minutes]
5, 10
9
4
8
3
2, 7

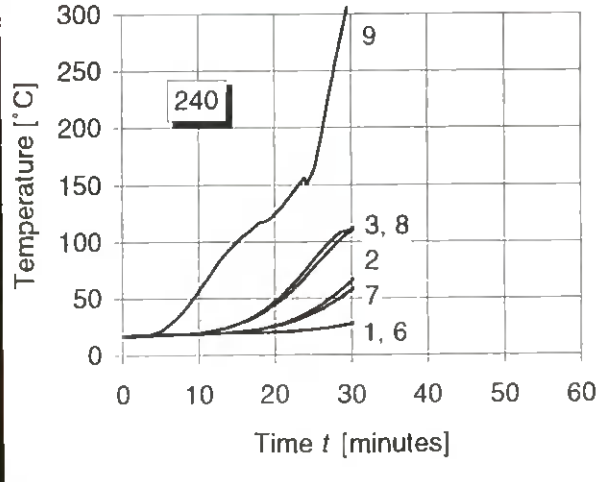
240
Temperature [°C]
Time t [minutes]
9
3, 8
2
7
1, 6

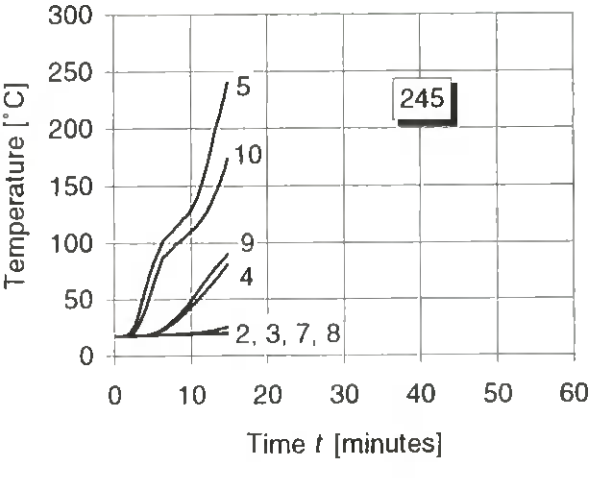
245
Temperature [°C]
Time t [minutes]
5
10
9
4
2, 3, 7, 8

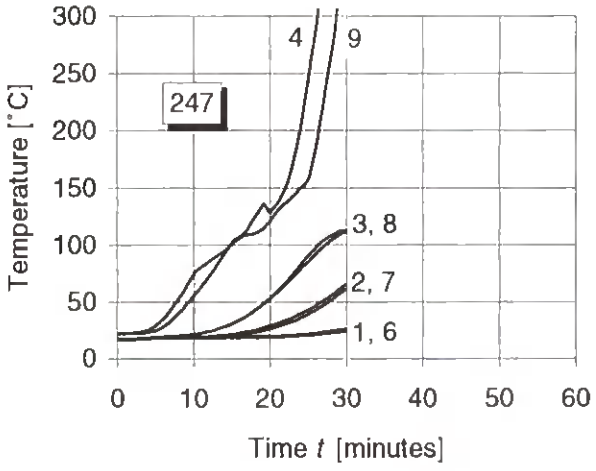
247
Temperature [°C]
Time t [minutes]
4
9
3, 8
2, 7
1, 6

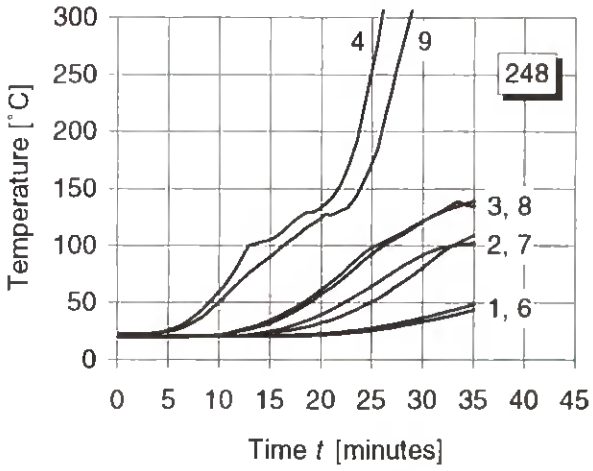
248
Temperature [°C]
Time t [minutes]
4
9
3, 8
2, 7
1, 6

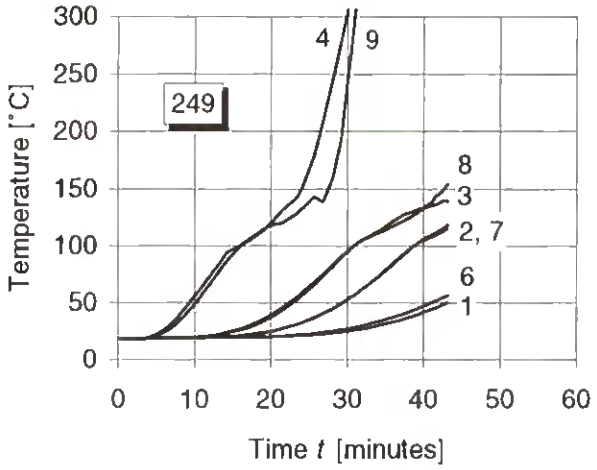
249
Temperature [°C]
Time t [minutes]
4
9
8
3
2, 7
6
1

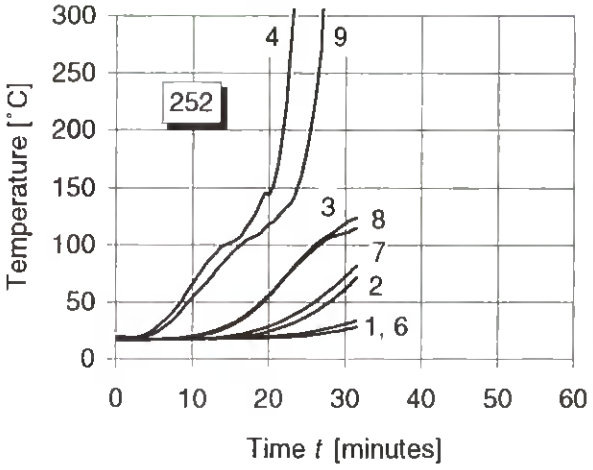
252
Temperature [°C]
Time t [minutes]
4
9
3
8
7
2
1, 6

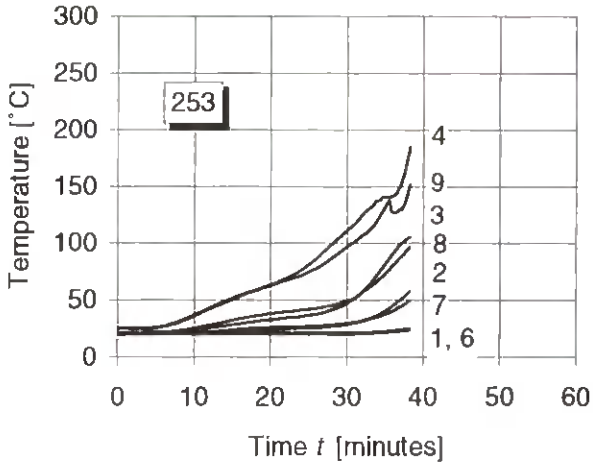
253
Temperature [°C]
Time t [minutes]
4
9
3
8
2
7
1, 6

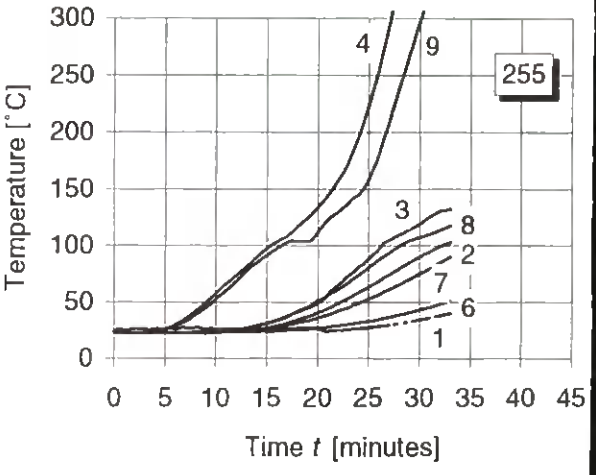
255
Temperature [°C]
Time t [minutes]
4
9
3
8
2
7
6
1

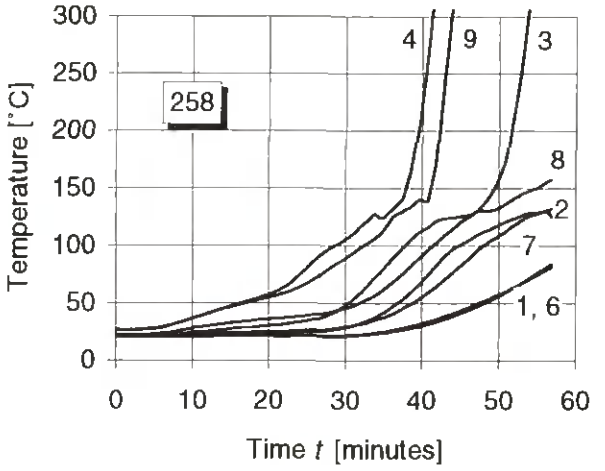
258
Temperature [°C]
Time t [minutes]
4
9
3
8
2
7
1, 6

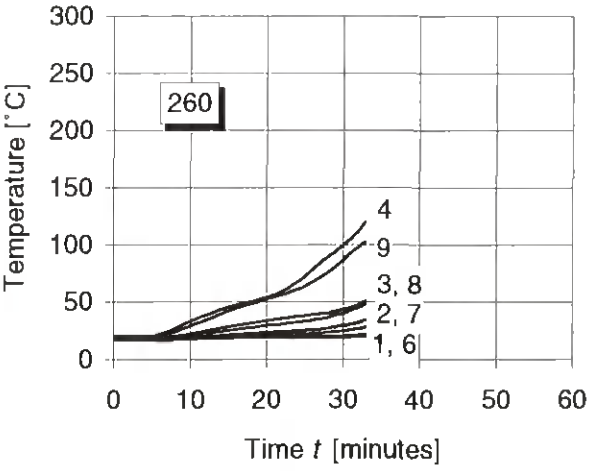
260
Temperature [°C]
Time t [minutes]
4
9
3, 8
2, 7
1, 6

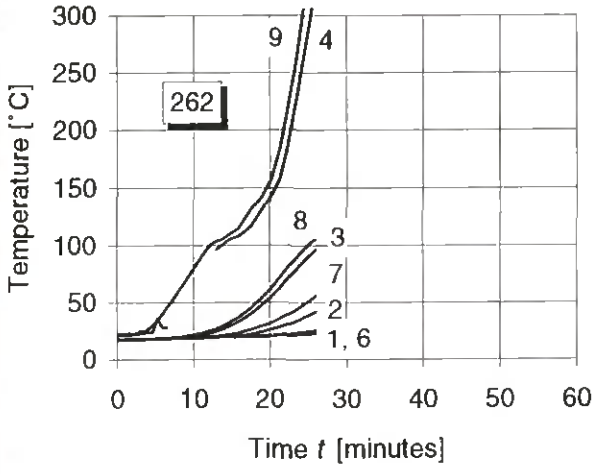
262
Temperature [°C]
Time t [minutes]
9
4
8
3
7
2
1, 6

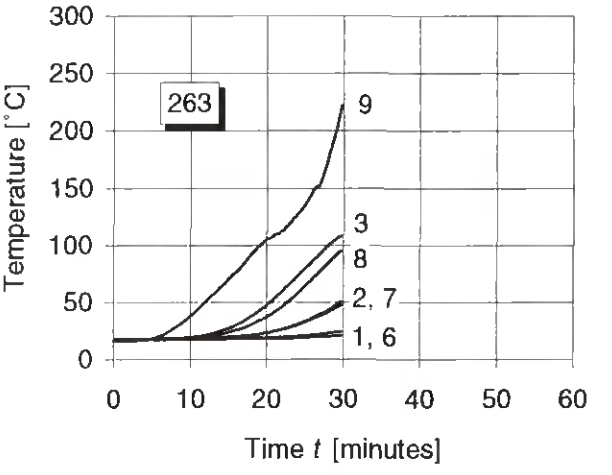
263
Temperature [°C]
Time t [minutes]
9
3
8
2, 7
1, 6

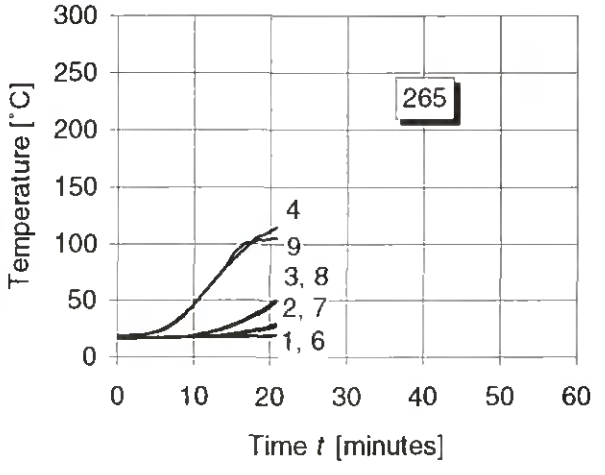
265
Temperature [°C]
Time t [minutes]
4
9
3, 8
2, 7
1, 6

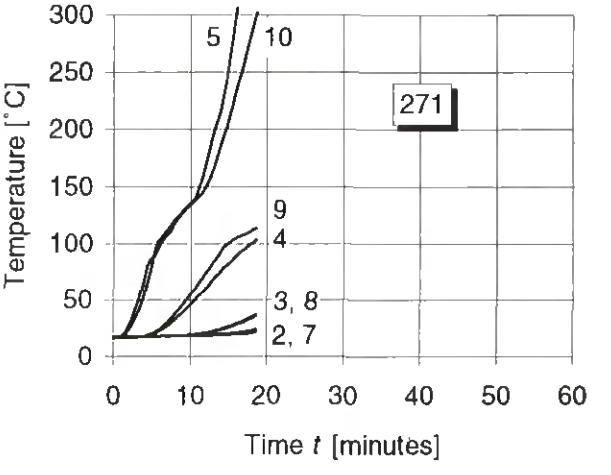
271
Temperature [°C]
Time t [minutes]
5
10
9
4
3, 8
2, 7

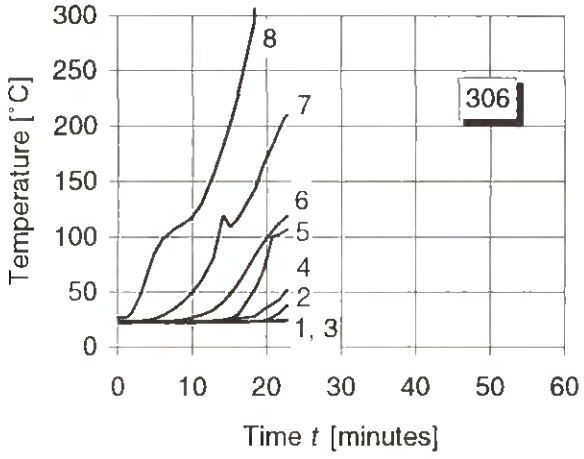
Temperature [°C]
300
250
200
150
100
50
0
0 10 20 30 40 50 60
Time t [minutes]
306
8
7
6
5
4
2
1, 3

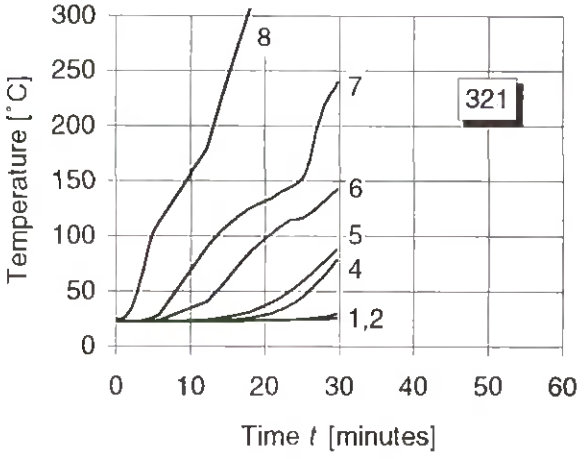
Temperature [°C]
300
250
200
150
100
50
0
0 10 20 30 40 50 60
Time t [minutes]
321
8
7
6
5
4
1,2

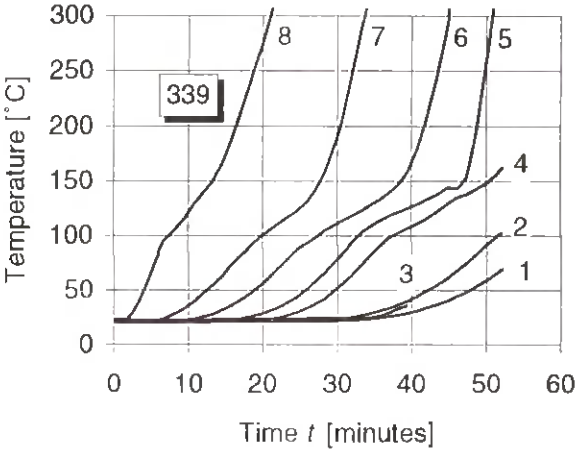
Temperature [°C]
300
250
200
150
100
50
0
0 10 20 30 40 50 60
Time t [minutes]
339
8
7
6
5
4
2
3
1

Detta digitala dokument
skapades med anslag från

**Stiftelsen Nils och Dorthi
Troëdssons forskningsfond**

Trätek

INSTITUTET FÖR TRÄTEKNISK FORSKNING

Box 5609, 114 86 STOCKHOLM
Besöksadress: Drottning Kristinas väg 67
Telefon: 08-762 18 00
Telefax: 08-762 18 01

Åsenvägen 9, 553 31 JÖNKÖPING
Telefon: 036-30 65 50
Telefax: 036-30 65 60

Skeria 2, 931 77 SKELLEFT
Besöksadress: Laboratorgrä
Telefon: 0910-652 00
Telefax: 0910-652 65